BEHAVIOUR OF CONTINUOUS CONCRETE SLABS REINFORCED WITH FRP BARS

Experimental and computational investigations on the use of basalt and carbon fibre reinforced polymer bars in continuous concrete slabs

Mohamed Elarbi Moh MAHROUG

A dissertation submitted for the award of
DOCTOR OF PHILIOSOPHY
PhD

School of Engineering, Design and Technology (EDT)

University of Bradford, UK

2013

BEHAVIOUR OF CONTINUOUS CONCRETE SLABS REINFORCED WITH FRP BARS

PhD Thesis,
School of Engineering, Design and Technology
University of Bradford, UK

Mohamed Mahroug

Signature: …….. Date: ……

PAPERS PRODUCED FROM THIS THESIS

1. M. E. M. Mahroug, A. F. Ashour and D. Lam "Experimental Response and Code Modelling of Continuous Concrete Slabs Reinforced with BFRP Bars" accepted for publication in the Composite Structures journal, Elsevier.

2. Mahroug, M. E. M., A. F. Ashour and Lam, D., "Tests of continuous concrete slabs reinforced with carbon fibre reinforced polymer bars", ACIC2013, Advanced Composites in Construction conference, 10-12 Sept. 2013, Queen's University, Belfast.

3. Mahroug, M. E. M., A. F. Ashour and Lam, D., "Tests of continuous concrete slabs reinforced with basalt fibre reinforced polymer bars", FRPRCS11 – 11th International Symposium on Fiber Reinforced Polymer for Reinforced Concrete Structures, Guimarães, June 26-28, 2013.

4. Mahroug, M. E. M., A. F. Ashour and Lam, D., "Flexural behaviour of continuous FRP reinforced concrete slabs", Structural Faults & Repair Conference, 3rd-5th July 2012, Edinburgh, Scotland.

The following papers are in preparation:

5. Mahroug, M. E. M., A. F. Ashour and Lam, D., "Flexural Behaviour of Continuous Concrete Slabs Reinforced with CFRP Bars" in preparation to be submitted for publication in Composites: Part B journal, Elsevier.

6. Mahroug, M. E. M., A. F. Ashour and Lam, D., "Code Modelling of Continuous Concrete Slabs Reinforced with FRP Bars" in preparation to be submitted for publication in the Composites for Construction, ASCE.

BEHAVIOUR OF CONTINUOUS CONCRETE SLABS REINFORCED WITH FRP BARS

Mohamed Elarbi Moh MAHROUG

ABSTRACT

Keywords: Concrete, slabs, Continuous, Failure, FRP Composites, Deflection, Moment, Shear, Capacity.

An investigation on the application of basalt fibre reinforced polymer (BFRP) and carbon fibre reinforced polymer (CFRP) bars as longitudinal reinforcement for simple and continuous concrete slabs is presented. Eight continuously and four simply concrete slabs were constructed and tested to failure. Two continuously supported steel reinforced concrete slabs were also tested for comparison purposes. The slabs were classified into two groups according to the type of FRP bars. All slabs tested were 500 mm in width and 150 mm in depth. The simply supported slabs had a span of 2000 mm, whereas the continuous slabs had two equal spans, each of 2000 mm. Different combinations of under and over FRP (BFRP/CFRP) reinforcement at the top and bottom layers of slabs were investigated. The continuously supported BFRP and CFRP reinforced concrete slabs exhibited larger deflections and wider cracks than the counterpart reinforced with steel. The experimental results showed that increasing the bottom mid-span FRP reinforcement of continuous slabs is more effective than the top over middle support FRP reinforcement in improving the load capacity and reducing mid-span deflections.

Design guidelines have been validated against experimental results of FRP reinforced concrete slabs tested. ISIS–M03–07 and CSA S806-06 equations reasonably predicted the deflections of the slabs tested. However, ACI 440–1R-06 underestimated the deflections, overestimated the moment capacities at mid-span and over support sections, and reasonably predicted the load capacity of the continuous slabs tested.

On the analytical side, a numerical technique consisting of sectional and longitudinal analyses has been developed to predict the moment–curvature relationship, moment capacity and load-deflection of FRP reinforced concrete members. The numerical technique has been validated against the experimental test results obtained from the current research and those reported in the literature. A parametric study using the numerical technique developed has also been conducted to examine the influence of FRP reinforcement ratio, concrete compressive strength and type of reinforcement on the performance of continuous FRP reinforced concrete slabs. Increasing the concrete compressive strength decreased the curvature of the reinforced section with FRP bars. Moreover, in the simple and continuous FRP reinforced concrete slabs, increasing the FRP reinforcement at the bottom layer fairly reduced and controlled deflections.

CONTENTS

LIST OF FIGURES

LIST OF TABLES

ACKNOWLEDGEMENTS

First of all, I express my deepest thanks to almighty **Allah** for blessing me with the health, wisdom, perseverance, patience, understanding and motivation needed to successfully complete this work.

I would like to express my sincere gratitude to my supervisors **Dr. Ashraf Ashour and Prof. Dennis Lam** for his invaluable guidance and advice, encouragement and support throughout this work.

Also, I wish to express my sincere thanks to **my late father**, who died on 01 July 2009. He and **my mother** have given all my academic endeavours unwavering encouragement and in the pursuit of my study this support substantially contributed to its completion.

My great gratitude and my sincere thanks are to be dedicated towards **my wife and kids, Ahmed, Arwa, Asma and Abdulrahman** for their invaluable encouragement and patience during my study. Without them, none of this would have been possible.

I am grateful to **all members and friends** of civil engineering for their great advice and encouragement during this research.

I wish to express my warm and sincere thanks also to **Dr. Xianghe Dai**, Lecture in Civil Eng., University of Bradford, for his assistance during the experimental investigation.

I am deeply grateful to **laboratory staff** in the Heavy Structural Laboratory for their technical support throughout the experimental investigation of this research.

Thanks also go to my friend Dr. **Abrahim Naser**, for his advice and assistance in the MATLAB operations during this research.

NOTATIONS

The following symbols are used in this thesis:

A_{bal}	=	area of balanced reinforcement;
A_f	=	area of FRP reinforcement;
A_s	=	area of steel reinforcement;
A	=	depth of each concrete segment in compressive or tensile ($= h/n$);
b	=	width of cross section;
c_b	=	neutral axis depth for balanced failure;
C_c	=	overall compressive forces in concrete
D	=	slab effective depth;
d_b	=	Bar diameter
E_c	=	modulus of elasticity of concrete;
E_f	=	modulus of elasticity of FRP reinforcement;
E_s	=	modulus of elasticity of steel reinforcement;
F_{ci}	=	concrete compressive forces in segment i;
F_{tj}	=	concrete tensile forces in segment j;
f'_c	=	cylinder compressive strength of concrete;
f_{ci}	=	concrete compressive stress in segment i;
f_{cu}	=	cube compressive strength of concrete;
f_{tj}	=	concrete tensile stress in segment j;
f_f	=	FRP stress at which concrete crushing failure mode occurs;
f_{fu}	=	ultimate tensile strength of BFRP bars;
f_r	=	modulus of rupture of concrete;

f_{ct} = tensile stress in a concrete;

h = height of slab;

I_{cr} = moment of inertia of transformed cracked concrete section;

I_e = effective moment of inertia of beam section;

I_g = gross moment of inertia of slab section;

K = ratio of neutral axis depth to reinforcement depth;

R = reaction force at the end of slab

L = slab span;

L_{ci} = lever arm for concrete compressive forces F_{ci};

L_{tj} = lever arm for concrete compressive forces F_{tj};

M_a = applied moment;

M_m = measured bending moment;

M_e = elastic bending moment;

M_{cr} = cracking moment;

M_{exp} = experimental failure moment;

M_{pre} = predicted failure moment;

$M_{support}$ = bending moment at the middle support of continuous slab;

M_{span} = bending moment at the mid-span of simple and continuous slabs;

M_r = bending moment at section number r along the slab span;

$M_{(r+1)}$ = bending moment at section number (r+1) along the slab span;

n = number of segments along the slab span;

n_f = modular ratio between FRP reinforcement and concrete ($=E_f/E_c$);

n_c = number of concrete segment in compression;

n_t = number of concrete segment in tension;

P = applied load;

P_{exp} = experimental failure load;

P_{cal} = Calculated failure load; *kN*

P_{cr} = first cracking load;

T_t = overall tensile forces in concrete;

w = crack width at tensile face of the slab;

x = segment location at the stress block;

β_d = reduction coefficient used in calculating deflection;

β = moment redistribution ration;

ε_c = compressive strain in concrete at the extreme fibre of a reinforced concrete cross-section;

ε_{ci} = concrete compressive strain at mid-depth of *i* segments

ε_{tj} = concrete tensile strain at mid-depth of *j* segments

ε_0 = strain of concrete corresponding to maximum stress of concrete f_c

ε_{cu} = ultimate strain of concrete;

ε_s = strain of steel reinforcement;

ε_t = tensile strain in concrete;

ε_r = concrete tensile strain corresponding to concrete tensile strength f_r;

ε_f = strain of FRP reinforcement;

ε_{fu} = ultimate strain of FRP reinforcement;

ε_y = yield strain of steel reinforcement;

ρ_{fu} = ultimate strain of BFRP reinforcement;

ρ_f = FRP reinforcement ratio; and

ρ_{fb} = balanced FRP reinforcement ratio.

$\varnothing$ = curvature along the slab length;

φ_r = curvature at section number r along the slab span;

φ_{r+1} = curvature at section number (r+1)r along the slab span;

θ = slope along the slab length;

θ_0 = slope boundary condition (θ_0=0);

θ_r = slope at section number r along the slab span;

$\theta_{(r+1)}$ = slope at section number (r+1)r along the slab span;

Δ = immediate mid-span deflection;

ΔL = length of sections (= L/n);

δ_n = deflection of the slab;

δ_r = deflection at section number r along the slab span;

δ_{r+1} = deflection at section number (r+1) along the slab span;

ABBREVIATION

The following symbols are used in this thesis:

AFRP	=	Aramid-fibre-reinforced polymer;
BFRP	=	Basalt-fibre-reinforced polymer;
CFRP	=	Carbon-fibre-reinforced polymer;
GFRP	=	Glass-fibre-reinforced polymer;
RC	=	Reinforced concrete;

CHAPTER ONE

INTRODUCTION

1.1 General

Steel reinforcements have a number of disadvantages such as corrosion, heavy weight and handling difficulties. In contrast, fibre reinforced polymer (FRP) reinforcing bars have many advantages including high strength-to-weight ratio, electromagnetic neutrality, ease of handling. As a result, during the past two decades, fibre reinforced polymer (FRP) materials have received a great deal of interest in concrete structures as an alternative to steel reinforcement. Corrosion of steel reinforcement in aggressive environments can cause cracking and deterioration of steel reinforced concrete structures. The use of FRP composites as reinforcement for such concrete structures provides a potential for increasing life, economic, and environment benefits. Thus FRP reinforcement can be used in places where steel cannot be used such structures may include dry docks, retaining walls, Magnetic Resonance Imaging (MRI) rooms, in hospital and research institutes, facades, floating pies, tanks, sea walls. FRP bars have mechanical properties different from steel bars, including elastic brittle stress-strain relationship and high tensile strength combined with low elastic modulus. Consequently FRP materials require a better understanding of behaviour of FRP reinforced concrete members.

There are several fabrication processes for FRP composites; these methods are well detailed and described in the ACI committee 440 reports (1996) for design and construction of reinforced concrete members with FRP bars. One of the most

common methods of fabricating composite material is pultrusion process, which is the only continuous fully automated manufacturing process, which allows the production of long straight constant section structural shapes made of reinforced polymeric composites.

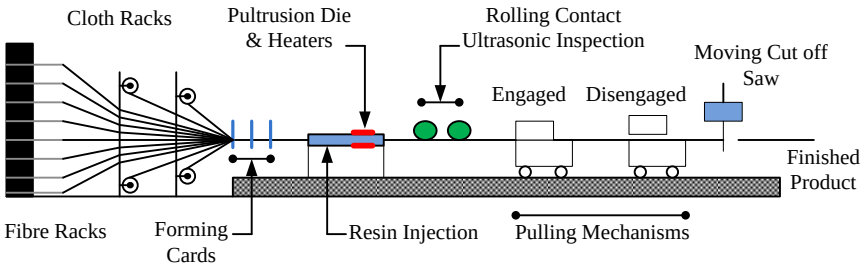

Figure 1–1: Pultrusion manufacturing procedure

In pultrusion, reinforcing materials in forms of continuous bars mats and other types of fabrics, one pulled though a resin matrix bath or other impregnation device, then carefully guided through a pre-shaping station followed by a heated, high precision die in which the resin matrix sets at high temperature to form the final product. Finally, the hardened profile is continuously pulled past a saw, activated to cut it into pre-determined lengths.

In recent years, a number of studies were conducted on simply supported concrete slabs/beams reinforced with FRP bars. The literature review which reported in chapter two shows that there has been very little studies into the behaviour of continuous concrete slabs reinforced with FRP bars, and many of studies finding from the investigations of simply supported slab are not applicable to continuous ones.

Many different types of FRP have been mainly used for concrete structures applications as presented in Figure (1–2); these include Carbon, Glass, and Armaid

fibres. This figure shows that fibre reinforced polymers do not have a yielding point and exhibit smaller failure strains compared with steel bars.

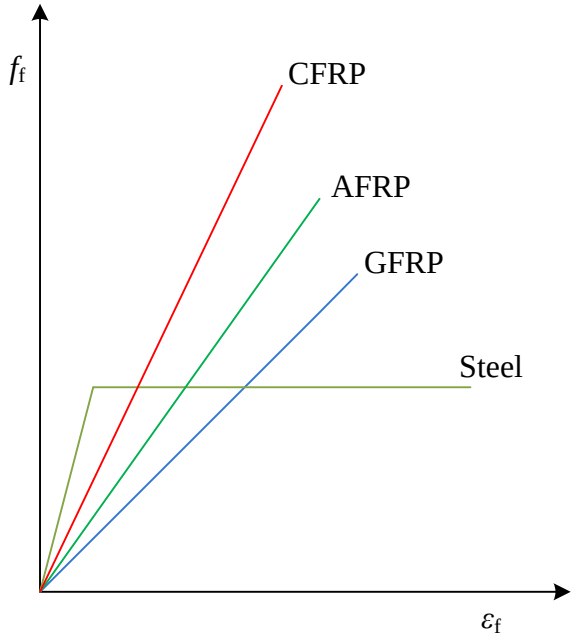

Figure 1–2: Typical stress-strain in tension for types of FRP bars and steel (Benjamin 1981)

The linear stress-strain diagram of FRP up to failure can be the cause of more fragile rupture, because of the lower stiffness of FRP bars. The geometrical shape, ductility, modulus of elasticity and bond qualities of FRP bars are likely to be different from that of steel bars. Thus the behaviour of FRP reinforced concrete should be independently investigated.

1.2 Research Aims and Objectives

The main aim of the research is to investigate the behaviour of continuously supported concrete slabs reinforced with basalt or carbon fibre reinforced polymer (BFRP or CFRP) bars. The project objectives are summarised below:

- To experimentally investigate the flexural behaviour of continuous concrete slabs reinforced with different FRP reinforcement configurations.

- To compare the behaviour of continuous concrete slabs reinforced with FRP and steel bars.
- To compare the behaviour of simply and continuously supported concrete slabs reinforced with FRP bars.
- To develop an analytical program for predicting the behaviour of continuously supported concrete slabs reinforced with FRP bars.
- To examine the applicability of design guidelines against the experimental results of continuous FRP reinforced concrete slabs.

1.3 Research Strategy

To achieve the research aims and objectives mentioned above, the following approach has been employed:

- Eight continuously and four simply supported concrete slabs reinforced with BFRP or CFRP bars were constructed and tested to failure in the laboratory. Two continuously supported steel reinforced concrete slabs were also tested for comparison purposes. Different combinations of under and over BFRP and CFRP reinforcements at the top and bottom layers of slabs were investigated.
- The design guidelines (ACI 440–1R-06, ISIS–M03–07 and CSA S806-06) have been evaluated against the experimental results.
- A computer program for sectional and longitudinal analyses has been developed using MATLAB (R2010a).
- Comparisons between the analytical results obtained from the current program and those obtained from the experimental result have been carried out.

1.4 Research Significance

Over the last couple of decades, several experimental studies have provided significant contributions in understanding the performance of FRP simple concrete members in shear and flexure. Many recommendations and proposals for design procedures have mainly arisen from these studies. However, limited investigations have been carried out on FRP continuous concrete members. In fact, no publications in the literature have been reported on the FRP continuous concrete slabs. Therefore, the existing research has attributed the following significance:

- The outcome of this investigation will provide valuable experimental results on continuous slabs reinforced with BFRP or CFRP bars.
- Design codes of FRP concrete members are mainly developed based on simply supported elements; therefore, the experimental results on continuous slabs can be used for design guidelines validation and develop new ones for continuous slabs if needed.
- Engineers and researchers will have a better understanding of the performance of CFRP and BFRP in concrete continuous slabs.
- The developed numerical technique can be used for further parametric studies to provide more insight into the behaviour of continuous concrete slabs reinforced with FRP bars.

1.5 Thesis Outlines

Chapter one presents general background of FRP materials, comparison between FRP and steel reinforcing bars, also background about fabrication process for FRP composites are highlighted. Finally the scope, the aim and the objectives of the research are presented. Chapter two gives a state of the art literature survey of the previous research on the behaviour of FRP reinforced concrete members. The

properties of FRP bars are highlighted early. Also it includes a general overview of the existing design codes and guidelines in the field of FRP reinforced concrete members. Finally, past work relating experimental and theoretical investigations of simple and continuous concrete members reinforced with FRP bars are presented in this chapter. Chapter three considers the experimental investigation of BFRP reinforced concrete continuous slabs. It includes a description of material properties, test procedure, the results and discussion of the tested slabs.

Chapter four presents the experimental investigations of CFRP reinforced concrete slabs. The material properties and methodology of the test program were presented. The test results and a discussion of the test program are also presented in this chapter. In chapter five, the design codes and their evaluation against the results obtained experimentally from this research were described. The failure load and deflection predictions for the BFRP and the CFRP reinforced concrete slabs were evaluated in this chapter.

Chapter six describes the numerical technique developed to predict the moment–curvature relationship, moment capacity and load-deflection of FRP reinforced concrete members. The influence of the FRP reinforcement ratio, concrete compressive strength and type of reinforcement on the performance of FRP material in the field of RC slabs has been investigated in chapter six. The experimental results detailed in chapters three and four used to validate the numerical techniques in chapter six. Chapter seven summarises the principal findings and the major conclusions of the research described in this thesis and gives recommendations and some suggestions for future work.

CHAPTER TWO

LITERATURE REVIEW

2.1 General

Fibre reinforced polymer (FRP) is becoming more frequently used for reinforcement of corrosion-prone concrete structures. This is due to their excellent corrosion resistance, a high tensile strength to weight ratio and good non-magnetization properties. However, FRP reinforced concrete members behave differently from traditional steel reinforced concrete structures because of their linear elastic stress-strain relationship up to failure. In addition, the lower modulus of elasticity of FRP causes a substantial decrease in the flexural stiffness of FRP reinforced concrete members after cracking and, consequently, larger deformations under service conditions. As a result, the design of FRP reinforced concrete members is often governed by the serviceability limit state. For this reason, a better understanding of the behaviour of FRP reinforced concrete members is required if they are to be used.

Many studies have investigated the flexural behaviour of simply supported beams and one way concrete slabs reinforced with different types of FRP reinforcing bars. However, the flexural behaviour of continuously supported FRP reinforced concrete beams has received little experimental attention. The literature survey presented in this chapter therefore describes the previous studies carried out on simply and continuously supported concrete members reinforced with FRP bars. In this chapter, a brief summary of the material properties and the main characteristics of FRP reinforcement bars are illustrated.

2.2 Development of fibre reinforced composite materials

The development of FRP as reinforcement can be traced back to the increased use of composites after the Second World War. Pultrusion offered an economic and fast manufacturing method to produce constant profile parts for commercial use. However, it was not until the 1960s that composite materials were seriously considered for use as reinforcement within concrete. The expansion of infrastructure projects and highway systems in the 1950s increased the need to provide year-round maintenance. Application of de-icing salts on highway bridges resulted in extensive corrosion of steel reinforcing bars (rebars) in these structures and corrosion was also prolific in structures subjected to marine environments. In the 1980s, the market demanded non-metallic reinforcement for specific advanced technology such as facilities for MRI medical equipment. FRP became the standard reinforcement used in this type of construction. Recently, FRP reinforcement began to be considered as a common solution for corrosion problems (see to Figure 2–1) (ACI 440 1R.06).

Figure 2–1: Application of FRP as reinforcement in civil and structural engineering (Val-Alain Bridge)

2.3 Constituent materials

Fibre reinforced polymers are composite materials essentially consisting of two basic components: reinforcing fibres and a matrix (resin). The fibres, which are responsible for carrying the load and providing strength, are ideally elastic, brittle and have high strength. The resin provides a cohesive environment to transfer stresses between fibres, holding the fibres together, and providing lateral support for the fibres against buckling. In addition, the resin plays an important role in protecting the fibres from mechanical and environmental damage. The fibres are significantly stronger than the resin material and control the elastic modulus and final strength of the composite (see to Figure 2–2). In order for fibres to provide a reinforcing function, the fibre-volume ratio should not be less than 55% of FRP bars and rods and 35% of FRP grids (ISIS Canada, 2007). The mechanical properties of the final FRP product also depend on a number of other parameters.

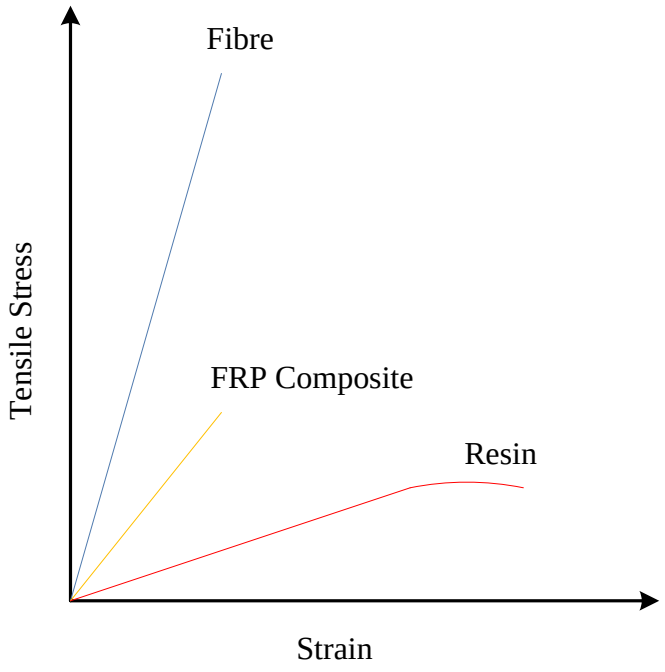

Figure 2–2: Stress-strain relationship for resin, fibres, FRP composite (reproduced from ISIS Canada, 2007)

2.4 Production and markets of FRP composites

Early applications for advanced composites were for military jets in those countries which had developed military industries, with the USA, the UK and France leading the field, closely followed by Germany and Italy. Japan has invested heavily from the outset, but with a much broader approach covering such areas as civil engineering and sports goods. China has also since become more and more involved in a large variety of composite products, so producers and markets are now distributed all around the world (Pilakoutas 2010).

Carbon fibre is the reinforcement of choice for many advanced polymer composites. They represent around 0.6% of the overall market but they account for approximately 12% of the total composite market value (Bunsell and Renard, 2005). Carbon fibre reinforced plastic (CFRP) composites have become a standard choice not only for the military applications but also for the civil engineering industry. Worldwide production of carbon fibre is estimated to be around 30 000 tones. It is expected that CFRP production will mature during the first part of the 21st century into a larger market now that it is finding applications in sectors such as the strengthening of civil engineering structures, reinforced and prestressed concrete members, hybrid load carrying elements for various structures, gas pressure vessels, wind turbines, offshore oil applications, sports goods and automobiles, alongside the traditional aerospace and military applications. Aramid fibres are another type of high performance fibre important for use in advanced polymer composites. They represent approximately 0.4% of the fibre reinforcement market and around 5% of its value. These fibres are also used in the internal reinforcing bars of concrete, and for structural rehabilitation of members made of reinforced concrete, masonry and timber, and cables among others (Pilakoutas 2010).

2.5 Manufacturing Process

There are three common manufacturing processes for FRP materials: pultrusion, braiding, and filament winding.

Pultrusion is the preferred technique for manufacturing continuous lengths of FRP bars that are of constant or nearly constant profile. A schematic representation of this technique is shown in Figure 2–3. Continuous strands of reinforcing material are drawn from creels, through a resin tank, where they are saturated with resin, and then passed through a number of wiper rings into the mouth of a heated die. The speed of pulling through the die is predetermined by the required curing time. To ensure a good bond with concrete, the surface of the bars is usually braided or sand-coated.

Braiding is a term used for interlocking two or more yarns to form an integrated structure.

Filament winding is a process whereby continuous fibres are impregnated with matrix resin and wrapped around a mandrel. During the latter process, the thickness, wind angle, and fibre-volume fraction are controlled. The final product is then cured using heat lamps. The most common products manufactured using this process are pipes, tubes, and storage tanks (ISIS Canada, 2007).

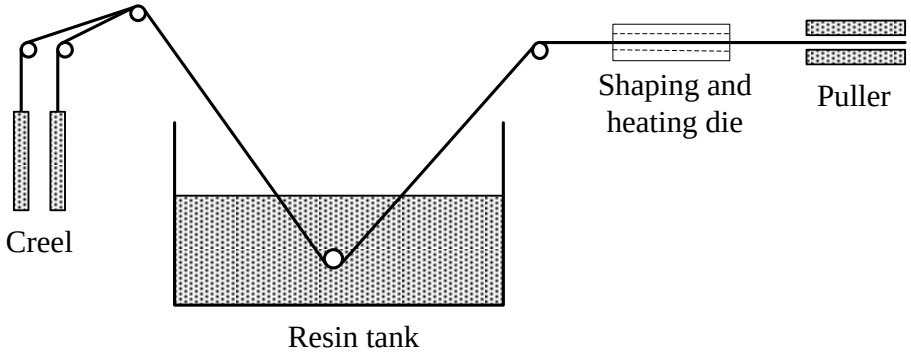

Figure 2–3: Pultrusion process

2.6 Properties of FRP Reinforcement

Fibre reinforced polymer (FRP) is produced from the manufacturing processes explained in the previous section. FRP bars typically have mechanical properties which are quite different to steel rebars. In addition, FRP bars have a lower Young's modulus, lower weight but higher strength than steel rebars.

2.6.1 Basalt Fibers

Basalt fibre is a material fibres commonly used in FRP. Basalt fibres are manufactured by the melting of quarried basalt rock. The molten rock is then extruded through small nozzles to produce continuous filaments of basalt fiber. The basalt fibres do not require any other additives during the production process, which gives an additional cost advantage. Basalt fibres have superior tensile strength in comparison to E-glass fibres, and a greater failure strain than carbon fibres. They also provide good resistance to chemical attack, impact load and fire damage, with lower levels of toxic fumes (Sim et al, 2005).

2.6.2 Carbon Fibers

Carbon fibres can be categorised into polyacrylonitrile fibres (PAN) and Pitch-based fibres. PAN fibres are characterized as having high strength (2500–4000 MPa) and high modulus of elasticity (350–650 GPa). However, pitch-based fibres are originally made from coal or petroleum. They are cheaper than PAN fibres, however, with lower strength and modulus. There are two types of Pitch fibres, ordinary and high modulus. Carbon fibres composites are expensive and sensitive to the processing conditions such as tension and temperature during manufacturing, and more brittle compared to glass and aramid fibres.

2.6.3 Glass Fibers

E-glass, Z–glass, A–glass, C–glass and S–glass are the most common types of glass fibres (Ganga Rao and Vijay 2007). Glass fibres are generally low cost, high tensile strength (1800–4900 MPa) (see Figure 2–4), high chemical resistance and excellent insulating properties. Due to the economical characteristic of the production process of glass fibres, this product is the most commonly used fibres in FRP composites products. In addition, glass fibres are insulators of both electricity and heat.

2.6.4 Aramid Fibres

Aramid fibres (aromatic polyimide) are manufactured first in Germany under the name of Kevlar. Aramid fibres offer excellent resistance to damage against impact, high tensile strength (see Figure 2–4) and the modulus is about 50% higher than glass. The density of aramid fibres is very low compared to carbon and glass. Furthermore, aramid fibres made from material exhibit excellent electrical and thermal insulation. However, the compressive strength of aramid fibres is very low.

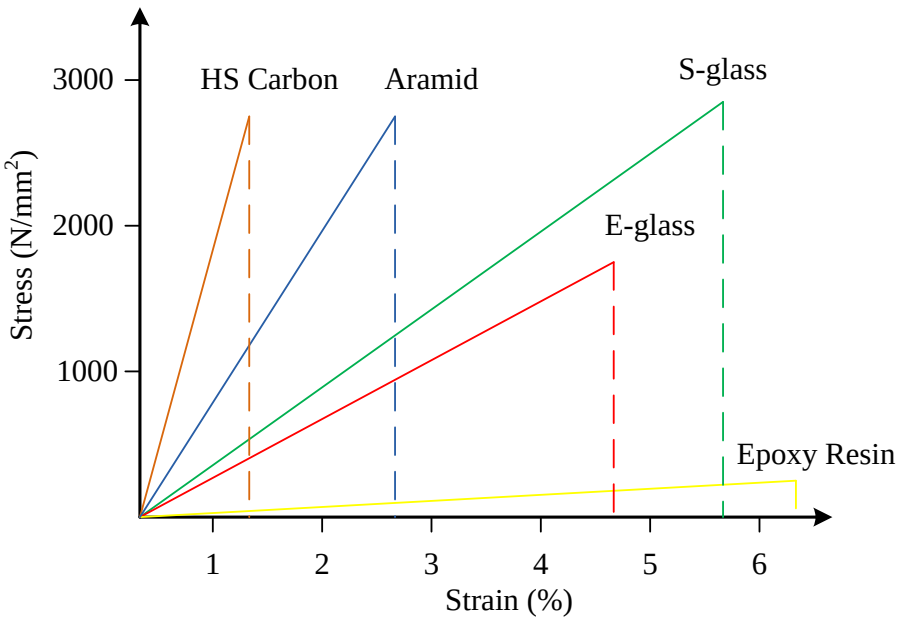

Figure 2–4: Stress–strain relationship to failure for E–glass, S-glass, Epoxy Resin, Aramid, and HS Carbon (Wu, 1990)

2.7 Existing FRP RC Design Guidelines

Over the last decade, numerous design guidelines have been published for concrete structures reinforced with fibre reinforced polymers (FRP). Currently, there are four main groups of design guidelines for FRP reinforced concrete structures, namely a) Japan (JMC, 1995; JSCE, 1997); b) Canada (CHBDC, 1996; ISIS–01, 2001; ISIS-07, 2007); c) America (ACI 440–96, 1996; ACI 440–98, 1998; ACI440.1R, 2001; ACI440.1R–03, 2003; ACI440.1R–06, 2006); and d) Europe (Clarke et al, 1995). The brittle linear-elastic behaviour of FRP reinforcement is an influencing factor behind all of the existing design codes (Pilakoutas 2010).

These design guidelines are mainly provided in the form of modifications to existing steel RC codes of practice, which predominantly use the limit state design approach. The modifications consist of basic principles which are heavily influenced by the unconventional mechanical properties of FRP reinforcement, and empirical equations based on experimental investigations of concrete elements reinforced with FRP. The brittle linear-elastic behaviour of FRP reinforcement is an influencing factor behind all of the existing design guidelines.

2.8 Flexural behaviour of FRP reinforced concrete members

2.8.1 Bond Behavior of FRP Reinforcement

Some manufacturers add a coating of sand and resin on the bar at the end of the manufacturing process which makes the bar surface even smoother. In addition, the stress-strain relation of GFRP bars is linear at all stress levels up to the point of failure, without exhibiting any yielding of the material. The modulus of elasticity of GFRP bars is approximately 20–25 present of that of steel bars. The tensile strength

varies from 500 to 1100 MPa, depending on the glass content, type of fibre and resin, and manufacturing process (Larrard et al. 1993).

The performance of bond between FRP reinforcing bars and the surrounding concrete is different to that of steel rebars (Faza and Ganga Rao, 1992). This is attributed to the fundamental differences between the interaction mechanisms, and the different material properties of FRP and steel rebars (Chaallal and Benmokrane, 1993). In addition, the outer surface roughness of the FRP reinforcing bars is controlled by using epoxy, fibres or sand coating which results in FRP bars exhibiting an inconsistent or poor bond. Thus, it has been argued that for FRP reinforcing bars, chemical adhesion and friction are the primary bond mechanisms (Larralde and Silva-Rodriguez, 1993; Benmokrane et al., 1996; Ehsani et al., 1993).

Makitani et al. (1993), Benmokrane et al. (1996) and Tighiouart et al. (1998) studied the influence of concrete strength on the bond performance of FRP reinforcing bars in concrete based on a number of experimental results and it was observed that the bond strength increase is proportional to the square root of concrete compressive strength ($\sqrt{f_c'}$).

The failure mode during bar pullout tests depends on the concrete compressive strength. Therefore, for high concrete strength, the bond strength of FRP reinforcing bars does not depend on the concrete compressive strength, since in such cases the failure interface takes place at the surface of the FRP reinforcement. Conversely, for low strength concrete, the concrete compressive strength directly influences the bond behaviour of FRP reinforcement, and the failure interface occurs within the concrete matrix (Achillides and Pilakoutas, 2004; Baena et al., 2009).

Ehsani et al., (1993); Kanakubo et al., (1993) and Defreese and Wollmann, (2002) noticed that concrete cover provides confinement pressure to the reinforcing bars

which improves the development of bond strength. ACI 440.1R-06 concluded that bond failure occurs during splitting of concrete which occurs when the reinforcing element does not have sufficient concrete cover. In general, it can be said that the bond failure mode of a reinforced member depends on the level of concrete cover.

The influence of the embedment length on the bond behaviour of FRP bars in concrete was investigated by some researchers (Makitani et al., 1993; Nanni et al., 1995; Benmokrane et al., 1996; Tighiouart et al., 1998 and Pecce et al., 2000). It was observed that when embedment length of FRP bars increases, the bond strength decreases. This attributed to the non-linear distribution of bond stresses along the length of bars (see Figure 2–5). Furthermore, it was shown that the rate of bond stress increase is greater for smaller embedment lengths (Achillides and Pilakoutas, 2004).

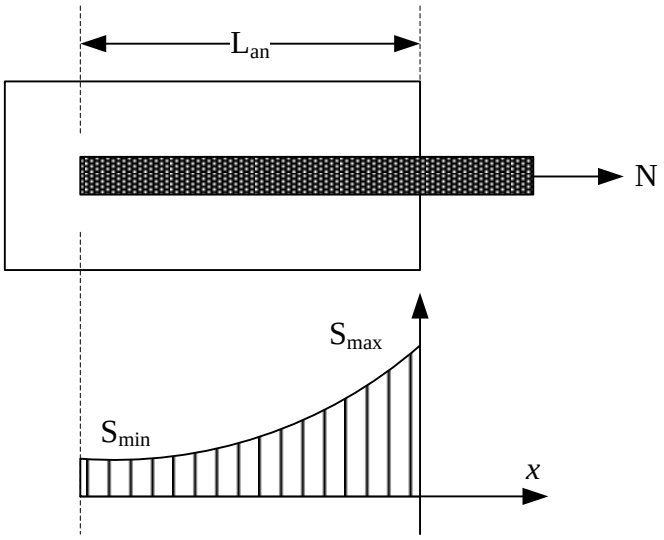

Figure 2–5: Bond stresses along the length of bar

Baena et al. (2009) conducted 88 pull-out tests on FRP bars and observed that when the failure is not occurring in the concrete matrix, the bar surface treatment has a significant effect on the bond strength.

The researchers also identified that in larger bars the difference between the maximum and minimum stresses increases which causes premature failure of the bar in bond caused by the orthotropic nature of the bar. These conclusions were based on post-failure observations of the bar in which pulverized resin and fibres were noted along the failure plane of the bar (Wang, 2004).

An experimental investigation was conducted by Janet and Chris (2000) to study the flexural performance of concrete prestressed with AFRP tendons. The influence of the bond between AFRP tendons and concrete on the flexural response of beams was studied by testing beams with fully-bonded tendons, unbonded tendons or partially-bonded tendons. It was found that, although the fully-bonded beams had a high ultimate load capacity, only limited rotation occurred prior to failure. In contrast, large rotations were noted in the unbonded beams, but the strengths of these members were significantly (25%) lower than those of the fully-bonded beams.

2.8.2 Deflection of FRP RC Members

2.8.2.1 Effective Moment of Inertia Approach

FRP reinforced concrete members behave differently from those reinforced with traditional steel rebars. FRP bars have higher strength, but lower modulus of elasticity than steel, and demonstrate linear elastic behaviour in tension up to failure. The lower modulus of elasticity of FRP causes a substantial decrease in the stiffness of FRP reinforced concrete beams after cracking, and consequently higher levels of deflection under service conditions (Zhao et al., 1997; Alsayed et al., 2000; Vijay and Ganga Rao, 2001). Hence, the design of FRP reinforced concrete members is typically governed by serviceability requirements. Analytical methods for predicting the service load deflections of FRP reinforced concrete members with reasonable degree of accuracy would be very beneficial (Ilker and Ashour, 2012).

The immediate short-term deflections of a cracked element reinforced with steel bars can be determined using an effective moment of inertia, given by Branson's equation (Branson, 1968; Branson, 1977) as presented in Eq. (2–1). It was observed that the ACI 318 equation leads to underestimated service level deflections in FRP RC beams (Benmokrane et al., 1996; Theriault and Benmokrane 1998; Massmoudi et al., 1998; Pecce et al., 2000; Razqpur et al., 2000 and Toutanji and Saafi, 2000). This is due to the fact that Branson's expression was only adjusted for moderately reinforced concrete beams (Bischoff, 2005; and Bischoff and Scanlon, 2007).

Nawy 1977 concluded that the deflections were found to be underestimated using Branson's expression. It was observed that the accuracy of deflection predictions for GFRP reinforced concrete beams varies with the amount of the reinforcement provided. A similar finding was reported by Kassem et al. (2003) and Yost et al. (2003) in which ACI steel equation underestimates the CFRP experimental deflection values.

Moreover, another experimental investigation was carried out by Al-Sunna et al. (2007) to study the deflection of FRP reinforced concrete beams. The authors concluded that the original version of Branson's equation for the effective moment of inertia works well for steel RC, but overestimates the effective moment of inertia and underestimates deflections for FRP RC.

In general, the studies presented in the literature have shown that the original version of Branson's equation for effective moment of inertia I_e may lead to significant errors when it is used for FRP reinforced concrete members.

Over the last two decades, a significant number of researchers have proposed modifications to Branson's equation to enable it to predict the effective moment of

inertia of FRP RC members. Most investigators modified Branson's original expression empirically to improve its agreement with other experimental results. Faza and Ganga Rao (1992) tested a series of simply supported beams reinforced with FRP bars. Their study was designed to quantify the load-deflection behaviour. They modified moment of inertia, I_m expressed as function of the effective moment of inertia, I_e and the moment of inertia of the cracked transformed section, I_{cr}. Thus, I_m replaces I_e in the calculation of deflection by ACI-318 procedure as given in equation (2–2) (see Table 2–1).

A further investigation concerning the effective moment of inertia was carried out by Benmokrane et al. (1996). They added two empirical factors to the expression originally developed by Branson and adopted by the ACI code such that it fits well with their experimental data of glass fibre reinforced polymer (GFRP) RC beams. One major criticism of Benmokrane's work is that their study was validated using only a limited number of tests. The effective moment of inertia was defined according to Eq. (2-3) for cases where the reinforcement type was FRP.

To predict short-term deflections of FRP RC members, ACI 440-01 recommended a modified form of Branson's equation for the effective moment of inertia, I_e, based on Gao et al. (1998) as shown in Eq. (2–4). ACI 440.1R-01 equations have been criticised by a number of researchers. Toutanji and Deng (2003) investigated the deflection prediction of FRP reinforced concrete beams. The main objective of the study was to verify the use of ACI 440.1R-01 equations to predict deflections of GFRP reinforced concrete beams by comparing their experimental results with ACI design code. They showed that the experimental measurements obtained in this research compared well with the predictions from the ACI 440.1R-01 equations.

Alsunah et al. (2007) also investigated the deflection of FRP–reinforced concrete beams with the main objective of evaluating the effective moment of inertia experimentally by comparing the results with deflection prediction by ACI provisions. They reported that the form of equation for I_e cannot be used to predict deflections of FRP reinforced concrete beams. Yost et al. (2003) studied the deflection behaviour of concrete beams reinforced with GFRP bars. The authors pointed out that the ACI model is over estimating the effective moment of inertia. However, they proposed an appropriate modification to this equation which allows more accurate calculation of the effective moment of inertia.

Mohamed et al. (2011) carried out flexural tests on an ensemble of GFRP RC beams. They observed that the theoretical data predicted using ACI 440 code showed good agreement with the experimental data, to within an error of around 20%. In addition, they found that the deflection predictions obtained from the Faza and Ganga Rao equation are adjusted to the experimental results.

Ashour and Habeeb (2008) also studied the accuracy of the ACI 440 1R-06 equations in predicting the deflections of simply and continuously supported RC beams. They noted that there is good agreement between the prediction from ACI 440-1R-06 and experimental measurements of simply supported CFRP RC beams. However, the ACI 440 1R-06 equations for the prediction of continuous CFRP reinforced concrete beam deflections have been adversely affected by the de-bonding of the upper CFRP bars from concrete.

Recently, Muhammad and Nadjai (2009) explored a comparison between the experimental load-deflection curves of FRP reinforced concrete members and the theoretical predictions based on the deflection model as suggested by ACI 440. From

this comparison they concluded that the modified expression provided consistent results and that the prediction agreed well with the experimentally measured curvature and deflection data.

Toutanji and Saffi (2000) presented a modification of the power of the (M_{cr}/M_a) term in Branson's equation to give reliable deflection calculations of FRP reinforced concrete members after cracking as shown in Eq. (2–5). In their study, the FRP modulus of elasticity and the reinforcement ratio were taken into account. The experimental results were then compared with deflections modelled by Branson's equation. Consequently, they concluded that the results for GFRP reinforced concrete beams were in good agreement with the proposed analytical models. In addition, GFRP reinforced beams demonstrated higher deflection values compared to their counterparts reinforced with steel. They attributed this finding to the lower elastic modulus of GFRP bars.

The ISIS Design Manual-01 (Rizkalla and Mufti, 2001) introduced a method for predicting the effective moment of inertia (I_e) for immediate deflection (δ) of FRP reinforced concrete members after cracking as defined in Eq. (2–6). This equation is derived from equations given by the CEB-FIP MC-1990. Comparisons between the effective moment of inertia predicted by Eq. (2–6) and the experimentally measured deflection of concrete beams reinforced with different types of FRP bars show good agreement (Ghali et al., 2001). The CSA S806-02 design code (2002) recommended the use of Eq. (2–7) (see Table 2–1) to calculate the effective moment of inertia (I_e) for FRP reinforced members.

More recently, an experimental study was conducted by El-Mogy et al. (2010) to evaluate the use of design codes for deflection prediction of FRP reinforced

continuous beams. It was observed that CSA/S806-02 design code progressively underestimates the deflections of FRP reinforced continuous concrete beams at loads higher than the cracking load. However, it has been reported that the deflection prediction by the CSA S806-02 equation showed very good agreement with the experimental results for three types (E-glass, C-glass and Z-glass) of GFRP bars (El-Gamal et al., 2010). Moreover, the equations given in CSA S806-02 were found to be the most accurate and conservative when used for calculating the deflection of CFRP reinforced concrete members (Carols et al., 2006). Ilker et al. (2012) studied the deflection of simple and continuous concrete structures reinforced with FRP bars. Their study found that while Bischoff's model gives good predictions for simply supported FRP reinforced concrete beam deflections, it progressively underestimates deflections of continuous FRP reinforced concrete beams. Moreover, in another major study, Barris et al. (2009) found that the predicted deflections provided by the Bischoff approach showed good agreement with the experimental data. However, for additional levels of applied load, this theoretical approach underestimates the deflections. Habeeb and Ashour (2008) investigated the deflection prediction of simply and continuously supported GFRP reinforced concrete beams. They introduced a correction factor, γ_G (=0.6) to the second term of the equation proposed in ACI 440 (2006) to predict the effective moment of inertia (I_e). The correction factor, as presented in Eq. (2-9) gives reasonable agreement with the experimental data, particularly at higher loading. In another study, El-Mogy (2010) concluded that the modified equation including the correction factor proposed by Habeeb and Ashour (2008) reasonably predicted deflections of FRP reinforced continuous concrete beams, especially at high loading stages. In a different study, Al-sunna et al. (2012) examined several existing approaches for the calculation of deflections of

FRP RC members and concluded that current design codes progressively underestimate the deflections.

Table 2–1: Deflection design equations for FRP reinforced concrete members

Author	Equation	No.
Branson (1977)	$I_e=\left(\frac{M_{cr}}{M_a}\right)^3 \times I_g + \left[1-\left(\frac{M_{cr}}{M_a}\right)^3\right] \times I_{cr} \le I_g$	2–1
Faza and Ganga Rao (1992)	$I_m=\frac{23 \times I_{cr} \times I_e}{8 \times I_{cr} + 15 \times I_e}$	2–2
Benmokrane et al. (1996)	$I_e=\alpha_0 I_{cr} + \left(\frac{I_g}{\beta_0} - \alpha_0 I_{cr}\right)\left[\frac{M_{cr}}{M_a}\right]^3$	2–3
Gao et al. (1998)	$I_e=\left(\frac{M_{cr}}{M_a}\right)^3 \beta_d \times I_g + \left[1-\left(\frac{M_{cr}}{M_a}\right)^3\right] \times I_{cr} \le I_g$	2–4
Toutanji and Saffi (2000)	$I_e=\left(\frac{M_{cr}}{M_a}\right)^m \times I_g + \left[1-\left(\frac{M_{cr}}{M_a}\right)^m\right] \times I_{cr} \le I_g$	2–5
ISIS Canada-01 (2001)	$I_e=\frac{I_e I_{cr}}{I_{cr} + \left(1-0.5\left(\frac{M_{cr}}{M_a}\right)^2\right)\left[I_g - I_{cr}\right]}$	2–6
CSA-02 (2002)	$I_e=\frac{I_{cr}}{1-\left(1-\frac{I_{cr}}{I_g}\right)\left(\frac{M_{cr}}{M_a}\right)^3}$	2–7
Bischoff and Scalon (2007)	$I_e=\frac{I_{cr}}{1-\left(1-\frac{I_{cr}}{I_g}\right)\left(\frac{M_{cr}}{M_a}\right)^2}$	2–8
Habeeb and Ashour (2008)	$I_e=\left(\frac{M_{cr}}{M_a}\right)^3 \beta_d \times I_g + \left[1-\left(\frac{M_{cr}}{M_a}\right)^3\right] \times I_{cr} \times \gamma_G \le I_g$	2–9

Note: I_e is the effective moment of inertia (mm^4), M_{cr} is the cracking moment (N.mm), M_a is the applied moment (N.mm), I_g is the moment of inertia of gross section (mm^4), I_{cr} is the moment of inertia of cracked section transformed to concrete (mm^4), α_0 and β_0 are equal to 0.84 and 7, respectively. The factor α_0 can reflect the reduced composite action between the concrete and FRP bars. The factor β_0 was introduced in the equation to enable a faster transition from I_g to I_{cr}.

In a comprehensive study, Mota et al. (2006) presented a critical review regarding to methods of deflection prediction. These methods are compared against the

experimentally measured deflection of 197 members conducted by other researchers. Their study indicates that the accuracy of the existing deflection formulae is dependent on both the modulus of elasticity of FRP and also on the relative reinforcement ratio. It has been shown that the equation given by Faza and Ganga Rao (1992) is the most accurate method of calculating the deflection of CFRP-RC beams, while the formula presented by Yost et al. (2003) gives satisfactory results for predicting the deflection of GFRP reinforced concrete beams.

The accurate results obtained by the methods of Toutanji and Saafi (2000), Faza and Ganga Rao (1992), Yost et al. (2003), and the Proposed ACI 440.1R-04, do not vary as greatly with the elastic modulus of the CFRP, as the methods proposed by ISIS M03-01 or CSA S806-02 (Mota et al., 2006).

2.8.2.2 Control of Deflections

The modulus of elasticity of FRP is generally smaller than that of steel. Therefore, members having the same concrete cross-section and the same loading typically exhibit larger deflection when FRP is used. However, by appropriate choice of the minimum thickness and by adopting an allowable stress in the FRP at service, the ratio of the span to the deflection can be the same as with steel-reinforced members (ISIS-07).

Because of the axial stiffness, brittle-elastic nature, and particular bond features of FRP reinforcement, deflections of FRP RC members are more sensitive to the variables affecting deflection than steel RC members of identical size and reinforcement layout (ACI 440 1R-06). Steel reinforced beams can exhibit a large increase in deflection with little change in load, due to yielding in the reinforcement. FRP reinforced beams however do not show any significant yielding. Deflection in

FRP reinforced concrete beams continues to increase as further load is applied, thereby exhibiting some ductility despite the brittle nature of FRP material (Benmokrane et al., 1995). Deflections are generally higher in concrete beams reinforced with FRP bars than in concrete beams reinforced with steel bars (Nanni, 1993, ACI 440 2006; Wegian and Abdalla, 2005; Habeeb and Ashour, 2008; El-Mogy et al., 2010). Depending on the load level and the number of loading and unloading cycles, the residual deflection of the FRP reinforced beams is 3 to 4 times that of identical conventional steel reinforced concrete beams, as is the ratio of instantaneous deflections. This ratio is mainly attributed to the difference of modulus of elasticity, and other physical and mechanical characteristics such as bond properties. The mid-span deflection decreases as reinforcement ratio increases (Masmoudi et al., 1998; Theriaul et al., 1998). In very early work, Nawy and Neuwerth (1977) presented a study on the behaviour of glass fibre RC slabs and beams. They found that once the concrete cracked, the beams deflected at a faster rate for a unit increase in load. They also noticed that by increasing the percentage of tensile reinforcement from 0.7% to 1.4%, the load at the allowable deflection of $L/180$ increased by approximately 25%. Others have observed that the ratio of span to experimental service load deflection is relatively high when compared to the usually accepted ratio of approximately $L/250$.

Almusallam et al. (1997) investigated the effects of different ratios of compression reinforcement on the deflection of concrete beams reinforced with GFRP rebars. They observed that the resulting impact on the deflection of the beams is small. These results are corroborated by further experimental work recently conducted to evaluate the flexural behaviour of FRP reinforced concrete beams. Three continuously and two simply supported concrete beams reinforced with carbon fibre

reinforced polymer (CFRP) bars were tested by Ashour and Habeeb (2008). Their experimental results showed that deflections were slightly reduced by increasing the top layer of CFRP reinforcement of continuous beams. However, increasing the bottom layer of CFRP reinforcement in simply and continuously supported concrete beams was also shown to be a key factor in controlling deflection.

2.8.2.3 Ultimate load and modes of failure

The flexural design of steel RC members usually results in under reinforced sections in order to ensure that yielding of the steel reinforcement occurs before the crushing of concrete. This is because yielding of steel provides ductility and a warning of failure of the member. However, in the case of FRP RC members, there is no such warning of failure due to the non-ductile behaviour of FRP reinforcement. In this case, failure would occur either due to crushing (compression failure) of the concrete, or rupturing (tension failure) of the FRP reinforcement. If flexural failure occurs due to rupture of FRP reinforcement, the failure is sudden and catastrophic. There would be a limited warning of impending failure in the form of extensive cracking and large deflection caused by the significant elongation that FRP reinforcement experiences before rupture. The concrete crushing failure mode is marginally more desirable for flexural members reinforced with FRP bars, since the members exhibit some plastic behaviour before failure (ACI 44o.1R-06).

Previous experimental results of FRP reinforced members indicate that when FRP bars ruptured (tension failure), the failure was sudden and led to the collapse of the member (Nanni, 1993; GangaRao and Vijay, 1997; and Theriault and Benmokrane, 1998). However, a more progressive and less catastrophic failure was observed when the member failed due to the crushing of concrete (compression failure). This

behavior results in higher deformability, which is defined as the ratio of energy absorption at ultimate to that at service level (Jaeger et al., 1997).

Nanni et al. (1993) studied the flexural behaviour of concrete beams reinforced with different GFRP bars (smooth or sand-coated) and steel deformed bars. It was noted that the sand-coated FRP increased the ultimate flexural capacity by approximately 25% compared with the equivalent uncoated rebars. The authors state that the ultimate strength could be predicted on the basis of the material properties of the concrete and reinforcement.

Mohamed et al. (2011) studied the influence of fibres on the flexural behaviour and ductility of GFRP reinforced concrete beams. Their tests showed that using GFRP as internal reinforcement for RC beams results in reasonable flexural strength. Furthermore, their results indicated that ACI 440.1R-06 strongly underestimated the moment capacities of FRP RC beams.

Ilker et al. (2012) adopted a numerical method for predicting the moment capacity of FRP concrete beams. Comparisons with experimental results show that the proposed numerical technique can accurately estimate moment capacity of RC beams reinforced with FRP bars. It was also noticed that the ACI-440.1R-06 formulae reasonably predicted the moment capacity of FRP reinforced concrete beams. Finally, it was shown that a large increase in FRP reinforcement produces a slight increase in the moment capacity of FRP over reinforced concrete beams. A parametric study concluded that concrete compressive strength has no effect on the moment capacity of FRP under reinforced concrete beams but a significant influence for the over reinforced equivalent.

Masmoudi et al. (1999) tested a number of FRP reinforced concrete beams subjected to static loading. The beams were tested in order to investigate the effects of reinforcement ratio on ultimate capacities and modes of failure. They observed from this study that as the reinforcement ratio increases, the ultimate moment capacity increases, but that this increase is limited by the concrete compression failure strain for the reinforced concrete beams. The results from the flexural tests of concrete beams reinforced with FRP rebars indicated that the use of GFRP rebars in concrete structures is possible and that optimal design is achievable if not only an appropriate reinforcement ratio is used, but also the appropriate height-to-span ratio is computed (Benmokrane et al., 1995). Other researchers, such as Habeeb and Ashour (2008) and Ashour and Habeeb (2008), noticed that over-reinforcing the bottom layer of either the simply or continuously supported GFRP beams is a key factor in enhancing the load capacity of concrete beams. Comparisons between the experimental results and those obtained from simplified methods proposed by the ACI 440 Committee show that ACI 440.1R-06 equations can reasonably estimate the load capacity of GFRP reinforced concrete beams under test.

Another experimental investigation was conducted by El-mogy (2010) to study the flexural behaviour of continuous concrete beams reinforced with different types of FRP bars. The test results were compared against the available design models and FRP codes. It was concluded that the Canadian Standards Association Code (CSA/S806-02) could reasonably predict the failure load of the tested beams; however, it fails to predict the failure location. It should be also mentioned that increasing the FRP reinforcement at the mid-span section, rather than the middle support section, had positive effects on load capacity. Other studies such as Muhammad et al. (2006) investigated the behaviour of FRP concrete beams. Their

study indicated that the behaviour of CFRP was similar to that of steel reinforced beams in many respects. Both types of beams failed according to their predicted modes of failure. The strength design method underestimated the nominal moment capacity of CFRP reinforced beams. During the early 90's, Vicki et al. (1993) studied the flexural performance of FRP reinforced concrete beams. In this study, the authors pointed out that strength design methods for RC beams reinforced with steel rebars adequately estimate the ultimate moment capacity of FRP reinforced concrete beams.

2.8.3 Cracking of FRP Reinforced Concrete Members

2.8.3.1 Cracking behaviour

At initial load level, the pattern and spacing of cracks in FRP reinforced concrete beams were similar to those in steel reinforced concrete beams, but as the load was increased, more cracks appeared with increased width when compared to steel reinforced concrete beams (Benmokrane et al., 1995; Alkhrdaji et al. 1999). Conversely, Muhammed et al. (2006) reported that the cracking behaviour of CFRP and steel reinforced concrete beams was similar. In another research, Michaluk et al. (1999) tested a number of one-way slabs reinforced with GFRP bars in order to study the flexural behaviour of such slabs. The study indicated that GFRP concrete slabs demonstrate larger crack widths when compared to counterparts reinforced with the same ratio of steel or CFRP reinforcements. This can be explained by the low elastic modulus of GFRP bars in comparison to steel rebars, and the debonding of the outer deformation of the particular bar used in this study. Other researchers such as Toutanji and Saafi (2000) investigated the flexural behaviour of FRP reinforced concrete beams. The study indicated that crack widths of FRP reinforced concrete beams are significantly larger than that of the steel reinforced counterparts.

This observation has been further confirmed by other researchers such as Masmoudi et al. (1999), Ashour and Habeeb (2008) and El-Mogy et al. (2010).

Masmoudi et al. (1999) concluded that the maximum observed crack width in beams reinforced with FRP reinforcing rods is 3 to 5 times that of identical beams reinforced with steel bars. It was also found that the residual crack width decreases as the reinforcement ratio increases; however, the results have shown that the residual crack width is not affected, after the first cycle of loading/unloading, by the number of loading/unloading cycles.

Kassem et al. (2011) reported that the crack width in FRP reinforced concrete beams varied linearly with the applied moment up until failure. The crack width was smaller for the beams with greater reinforcement ratios. Similarly, Theriaul et al. (1998) noted that the residual crack width decreases as the reinforcement ratio increases. The beams reinforced with sand-coated bars exhibited a greater number of cracks as opposed to those reinforced with ribbed-surface bars. This suggests that the tested sand-coated bars provided a better bond with the concrete than the ribbed-surface bars (Kassem et al., 2011).

2.8.3.2 Cracking Prediction

Due to their different mechanical properties, the behaviour of FRP reinforced concrete members is quite different from that of traditional steel reinforced concrete (Faza and Ganga Rao, 1993 and Masmoudi et al., 1996). Because of the lower stiffness of FRP bars when compared to steel, deformations and crack widths at service loads are usually larger for GFRP RC than for steel reinforced concrete (SRC). For this reason, the prediction of their behaviour plays an important role in the design of GFRP RC flexural elements, and this is often governed by the

serviceability limit states (ISIS design code, 2001). In this sense, the study of the interaction between FRP reinforcement and surrounding concrete is necessary in order to calculate deformations in FRP reinforced concrete to a sensible accuracy (Baena et al., 2009). The original formula (Eq. 2–10) in Table 2-2 developed by Gergely and Lutz (1968) to predict the maximum crack width for steel reinforced concrete members (ACI 318R-95) was also recommended for FRP reinforced concrete members (ACI 440R-01), but is significantly modified in order to account for both the mechanical and bond properties of FRP reinforcements. Masmoudi et al. 1999 reported that crack width in FRP reinforced concrete beams can be predicted using the modified Gergely-Lutz equation. For practical prediction, the coefficient K_g = 41 for the FRP reinforcing rod used in their study.

El-Salakawy and Benmokrane (2004) concluded that the experimental crack widths measured on their tested slabs gave good correlation with those obtained by the ACI 440.1R-01 formula using a bond factor, k_b=1. Moreover, Toutanji and Deng (2003) reported that ACI 440.1R-01 approach gave better predictions of crack width when FRP reinforcing bars were located in one layer.

Conversely, Faza and Ganga Rao (1993) modified the Gergely-Lutz formula to calculate the maximum crack width for FRP reinforced concrete beams, while taking into account the effect of the relative low modulus of elasticity of FRP bars compared to steel reinforcing bars by increasing the crack width at the same stress level as given in Eq. (2–10).

Based on the formula developed by Frosch (1999) (see Eq. 2–11 of table 2–2), ACI 440.1R-06 calculates the maximum crack width of FRP reinforced concrete beams, taking into account the maximum distance from the centre of the bar to the concrete

surface. Another formula (Eq. 2–12) has been proposed by Toutanji and Saffi (2000) to calculate the maximum crack width for FRP reinforced concrete beams as presented in Table 2–2. El-Gamal et al. (2009) suggested that the ACI 440.1R-06 formula (Eq. 2-13) with a k_b coefficient of 1.4 gave better predictions of the crack width for the experimental results recorded in their study.

Table 2–2: Crack widths design formulae for FRP reinforced concrete members

Author	Formula	No.
Ggergely and Lutz (1968)	$w = 11\left(\frac{E_s}{E_f}\right)\sigma_f k_b \beta \sqrt[3]{d_c \times A \times 10^{-6}}$	2–10
Frosch (1999)	$w = 2\left(\frac{\sigma_f}{E_f}\right)k_b \beta \sqrt[3]{d_c \times \left(\frac{s}{2}\right)^2}$	2–11
Toutanji and Saffi (2000)	$w = 10^{-6} \times \left(\frac{\sigma_f}{E_f}\right)\rho_f^{-0.5} f_f \times \left(\frac{h_1}{h_2}\right) \times \sqrt[3]{d_c \times A}$	2–12
ACI 440.1R-06	$w = \left(\frac{2.2}{E_f}\right)\beta f_f k_b \sqrt[3]{d_c \times A}$	2–13

Note: A= tension area per bar; d_c= concrete cover of outermost bar measured from the center of that bar; f_f = tensile stress in longitudinal FRP bars; w= crack width measured at the extreme beam bottom level; and β = ratio of distances to the neutral axis from the extreme beam bottom level and from the centroid of longitudinal bars. k_b equals 1.0 for FRP bars having similar bond characteristics to that of steel; a value of 1.2 is assumed if k_b is not experimentally obtained.

2.8.4 Shear Capacity in FRP RC Members

The shear resistance provided by both aggregate interlock (see Figure 2–6) and compressed concrete is smaller. Investigations on the shear capacity of flexural elements without shear reinforcement have indicated that the concrete shear strength is influenced by the stiffness of the tensile (flexural) reinforcement (Zhao et al. 1995; JSCE 1997b; Michaluk et al. 1998; Tureyen and Frosch 2002, 2003). Failure of RC elements due to shear takes place under combined stresses resulting from applied shear force and bending moment as presented in Figures (2–7).

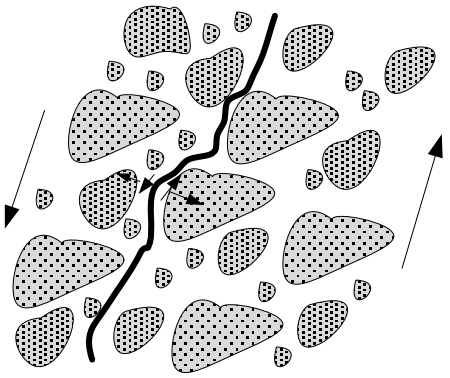

Figure 2–6: Transfer of forces across cracks due to aggregate interlock

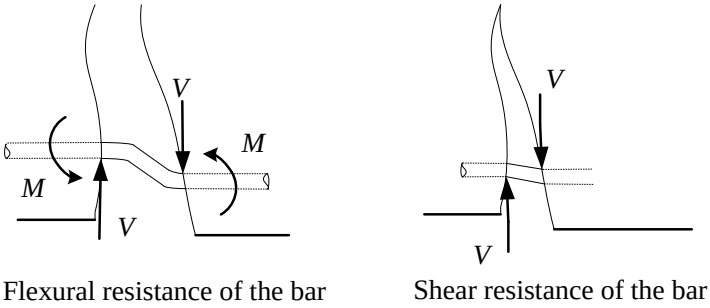

Figure 2–7: Mechanisms of flexural bars crossing a crack

Generally, the shear strength of RC members without shear reinforcement is proportional to the axial stiffness of the longitudinal reinforcing bars. As the reinforcement ratio increases, the shear strength increases accordingly (Ahmed et al., 2006). However, failure of a beam without shear reinforcement is sudden and brittle. Therefore, a minimum amount of shear reinforcement is required when the factored shear force, V_f, exceeds 0.5Vc. This reinforcement is not necessary for slabs, footings, and beams with a total depth not greater than 300 mm (ISIS-07).

Several researchers have studied experimentally the shear behaviour of concrete members with FRP reinforcement bars. During the lately 90's, Doranovic, Pilakoutas and Waldron (1997) investigated the shear capacity of beams reinforced with steel and GFRP bars. Three different approaches to shear design were investigated by considering the stiffness, area and strength of reinforcement. It was experimentally demonstrated that shear capacity is predictable by introducing modifications to the

equations proposed by Clarke et al. (1997). However, the strength of GFRP links appears to be limited due to a number of factors. To evaluate the flexure and shear capacities of FRP reinforced concrete beams, eleven such beams were tested by Wegian and Abdalla (2005). Five of the specimens contained GFRP (Isorod) reinforcing bars, two specimens had steel bars, one specimen had CFRP (Leadline) rods and the other three slabs had CFRP reinforcing bars. In their tests, they examined the use of the ACI-440 equations developed for estimation of the shear capacity of concrete members reinforced with steel. These equations were found to significantly over-estimate the shear capacity of FRP reinforced concrete members. They further asserted that the estimation of shear capacity according to equations proposed in their study was in good agreement with their experimental data and with that of other researchers. Ashour (2006) presented a comprehensive study on the shear capacities of 12 GFRP reinforced concrete beams, all of which contained no transverse shear reinforcement. The main variables in his research were the amount of GFRP reinforcement and the beams' depth. Ashour found from the study's results that under reinforced beams failed in flexural mode due to GFRP bar rupture, whereas shear failure occurred for over reinforced beams. Ashour focused on comparisons between the shear capacity estimated from the methods of several different studies and that calculated in the proposed study. These comparisons show inconsistent agreement, but very good correlation with the ACI-440 and Michalule et al. (1998) methodologies. The method proposed by Deitz et al. 1999 provided a reasonable estimate for the shear capacity of the GFRP reinforced concrete beams. It was recommended that further research be conducted into the shear capacity of RC beams reinforced with FRP bars.

In addition, Tureyen and Frosch (2003) and Yost et al. (2001) confirmed that the ACI 440 method provided very conservative shear strength predictions for FRP RC members; whereas the ACI 318-99 design method provided predominantly un-conservative computations of shear strength.

According to results of experimental studies on shear behaviour (Goodspeed et al., 1990; Yost, 1994), it has been shown that the shear strength of concrete beams reinforced by FRP bars is significantly lower than the shear strength calculated using formulae developed for steel reinforced concrete beams.

In recent years, Ilker (2011) studied the prediction of shear strength for FRP reinforced concrete beams without shear reinforcement. It was found that shear provisions of ACI 440 are strongly conservative in predicting the shear strength of FRP reinforced concrete beams as shown in Figure 2–8. Furthermore, all other shear design codes (CSA S806-02, 2002; ISIS Canada-01, 2001; JSCE-97, 1997) give conservative results.

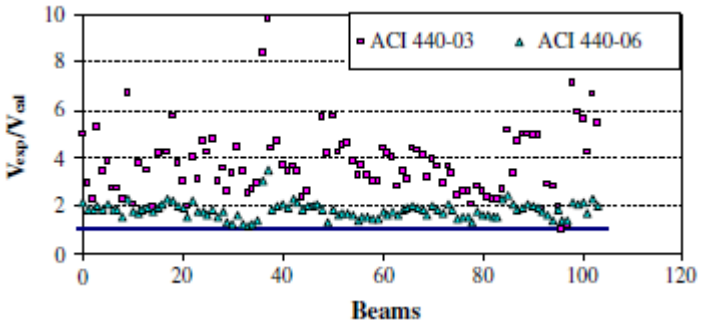

Figure 2–8: Performance of ACI 440 equations in calculating shear capacity of FRP reinforced concrete beams without stirrups (Ilker, 2011)

In another study conducted by Niwa et al. (1997), the effect of size of the FRP reinforced concrete beams without shear reinforcement was investigated. They reported that the shear strength of concrete beams reinforced with FRP rebars decreases with a decrease in young's modulus of the FRP rods. However, the

tendency of the size effect is similar regardless of young's modulus. Alkhardaji et al. (2001) carried out an experimental investigation to examine the shear performance of GFRP RC beams. One of the main conclusions of this study was that the contribution of concrete to the internal shear resistance is influenced by the reinforcement ratio. However, in agreement with many other experimental studies, El-Sayed et al. (2006) observed that the shear strength of concrete beams increases with an increase in the amount of reinforcement. The behaviour and shear strength of slender concrete beams reinforced with FRP bars were also investigated by Ahmed et al. (2006). The authors tested a total of nine (large-scale) reinforced concrete beams without stirrups, subjected to four-point bending. The test variables under investigation were the reinforcement ratio and the modulus of elasticity of the longitudinal reinforcing bars. From the experimental results, the authors found that the shear strength of reinforced concrete beams without stirrups is proportional to the axial stiffness of the longitudinal reinforcing bars. In the same study they reported that the ratio of shear strength of concrete beams flexurally reinforced with FRP bars to that of beams reinforced with steel bars $\left(\frac{V_{c,f}}{V_c}\right)$ is not directly proportional to the ratio of axial stiffness between FRP and steel reinforcing bars. However, Ehab et al. (2010) investigated the shear strength of concrete beams reinforced with GFRP stirrups. They tested an ensemble of four large-scale RC beams with a total length of 7000 mm and a T-shaped cross-section. The test variables examined were reinforcement type and the ratio of shear reinforcement (stirrups). Their results showed that the presence of GFRP stirrups in the beam specimens, similar to steel stirrups, enhances the concrete contribution after the formation of the first shear crack. At shear failure, the inclination angle of the shear crack in concrete beams reinforced with GFRP stirrups was in good agreement with the traditional 45° degree

truss model. Tureyen and Frosch (2002) investigated the shear behaviour of concrete beams reinforced with FRP bars without shear reinforcement. They used in their study two types of glass FRP and one type of aramid FRP along with two types of steel reinforcement with varying yield strengths. They found that flexural concrete members reinforced in the longitudinal direction with FRP bars can fail at shear at loads considerably lower than those reinforced by an equivalent area of steel bars. Experimental studies by other researcher (Yost et al., 2001) indicate that the amount of longitudinal reinforcement has no significant influence on the shear capacity of beams reinforced with GFRP rebar for the reinforcement ratios tested.

Table 2–3: Shear design equations for FRP reinforced concrete members without shear reinforcement.

Model	Equation	Committee	No.
ACI 318-1999	$V_{c,f}=\left(0.16\sqrt{f_c'}+17.2\rho\frac{V_u d}{M_u}\right)bd$	$V_{c,f}\le 0.29\sqrt{f_c'}\,bd$	2–14
ACI 440-03	$V_{c,f}=\frac{\rho_f E_f}{90\beta_1 f_c'}V_c$	$V_{c,f}\le V_c,\ V_c=b_w d\sqrt{f_c'}$	2–15
ACI 440-06	$V_{c,f}=\frac{2}{5}\sqrt{f_c'}\,b_w C$	$C=kd$ $k=\sqrt{\left(2\rho_f n_f+(\rho_f n_f)^2\right)}-\rho_f n_f$ $and\ n_f=\frac{E_f}{E_s}$	2–16
CSA S806-02	$V_{c,f}=0.035 b_w d\left(f_c'\rho_f E_f\frac{V_f d}{M_f}\right)^{1/3}$	$0.1 b_w d\sqrt{f_c'}\le V_{c,f}\ge 0.2 b_w d\sqrt{f_c'}$ $for\ d\le 300\ mm$	2–17
ISIS Canada-01	$V_{c,f}=0.2 b_w d\sqrt{f_c'\frac{E_f}{E_s}}$	$for\ d\le 300\ mm$	2–18

Note: f_c' = compressive strength of concrete, b_w and d = beam's width and effective width, respectively, ρ_f = longitudinal reinforcement ratio; E_c, E_s and E_f = modulus of elasticity of concrete, steel and FRP longitudinal bars, respectively; M_f and V_f = moment and shear force at critical section, respectively.

2.9 Analytical investigations on FRP reinforced concrete members

Alsayed (1997) conducted a study on the flexural behaviour of concrete beams reinforced with FRP bars. The numerical technique developed in this study was carried out using the computer model proposed by Faza and Ganga Roa (1991), (1992). The results of the comparison made between the computed and the experimental load-deflection relationships for nine GFRP reinforced concrete beams and three similar steel reinforced concrete beams were presented. The author stated that the error in the actual service load deflection predicted by ACI model of the GFRP reinforced concrete beams is approximately 70%, while that predicted by the modified model is in error by less than 15%. The researcher recommended that the developed computer model can be extended by using other types of FRP materials for proposed modifications.

Gravina and Smith (2008) conducted a theoretical study on the flexural behaviour of two-span concrete beams reinforced with fibre reinforced polymer (FRP) bars using a local deformation model developed by the authors. Their model is applied simultaneously to regions of high moment in a continuous beam to predict the bending moment distribution, crack spacing, flexural cracks and crack width. In order to model local deformations, the bond-slip relation between the FRP reinforcing bars and concrete for various types of FRP bars are considered. They pointed out that the analytical procedure can be used to investigate the influence different bar bond properties have no ductility and moment distribution. The authors also concluded that further studies are required to investigate the range of parameters that influence the flexural behaviour of continuous reinforced concrete with FRP bars.

2.10 Experimental investigations on FRP reinforced continuous members

Several studies investigated the flexural behaviour of simply supported beams and one way concrete slabs reinforced with different types of FRP reinforcing bars (Benmokrane et al., 1995, 1996; Almusallam 1997; Benmokrane et al., 1998; Grace et al., 1998; Alsayed et al., 1998, 2000; Pecce et al., 2000; Razaqpur et al., 2000; Toutanji and Saffi, 2000; Vijay and GrangaRao, 2001; Abdalla, 2002; Yost and Gross, 2002; Yost et al., 2003; Rashed et al., 2004; Benmokrane, 2004; El-salakawy and Benmokrane, 2004; Bischoff 2007). To date, unlike simply supported members, relatively few studies have experimentally examined the flexural behaviour of continuously supported FRP reinforced concrete beams (Tezuka et al., 1995; Grace et al., 1998; Razaqpur and Mostofinejad, 1999; Habeeb and Ashour, 2008; Ashour and Habeeb, 2008; El-Mogy et al., 2010).

Tezuka et al. (1995) studied the moment distribution of two-span concrete beams, either reinforced or pretensioned with FRP longitudinal bars or steel wires. AFRP, CFRP and conventional steel wires were used in this study. They concluded that a moment-curvature relationship can be accurately predicted using a very simple non-linear analysis, taking into consideration the non-linearity of the materials used. It was observed that the curvatures tended to be higher in the analytical data than in the experimental data for the same applied moment. It was also found that experimental findings of the moment-curvature relationship obtained at the central support indicated that the slope of the curve hardly changed up until failure.

Moreover, Grace et al. (1998) tested seven two-span concrete T-beams reinforced with different arrangements of longitudinal and shear reinforcements formed of CFRP, GFRP and steel bars. The main aim of the research was to investigate the behaviour and ductility of simply and continuously supported FRP reinforced

concrete beams. Their work concluded that beams with different FRP combinations showed the same load capacity as beams reinforced with steel but that the failure modes and ductility were different. Moreover, FRP continuous beams exhibited higher deflections when compared to the steel reinforced beams.

Likewise, Razaqpur and Mostofinejad (1999) presented experimental results for four continuously supported CFRP reinforced concrete beams with steel stirrups or a CFRP grid as shear reinforcement. The main studied parameters in this work were the shear reinforcement material and the reinforcement ratio. The study concluded that continuous FRP reinforced concrete beams with an over-reinforcement ratio demonstrated a semi-ductile behaviour. This was exhibited in the experimental results of the tested beams, which did not collapse when the load corresponding to the flexural capacity of the middle support region was reached. It was also observed that the presence of a CFRP grid in the specimens tested had a similar performance to the steel stirrups. Furthermore, Ashour and Habeeb (2008), and Habeeb and Ashour (2008) introduced experimental results of four simply and six continuously supported concrete beams with different types (CFRP or GFRP) and ratios of FRP bars. The main variable studied in this investigation was the amount of FRP reinforcement. They concluded that the continuous FRP reinforced concrete beams developed earlier and wider cracks when compared with their counterpart steel reinforced concrete slabs. It should also be noticed that continuously supported FRP reinforced concrete beams did not demonstrate any significant load redistribution. The study also indicated that ACI 440 1R–06 equations can reasonably predict load capacity and deflection of simply supported FRP beams, but progressively underestimate deflections of continuously supported FRP reinforced concrete beams after the first cracking.

Recently, El-Mogy et al (2010) presented the experimental results of seven GFRP and two CFRP reinforced concrete continuous beams. The main objective of this research was to investigate the range of moment redistribution that can be achieved by CFRP and GFRP reinforced continuous beams and the flexural behaviour with different arrangements. The experimental results were compared to FRP code equations and available design models. This comparison showed that the Canadian Standards Association Code (CSA-02) could reasonably predict the failure load of the tested beams. It was also observed that increasing the GFRP reinforcement at mid-span sections had a more positive effect on reducing mid-span deflections and improving load capacity, than over the middle support regions, consistent with the findings reported by Habeeb and Ashour (2008).

In another different study, Mohamed (2011) presented research about the behavior of cantilever concrete beams reinforced with glass fiber reinforced polymers (GFRP) bars. The experimental program consists of testing six cantilever concrete beams. The tested beams were classified into three groups. They had cross section dimensions of 150 × 250 mm and 2000 mm total length. It was observed that steel reinforced cantilever beams generally recorded higher experimental ultimate loads than the corresponding GFRP reinforced cantilever beams. A summary of works carried out on the experimental investigations of FRP continuous members is given in Table 2–4.

Table 2–4: Selected flexural behaviour tests on FRP continuous members

Reference	FRP Material	Variables Studied	Objectives
Tezuka et al. (1995)	AFRP & CFRP	• Material	To investigate the moment distribution of FRP two-span concrete beams
Grace et al. (1998)	GFRP & CFRP	• Reinforcement Ratio • Material	To study the behaviour and ductility of FRP continuous concrete beams
Razaqpur and Mostofinejad (1999)	CFRP	• Reinforcement Ratio	To investigate the use of CFRP grid as shear reinforcement for continuous concrete beams
Ashour and Habeeb (2008)	CFRP	• Reinforcement Ratio	To study the use of CFRP bars as longitudinal reinforcement for continuous concrete beams
Habeeb and Ashour (2008)	GFRP	• Reinforcement Ratio	To investigate the application of GFRP bars as longitudinal reinforcement for continuous concrete beams
El-Mogy et al. (2010)	GFRP & CFRP	• Material • Reinforcement Ratio	Ability of FRP materials to redistribute loads and moments in continuous beams
Mohamed (2011)	GFRP & Steel	• Ratio of GFRP bars • Type of bars • Strength of concrete	to investigate the behavior of concrete cantilever beams when using locally produced GFRP bars

2.11 Concluding Remarks

Based on the results of previous research described in this chapter, the following conclusions can be drawn:

- Previous studies show that the behaviour and structural performance of FRP reinforced concrete members is typically significantly different to those of steel reinforced members.
- Plastic behaviour (yielding) in the reinforcement bars of the steel reinforced beams led to a large increase in deflection with little change in load, whereas the FRP reinforced beams do not show any plastic behaviour. For this reason, FRP reinforcement should be avoided in places where moment redistribution is required, for example in moment frames.
- Based on the previous studies, existing approaches to estimate deflection, moment capacity and shear strength of FRP reinforced concrete members appear in general to give scattered results in comparison with experimental data.
- It can be seen that the bond strengths achieved by FRP bars can be distinctly lower than those provided by steel reinforcing bars. On the other hand, the bond failure mode of a member depends on the concrete cover, concrete compressive strength and embedment lengths within the concrete.
- Test parameters such as type of FRP materials, reinforcement configurations and different load cases, still require rational experimental studies.
- Several studies investigated the flexural and shear behaviour of simply supported beams and one-way concrete slabs reinforced with different types of FRP bars.

However, very limited experimental investigations have been conducted regarding the flexural behaviour of continuously supported FRP reinforced concrete beams.

2.12 Topics for Further Research

The main aspects of structural behaviour that would still benefit from further research are summarised as follows:

- There would appear to be a lack of computational research on the analysis of continuous members reinforced with FRP rebars.
- Simply and continuously supported FRP reinforced concrete beams have been investigated extensively in experimental researches. On the contrary, there seems to be no systematic research for the flexural behaviour of FRP continuous slabs.
- There is a need to carry out experimental studies on the effect of different parameters of behaviour performance of FRP continuous slabs as it has been carried out before on FRP simple slabs.
- There is no evidence of investigations to compare between the results data of existing FRP codes and experimental results of continuously supported FRP RC slabs.

In this thesis, the research done is devoted to investigate the above mentioned topics.

CHAPTER THREE

EXPERIMENTAL INVESTIGATION OF BFRP CONCRETE SLABS

3.1 Introduction

This chapter describes the main experimental program, which was developed to investigate the behaviour of BFRP reinforced concrete continuous slabs. A series of four continuously and two simply supported concrete slabs reinforced with BFRP bars were tested. Additionally, one continuously supported steel reinforced concrete slabs were also tested for comparison purposes. In particular, the main parameters investigated in the testing of slabs were the different combinations and type of reinforcement of the BFRP reinforcing bars used in this study. The results of these slabs are presented in this chapter. Furthermore, the experimental results including the deflection and ultimate load would be used in chapter five and six for validation purposes.

3.2 Test Specimens

Two simply and four continuously supported BFRP reinforced concrete slabs were tested in flexure. In addition, a continuously supported slab reinforced with conventional steel rebars was also tested as a reference slab. All slabs tested were 500 mm in width and 150 mm in depth. The simply supported slabs had a span of 2000 mm as shown in Figure 3-1, while the continuous slabs comprised of two equal spans, each of 2000 mm, as shown in Figure 3-2. A concrete cover of 25 mm thickness was kept constant for all reinforcement.

The BFRP reinforcing bars were selected to investigate two modes of flexural failure, namely BFRP reinforcement rupture and concrete crushing. The first mode is achieved by using a reinforcement ratio ρ_f less than the balanced reinforcement ratio ρ_{fb} according to the ACI 440.1R-06 guidelines, whereas the second mode by using a reinforcement ratio higher than ρ_{fb} as presented in Table 3-1. The reinforcement ratio, ρ_f and balanced reinforcement ratio, ρ_{fb} can be respectively, determined from Eqs. (3–1) and (3–2) below, as defined in the ACI 440.1R-06 guidelines:

$$\rho_f = \frac{A_f}{bd} \tag{3–1}$$

$$\rho_{fb} = 0.85\beta_1 \frac{f'_c}{f_{fu}} \frac{E_f \varepsilon_{cu}}{E_f \varepsilon_{cu} + f_{fu}} \tag{3–2}$$

where A_f is the area of FRP reinforcing bars, f'_c is the cylinder concrete compressive strength (MPa), b is the width of the slab section (mm), d is the effective depth of the slab section (mm), f_{fu} is the ultimate tensile strength of FRP bars (MPa), ε_{cu} is the ultimate concrete strain, E_f is the modulus of elasticity of FRP bars (MPa) and β_1 is the strength reduction factor, which can be determined based on the ACI 440.1R-06 equation (3–3) in SI units, as given below:

$$\beta_1 = 0.85 - 0.05\left(\frac{f'_c - 27.6}{6.7}\right) \tag{3–3}$$

The position and number of reinforcing bars were the main parameters investigated, as summarised in Table 3–1 and Figures 3–1 and 3–2. The BFRP reinforced concrete continuous slabs were reinforced with three different reinforcement combinations at the top and bottom layers. The slab C–B–UO was reinforced with three BFRP longitudinal bars of 8 mm diameter (under reinforcement) on the bottom side and five 10 mm diameter BFRP bars (over reinforcement) on the top side, whereas slab C–B–OU was

reinforced with an opposite arrangement of BFRP. On the other hand, the bottom reinforcement of slabs C–B–UU and C–B–OO was the same as the top reinforcement; three BFRP bars of 8 mm diameter (under reinforcement) and five BFRP bars of 10 mm diameter (over reinforcement) were used in C–B–UU and C–B–OO slabs, respectively. The simply supported slabs, S–B–O and S-B-U, were reinforced with five BFRP bars of 10mm diameter (over reinforced) and three BFRP bars of 8mm diameter (under reinforced), respectively, on the bottom side. Slab C–S–UU was reinforced with four steel bars of 10 mm-diameter (under reinforced) on both the bottom and top sides to achieve a typical ductile failure mode by yielding of steel reinforcement first, followed by concrete crushing. The amount of steel in slab C–S–UU was selected to have similar strength to that used in slab C–B–UU. In all slabs, top reinforcing bars were curtailed beyond the mid-span point load, whereas bottom bars continued throughout the slab length as shown in Figures 3–1 and 3–2.

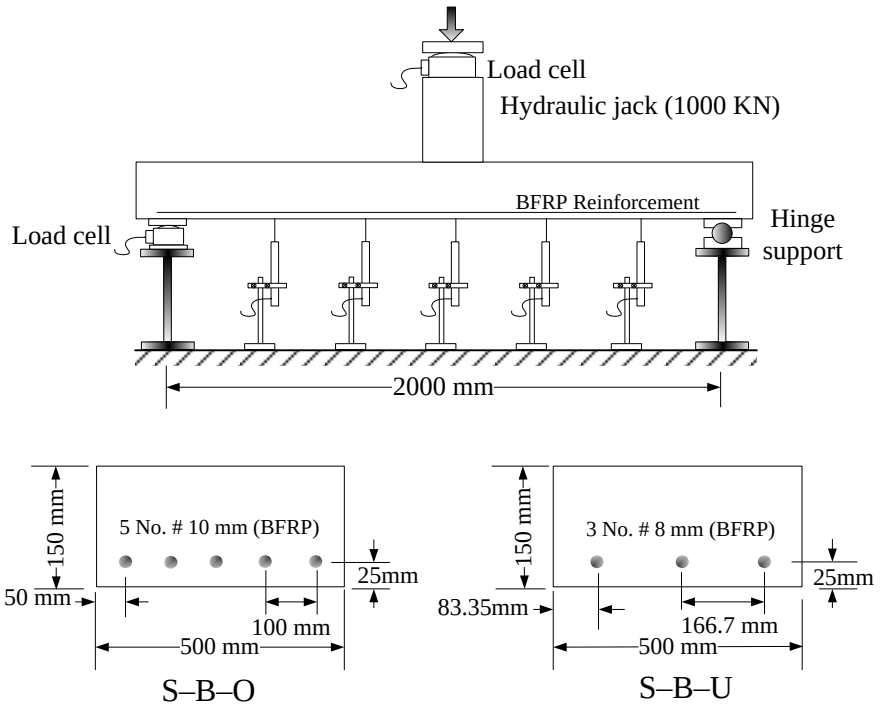

Figure 3–1: Experimental setup and details of BFRP simple slabs

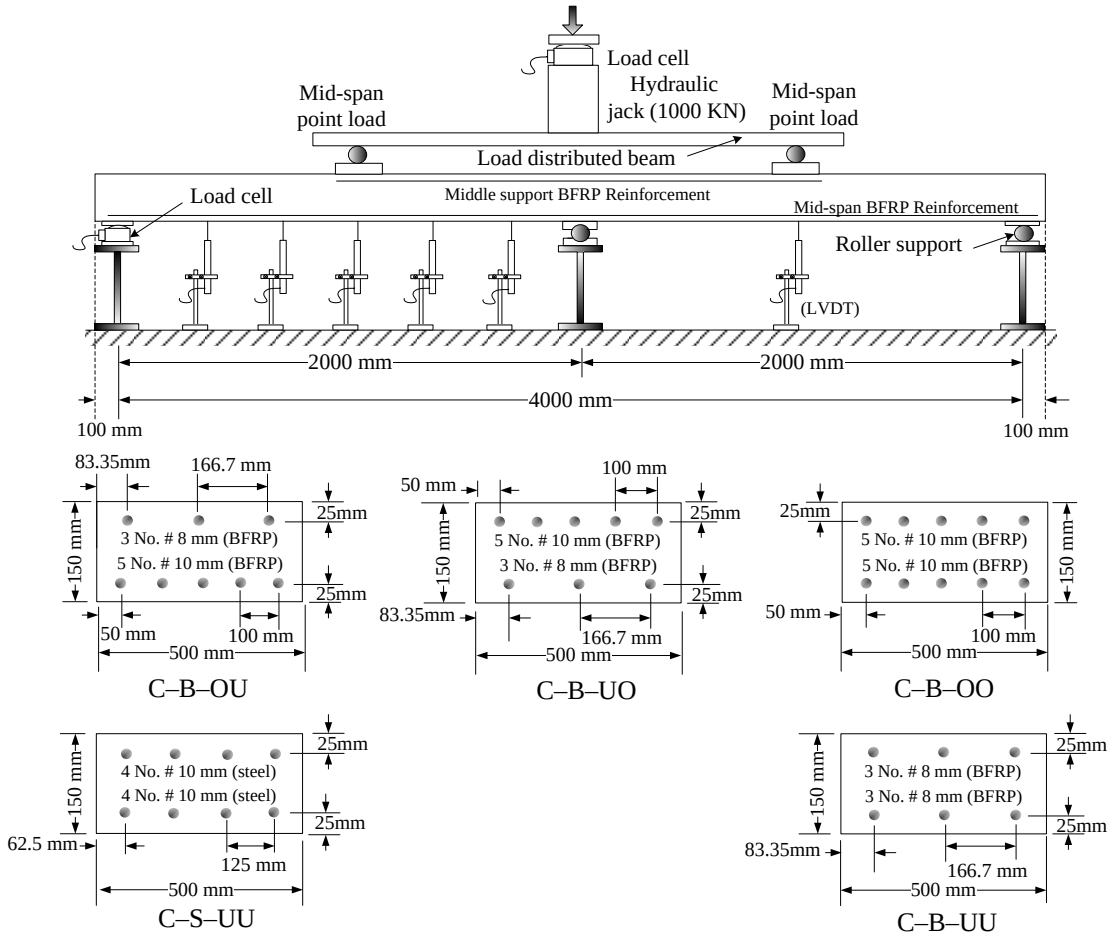

Figure 3–2: Experimental setup and details of BFRP continuous slabs

3.3 Materials Properties

3.3.1 Concrete

The slabs were constructed using ready-mixed, normal weight concrete with a target compressive strength of 50 MPa at 28 days. Five 100mm cubes and three 150mm diameter×300mm high cylinders were made and tested immediately after testing of each slab to provide the average values of the cube compressive strength, f_{cu}, and splitting tensile strength, f_{ct} (see Table 3–1). Two 100×100×500 mm prisms were also tested for each group of slabs to obtain the modulus of rupture, f_r, as listed in Table 3-1. After concrete casting, all specimens were covered with polyethylene sheets to keep down moisture loss at all times during the period of curing and stored in the laboratory under the same condition until the day of testing.

Table 3–1: Designation of slabs and characteristics of longitudinal reinforcement and concrete

Slab notation	Longitudinal reinforcing bars								Concrete properties	
	Bottom bars at mid-span				Top bars at central support					
	No.	Bar Diameter: mm	ρ_f%	$\frac{\rho_f}{\rho_{fb}}$	No.	Bar Diameter: mm	ρ_f%	$\frac{\rho_f}{\rho_{fb}}$	f_{cu}: MPa	f_{ct}: MPa
C–B–OU	5 BFRP	10	0.63	2.52	3 BFRP	8	0.24	0.82	53.7	4.3
C–B–UO	3 BFRP	8	0.24	0.82	5 BFRP	10	0.63	2.52	56.2	4.4
C–B–OO	5 BFRP	10	0.63	2.52	5 BFRP	10	0.63	2.52	52.5	4.1
C–B–UU	3 BFRP	8	0.24	0.82	3 BFRP	8	0.24	0.82	53.7	4.2
S–B–O	5 BFRP	10	0.63	2.52	N/A	N/A	N/A	N/A	55.0	4.7
S–B–U	3 BFRP	8	0.24	0.82	N/A	N/A	N/A	N/A	51.2	4.5
C–S–UU	4 steel	10	0.50	0.22	4 steel	10	0.50	0.22	53.7	4.6

3.3.2 FRP and steel reinforcement

The Basalt and Carbon FRP bars used in this investigation are manufactured and funded by Magmetech Ltd. (UK), which are formed by the pultrusion technique. The surface of these bars is coated with a coarse silica sand to improve bond and force transfer between reinforcing bars and concrete increase bonding with the concrete matrix. The mechanical characteristics of these reinforcing bars were obtained by carrying out tensile tests on a number of specimens of each diameter. Anchorage systems have been proposed to avoid premature failure of FRP bars during tensile tests at the steel jaws of the testing machine. Referring to previous successful systems for applying tensile loading of FRP bars, it was decided to explore the system developed by researchers at West Virginia University. In this technique, the length of the two anchorages was 300 mm each based on previous research (Micelli and Nanni 2001) as shown in Figures 3–3 and 3–4. In addition, a free length of 400 mm was provided as recommended by unpublished ACI provisions. The specimens were initially prepared by embedding the ends of bar into steel pipes filled with expansive grout in vertical position by using wooden formwork (see Figures 3–5a and 3–5b). All prepared specimens were tested

using a 500 KN-capacity, universal testing machine as shown in Figure 3–6a. A tensile test machine with an extensometer attached on the backside of the sample was used for measuring the modulus of elasticity; the DIC system with a high speed camera was set in the front of the sample on a stable tripod as shown in Figure 3–6b. The mechanical and design properties of the BFRP and steel bars are provided in Table 3–2.

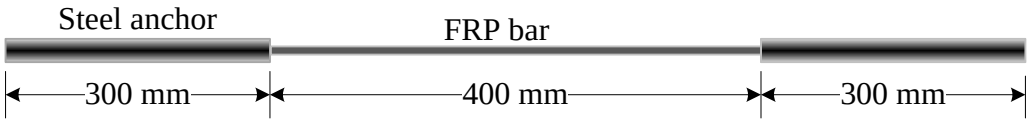

Figure 3–3: Longitudinal details of tested Specimen

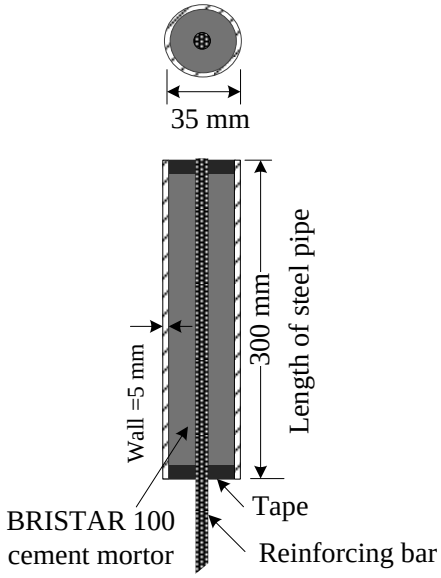

Figure 3–4: Cross-sectional details of the anchorage

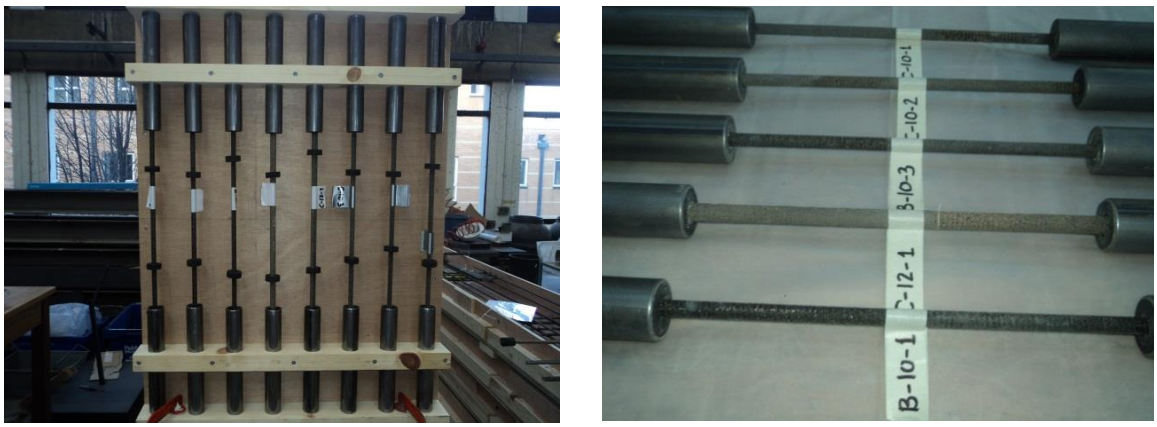

(a) before casting (b) After construction

Figure 3–5: Specimens of FRP bars before and after filling with adhesives

(a) Universal testing machine

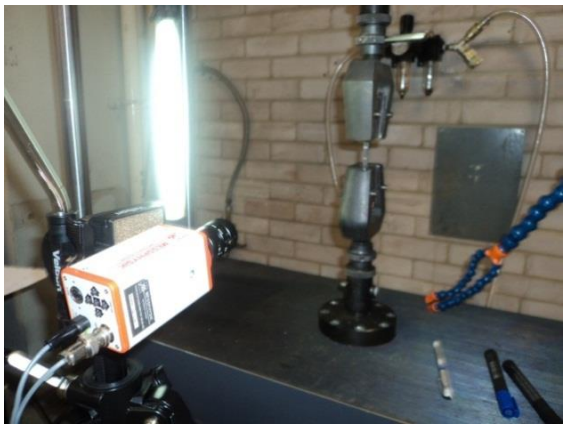

(b) Digital image correlation (DIC)

Figure 3–6: Arrangement of tensile-test specimen

Table 3–2: Mechanical Properties of FRP and Steel Reinforcing Bars

Type of bars	Bar diameter: mm	Modulus of elasticity: Gpa	Tensile strength: MPa	Ultimate strain	Yield strength: MPa
BFRP	8	50	1250	0.025	N/A
BFRP	10	50	1350	0.027	N/A
Steel	10	200	645	0.003	575

3.4 Slabs Notations

The slab notation was defined according to the type of reinforcement, support system and amount of reinforcement. The first letter in the notation indicates the type of supporting system, ‘C’ for continuously supported slabs and ‘S’ for simply supported slabs. The second letter corresponds to the type of reinforcement, either ’B’ or ‘S’ for BFRP and steel reinforcement, respectively. The third letter reflects the reinforcement ratio on the bottom mid-span region of the simply or continuously supported slab, ‘U’ for under-reinforcement or ‘O’ for over-reinforcement ratio. The last letter, ‘U’ or ‘O’, is used only for the continuously supported slabs, illustrating the over middle-support reinforcement ratio. For example, the slab notation C–B–UO indicates a continuously supported slab reinforced with BFRP bars having under and over reinforcement ratios of BFRP bars at the mid-span and over middle-support regions, respectively.

3.5 Test Preparations

Plywood forms were carried out to accommodate the required reinforcement cages as shown in Figure 3–7a. The reinforcement cages were placed inside the forms after cleaning and brushing all internal sides with oil to simplify their removal after casting of the concrete. The reinforcement cage rested on transverse rods to maintain a 25-mm clear concrete cover. Each of four slabs was cast on the day, together with several cubes, cylinders and prisms to determine the concrete characteristics. During casting, the concrete was vibrated using electrical vibrator and the surface of the concrete was levelled (see Figure 3–7b). In the same environmental conditions, the slabs were stored and covered with a plastic sheet the first days. Before testing, each slab was painted white in order to trace the crack patterns during testing.

a) Reinforcement cages in forms b) Test specimens after casting

Figure 3–7: Construction stages of test specimens

3.6 Test Setup and Instrumentations for Tested Slabs

Figures 3–1 and 3–2 above show the experimental setup of the simply and continuously supported slabs tested, respectively. Each span of the continuous slabs was loaded at its mid-point and supported on two end rollers and a middle hinge support. Each slab was instrumented with two load cells to measure the reactions at one end support and the main applied load from the hydraulic ram. Moreover, deflections at the two mid-spans

of continuously supported slabs and the mid-span of simple slabs were measured using linear variable differential transducer (LVDTs). Additional four LVDTs were located at equal spacing of *L*/6 on one span of the continuous slabs and along the simple slab span to measure the deflections at these locations, where *L* is the span length. Two additional LVDTs were installed at the end and middle supports of continuous slabs to measure any movement at supports. Load cell and LVDT readings were automatically registered at each load increment using a data logger.

3.7 Test Results and Discussion

3.7.1 Crack propagation and failure modes for BFRP slabs

The first visible cracking load of all slabs tested is presented in Table 3–3. The steel reinforced concrete slab exhibited a higher first cracking load than slabs reinforced with BFRP owing to the higher axial stiffness of steel bars than that of BFRP bars. The amount of BFRP reinforcement at different locations for each slab tested has also affected the first cracking load; for example slabs C–B–OU and C–B–UO experienced the first crack at the lower reinforcement location.

Figure 3–8 sketches the cracks occurred in the continuous slabs tested. Slabs C–B–UU and C–B–UO had deeper cracks at the mid-span region than the rest of the slabs as they were under reinforced at the mid-span region. In general, the crack spacing and crack depth for all slabs reinforced with BFRP bars were clearly larger than these of the slab reinforced by steel due to the low elastic modulus of BFRP bars in comparison with steel bars.

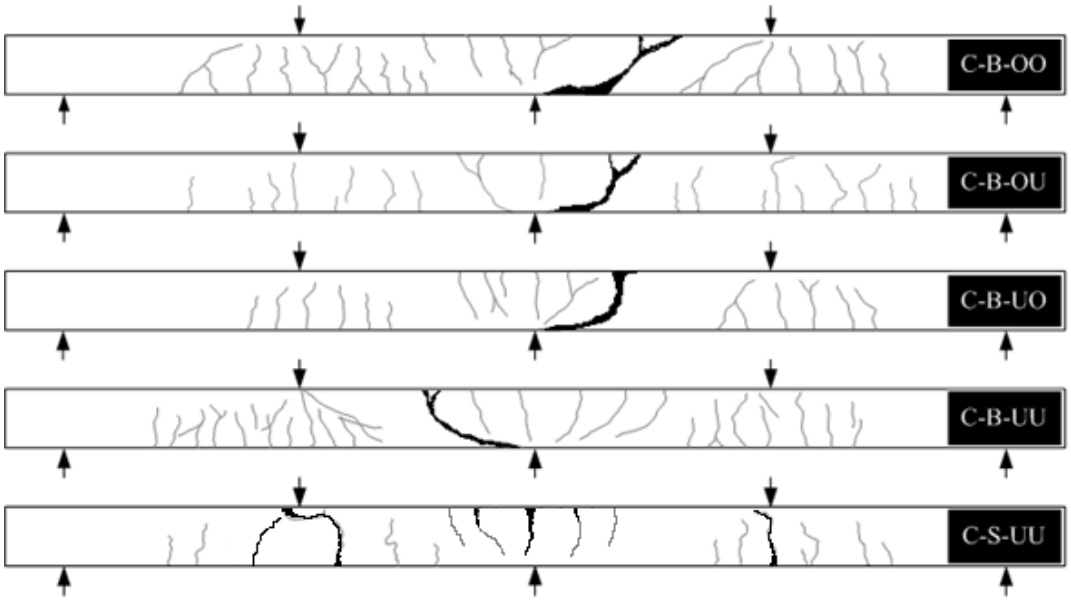

Figure 3–8: Crack patterns at failure of BFRP reinforced concrete continuous slabs

Table 3–3: First cracking and total experimental failure loads of slabs tested

Slab Notation	First cracking loads, P_{cr}: kN		Total experimental failure load, 2*P*: kN	Observed failure mode
	sagging	*hogging*		
C–B–OO	15.4	18.5	195.0	Flexure-shear failure at middle support
C–B–OU	17.5	13.9	140.0	Flexure-shear failure at middle support
C–B–UO	16.5	18.4	130.0	Flexure-shear failure at middle support
C–B–UU	18.6	14.4	128.0	Flexure-shear failure at middle support
S–B–O	16.2	N/A	84.8[a]	Flexure-shear failure at end support
S–B–U	12.7	N/A	42.0[a]	BFRP bar rupture at mid-span
C–S–UU	22.6	22.6	144.0	Flexural-Tension Failure at both mid-span and middle support

[a]Just *P* for the simply supported slabs

Figures 3–9 and 3–10 illustrate the main crack width at both mid-span and middle support regions for all slabs tested, respectively. The control slab C–S–UU had considerably less crack width at both mid-span and middle support regions among all slabs tested due to the higher axial stiffness of steel reinforcement than that of BFRP reinforcement. For the BFRP continuous slabs, wider cracks at the mid-span region were observed in slabs C-B-UU and C–B–UO with under reinforcement ratio than the over reinforced BFRP slabs, C–B–OO and C–B–OU, at their mid-span regions. It was not expected that slab C–B–UU had less crack width at middle support region than slab

C–B–OU. This may be as a result of local de-bonding between top BFRP bars and concrete.

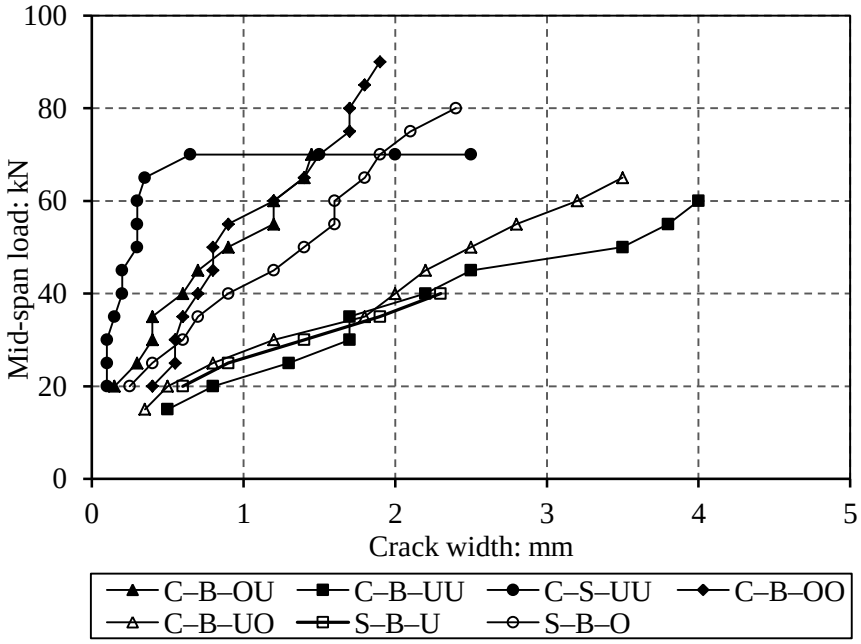

Figure 3–9: Total applied load versus crack width at mid-span of all slabs tested

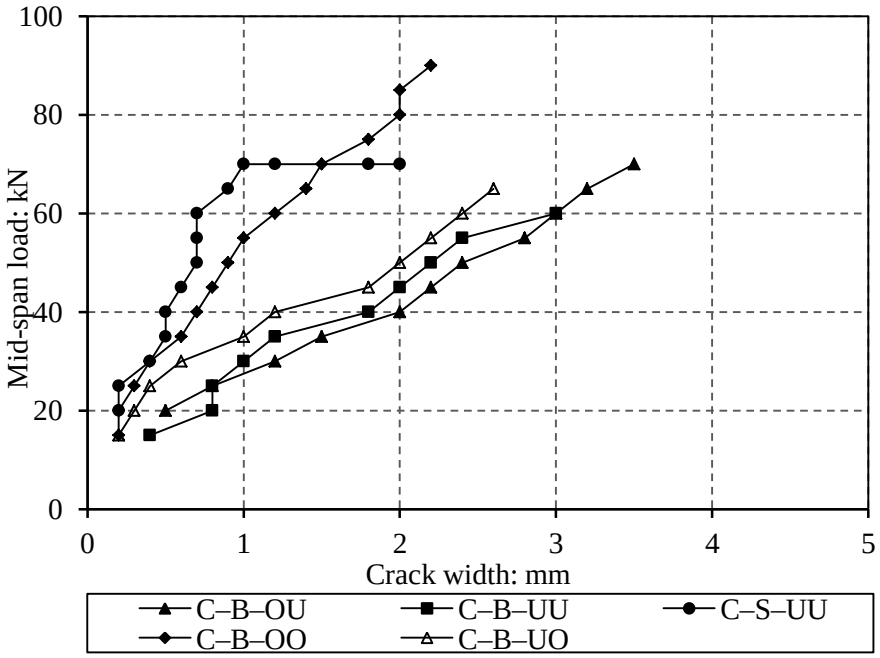

Figure 3–10: Total applied load versus crack width at middle support of continuous slabs tested

Three different failure modes were observed in the experimental tests as shown in Figures 3–11 to 3–18, and summarised in Table 3–3 and explained below:

Mode 1: Combined flexural and shear failure–This type of failure was observed in BFRP slabs C–B–OO, C–B–UO, C–B–UU, C–B–OU and S–B–O. The failure initiated at the compression side of the middle support region, followed by a major, sudden diagonal shear crack at the same location for continuous slabs C–B–OO, C–B–UO, C–B–UU and C–B–OU as shown in Figures 3–11 to 3–14. However, the shear failure occurred close to the end support in case of S-B-O slab as presented in Figure 3–15. This is mainly attributed to the low modulus of elasticity of BFRP that significantly reduces the shear resistance of the BFRP slabs tested.

Figure 3–11: Compressive flexural-shear failure at middle support of slab C–B–OO

Figure 3–12: Flexure–shear failure at middle support of slab C–B–UO

Figure 3–13: Flexure–shear failure at middle support of slab C–B–UU

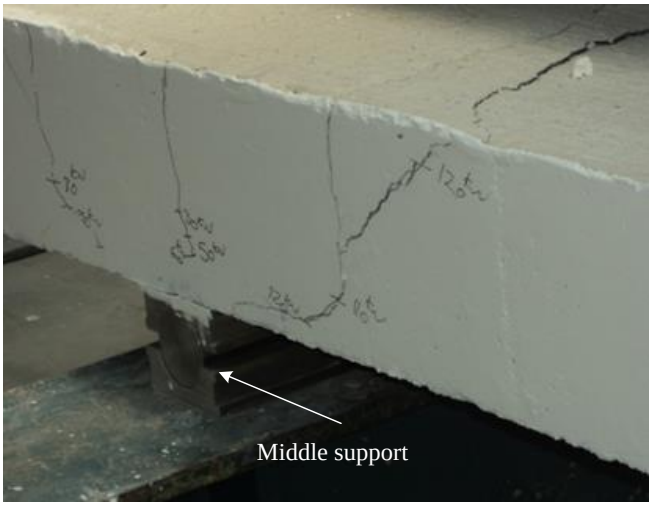

Figure 3–14: Flexure–shear failure at middle support of slab C–B–OU

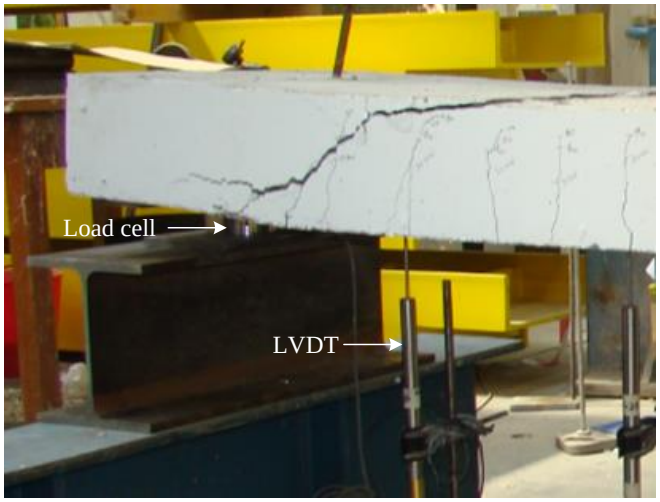

Figure 3–15: Flexure–shear failure at end support of slab S–B–O

Mode 2: Conventional ductile flexural failure–This mode occurred due to yielding of tensile steel reinforcement followed by concrete crushing at both mid-span and middle support regions for the control slab C–S–UU as shown in Figures 3–16 and 3–17. Hogging flexural failure at the central support was observed earlier than that at the slab mid-span.

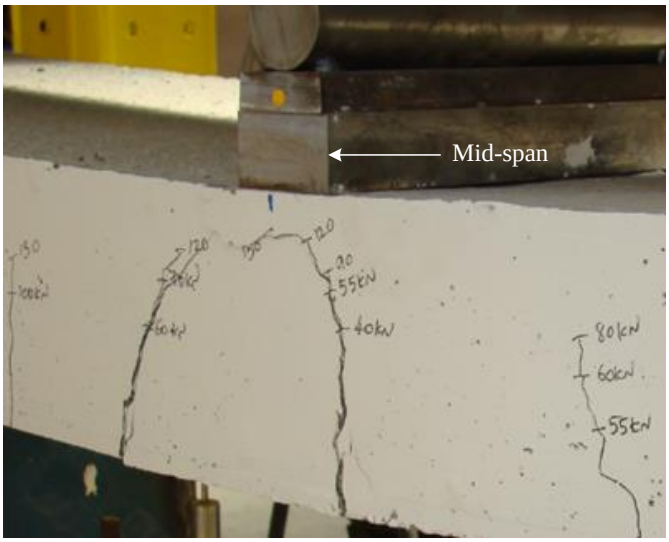

Figure 3–16 Flexural–tension failure at mid-span of slab C–S–UU

Figure 3–17: Flexural–tension failure at middle support of slab C–S–UU

Mode 3: BFRP Bar rupture–This mode was experienced by slab S–B–U, that was reinforced with an under reinforcement ratio of BFRP bars at the mid-span region as shown in Figure 3–18. It was therefore expected that the strain in BFRP reinforcement would reach its ultimate limit, at the mid-span section, before the full exhaustion of the concrete ultimate strain, which usually results in such failure mode. It should be mentioned that rupture of BFRP bars was sudden and accompanied by a loud noise indicating a rapid release of energy.

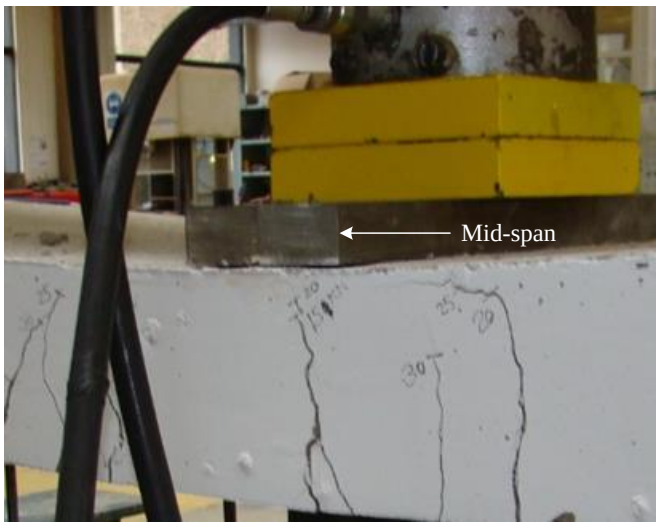

Figure 3–18: BFRP bar rupture failure at mid-span of slab S–B–U

3.7.2 Load capacity

Table 3–3 above and Figure 3–19 below present the failure loads of the BFRP slabs tested. Slab C–B–OO that was over reinforced at both mid-span and middle support regions tolerated more load than slab C–B–OU or C–B–UO that was over reinforced in only one region. The failure load of slab C–B–OU was slightly higher than that accomplished by the slab C–B–UO having an opposite reinforcement arrangement. Despite the fact that the reinforcement ratio in slab C–B–UO was around 2.6 times that in slab C–B–UU at middle support, slab C–B–UO accomplished a failure load similar to that of slab C–B–UU as they failed in combined shear and flexure. The load capacities

of BFRP reinforced concrete continuous slabs C–B–UU and C–B–UO were around 3.2 times that of BFRP reinforced concrete simple slab S–B–U. However, it can be seen that the load capacities of slabs C–B–OO and C–B–OU were about 2.30 and 1.65 times that achieved by the simple BFRP reinforced concrete slab S–B–O. Although slab C–S–UU was reinforced with an under reinforcement ratio of steel bars having similar strength to that used in slab C–B–UU, it exhibited a higher load capacity than that of slabs C–B–UU and C–B–UO but nearly similar load capacity to that of slab C–B–OU.

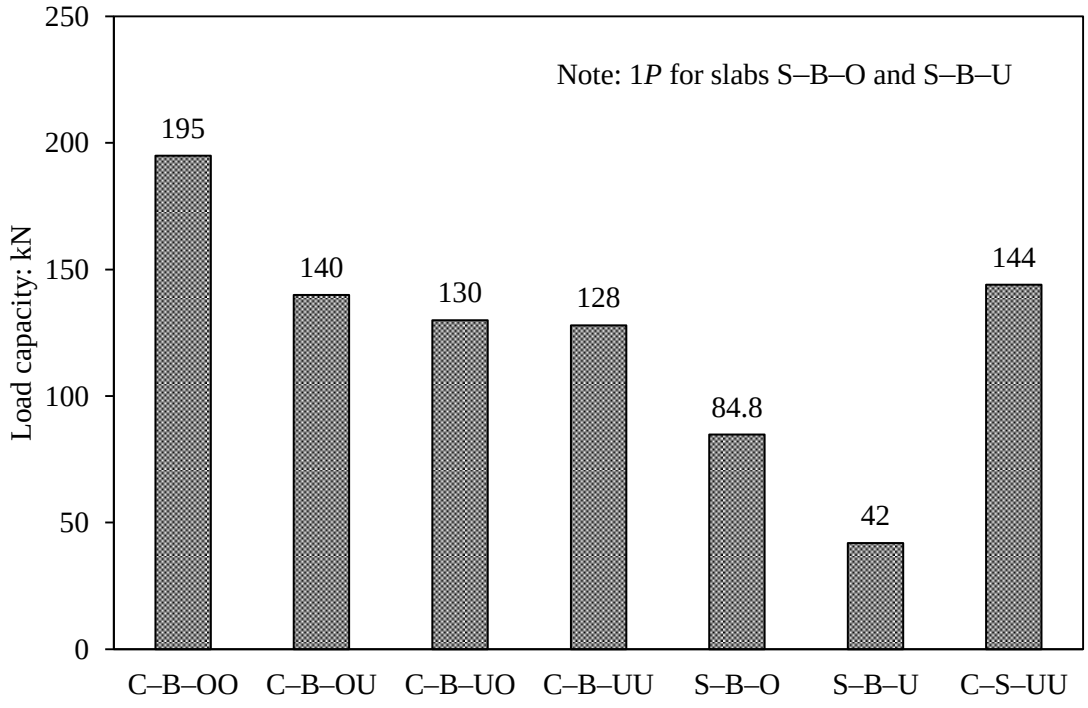

Figure 3–19: Experimental load capacities of slabs tested

3.7.3 Redistribution of load and bending moment for BFRP Slabs

Figure 3–20 presents the measured end support reaction versus the total applied load for each continuous slab tested. The end support reaction obtained from an elastic analysis, assuming uniform flexure stiffness '*EI*' along the span of slabs, is also plotted in Figure 3–20 to assess the amount of load redistribution. At the initial stages of loading before concrete cracking, the measured end support reaction of continuous slabs tested was

very close to these obtained from the elastic analysis owing to the linear elastic characteristics of concrete, BFRP bars and steel bars before reaching the cracking load. For slab C–B–OU, the end support reaction was slightly larger than the elastic reaction, indicating signs of load distribution from the middle support region to the mid-span region due to the higher stiffness at mid-span region and cracks over the middle support. On the other hand, slab C–B–UO demonstrated opposite redistribution to slab C–B–OU due to the reverse reinforcement configuration. Other continuous slab reactions were very close to that from elastic analysis as depicted in Figure 3–20.

Figures 3–21 to 3–24 show the experimental and elastic bending moment distributions at failure along the BFRP continuous slab span. The predicted moment capacities at both mid-span and over support sections calculated from the ACI 440.1R–06 are also presented in Figures 3–21 to 3–24. The amount of moment redistribution, β, can be calculated by comparing the experimental and elastic bending moments and given by:

$$\beta = \left(\frac{M_m - M_e}{M_e}\right) \times 100\% \tag{3-4}$$

where M_m is the bending moment obtained from experiments using the measured end support reaction and mid-span load and M_e is the bending moment calculated from elastic analysis at failure load. The amounts of moment redistribution, β, for the mid-span and over support sections are calculated from Eq. (9) and given in Figures 15 to 18.

Figures 3–21 to 3–24 indicate that the experimental bending moment distribution is different from that obtained from linear elastic analysis at failure load for many slabs. The value of β at the middle support sections is always larger than that of mid-span sections for all BFRP continuous slabs tested. Redistribution of moment from the middle support section to the mid-span section occurred in C–B–OO, C–B–UU and C–

B–OU slabs. However, redistribution of moment from the mid-span section took place in only C-B-UO slab. Slab C–B–OU exhibited the largest moment redistribution at mid-span (25%) and over middle support (41%). In all slabs but C–B–UU at mid-span section, neither the middle support nor mid-span section reached the corresponding predicted moment capacity as depicted in Figures 3–21 to 3–24. This indicates that the moment redistribution occurred is likely to be attributed to cracks, variation of flexural stiffness along the slab or slight debonding of BFRP reinforcement from concrete.

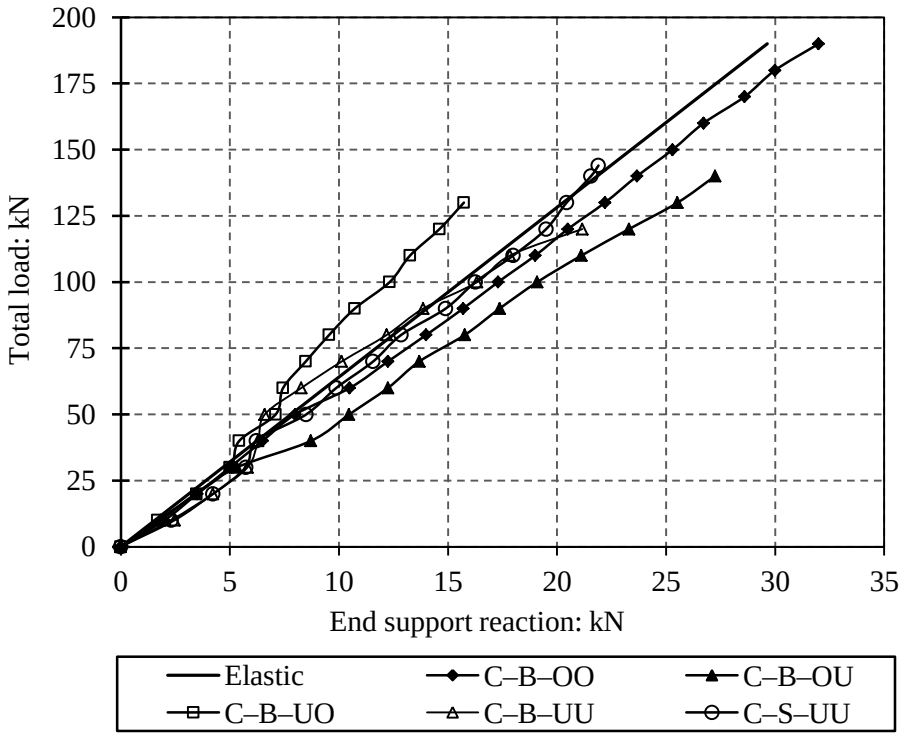

Figure 3-20: Total applied load versus end support reaction of continuous slabs tested

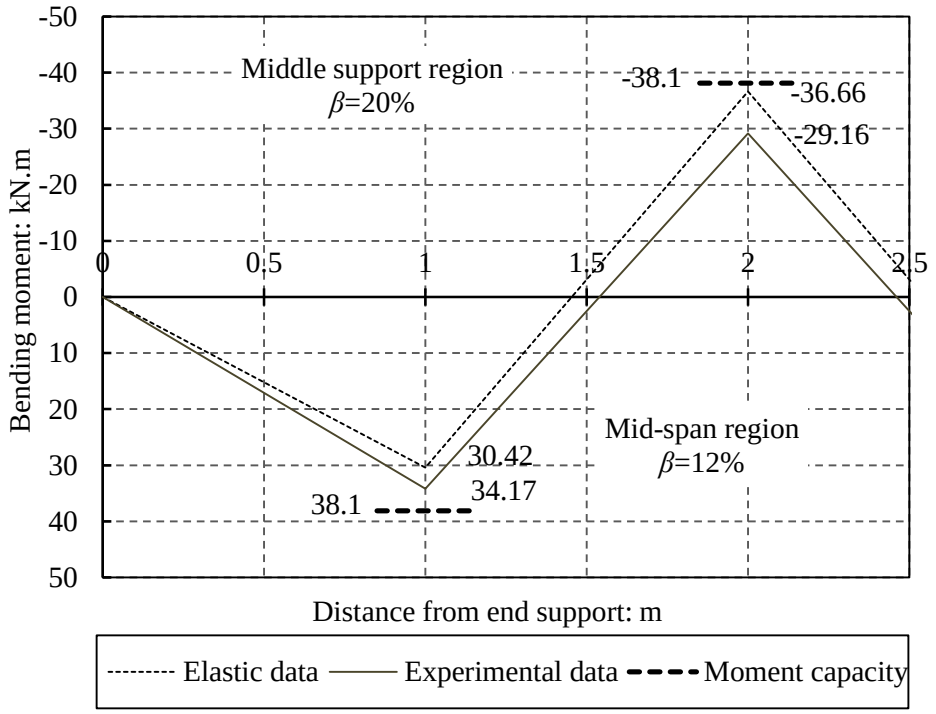

Figure 3-21: Elastic and experimental bending moments relations at failure for slab C–B–OO

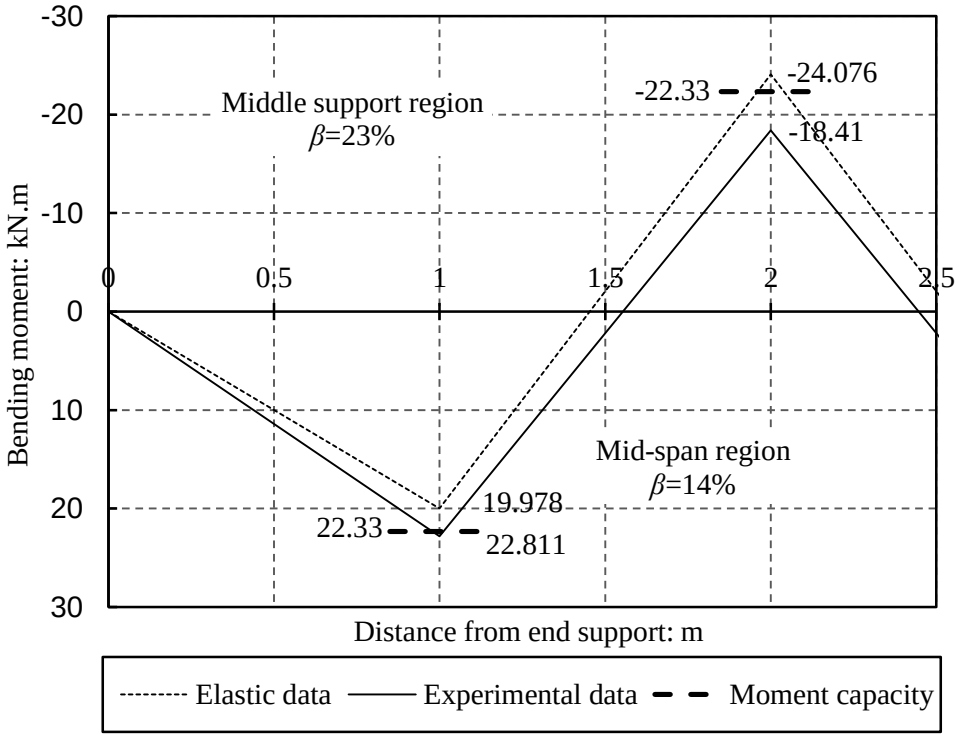

Figure 3-22: Elastic and experimental bending moments relations at failure for slab C–B–UU

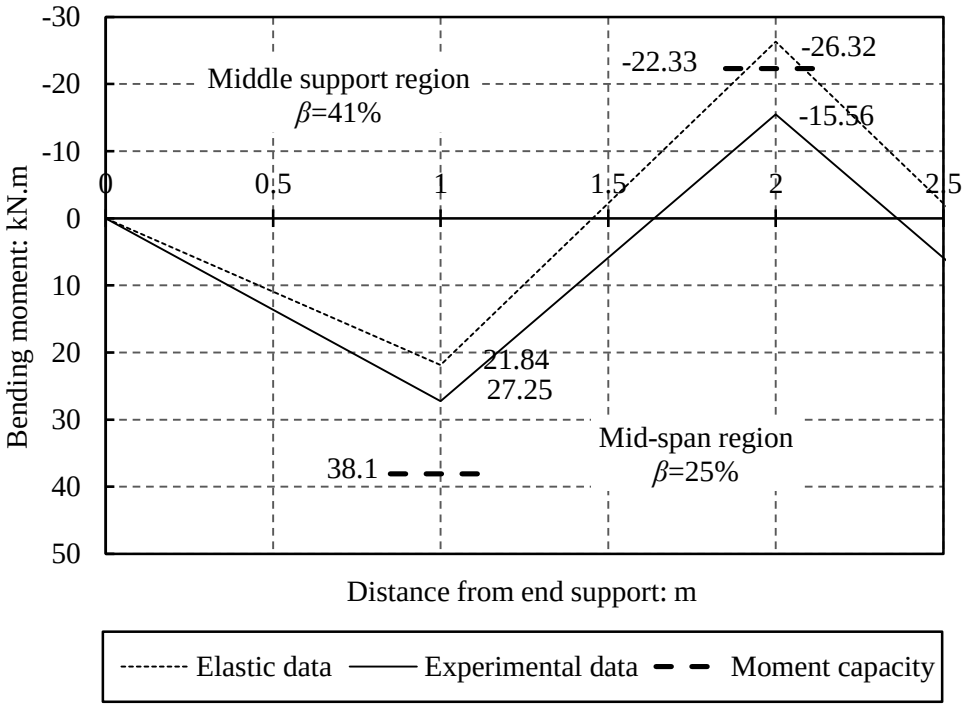

Figure 3-23: Elastic and experimental bending moments relations at failure for slab C–B–OU

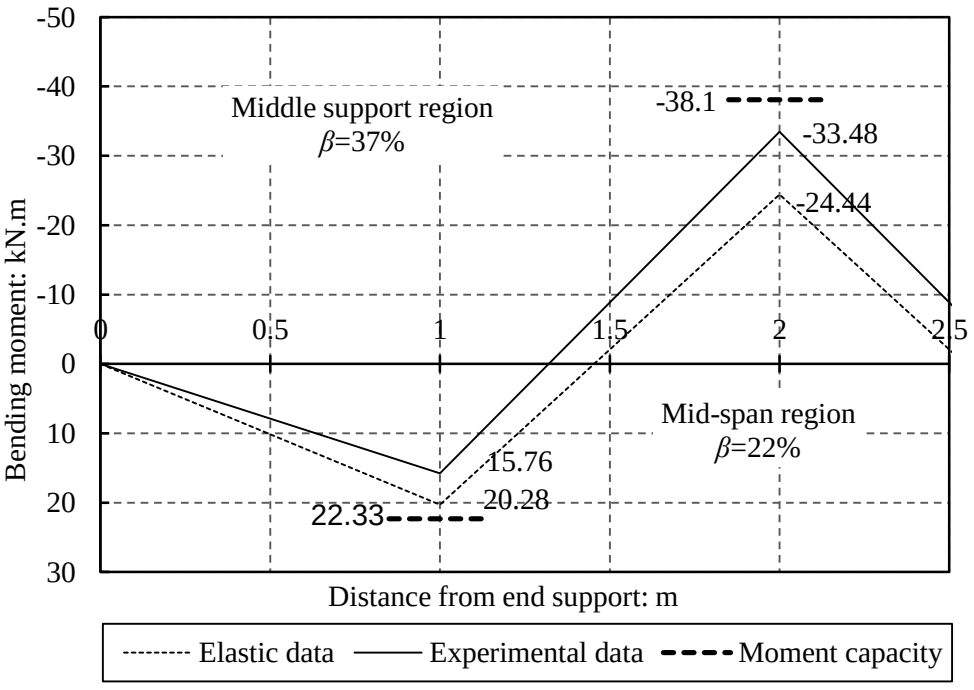

Figure 3-24: Elastic and experimental bending moments relations at failure for slab C–B–UO

3.7.4 Load-Deflection Response

Figure 3–25 illustrates the relationship between the mid-span point load versus the recorded mid-span deflections of all slabs tested. The LVDTs at the end and middle supports did not record any noticeable movement; therefore not presented. At early stages of loading, all slabs exhibited linear load-deflection behaviour before cracking due to the linear elastic characteristics of concrete and BFRP bars. After cracking, there is a clear reduction in the flexural stiffness; as the load increased, the stiffness of slabs further reduced due to the occurrence of more additional cracks. As expected, due to the higher axial stiffness of steel bars, C-S-UU slab demonstrated the lowest deflection of all slabs tested before yielding of steel. Overall, the amount of BFRP reinforcement used had a significant effect on the flexural stiffness and, consequently, deflections of the slabs tested. It could be noticed that slab C–B–UO demonstrated higher deflection than C–B–OU as the mid-span flexural stiffness of slab C–B–OU is higher than that of C–B–UO. The under reinforced simply supported slab S-B-U showed unacceptable large deflection compared with its span ($>L/30$). Figure 3–26 presents the deflection curve of continuous slabs tested, measured at 5 points along the slab span at a mid-span point load of 40kN. The test results illustrate the largest deflection of all continuous slabs tested belongs to slab C–B–UO with the smallest amount of BFRP reinforcement at the mid-span region, whereas the lowest deflection exhibited by the steel reinforced concrete slab C–S–UU owing to the higher axial stiffness of steel reinforcement used, followed by C-B-OO.

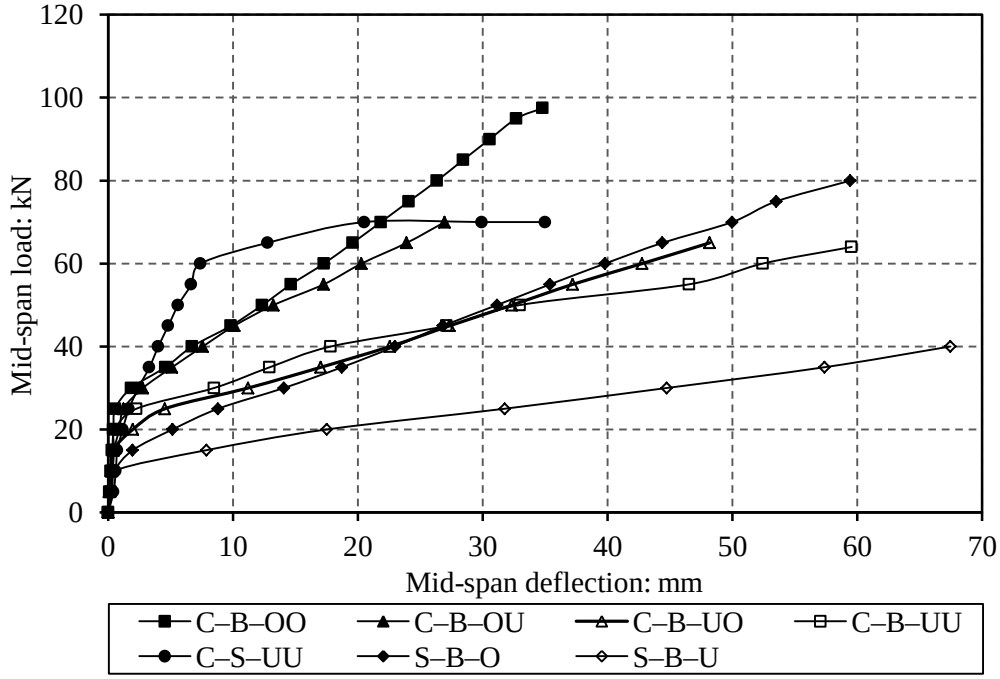

Figure 3-25: Load-deflection at mid-span for continuous slabs tested

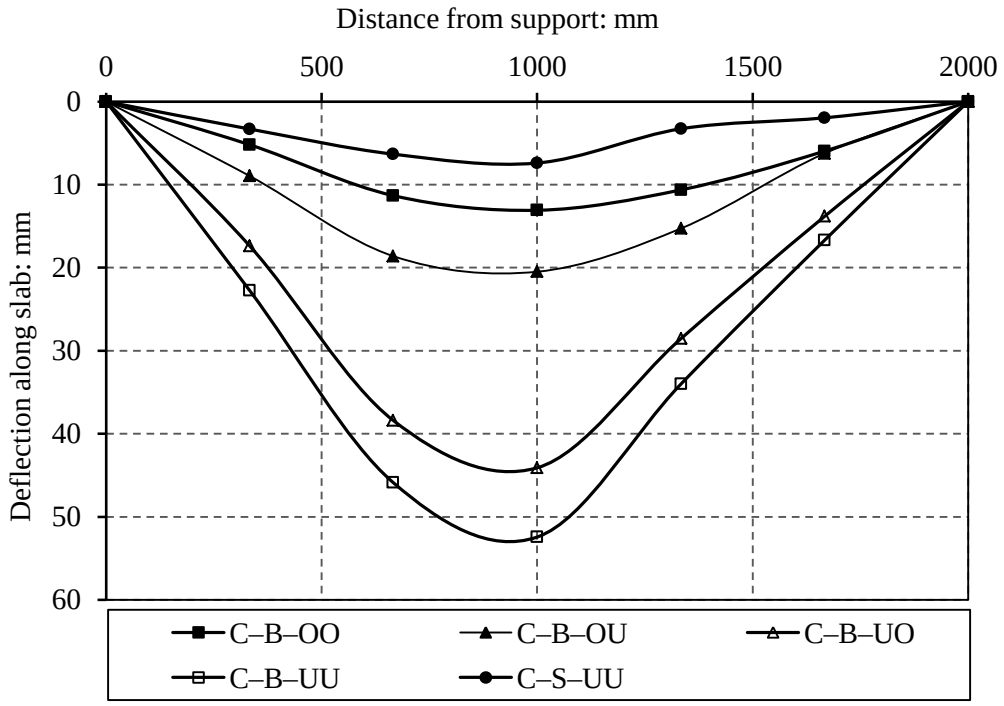

Figure 3-26: Experimental profile of deflections along continuous slabs tested at a midspan load of 40 kN

3.8 Conclusions

Tests results and code modelling of two simply and four continuously supported concrete slabs reinforced with BFRP bars have been presented in this paper. The following conclusions are drawn:

- The continuously supported BFRP reinforced concrete slabs developed earlier and wider cracks, and larger deflections than the control concrete slab reinforced with steel owing to the lower elastic modulus of BFRP reinforcing bars.
- At initial stages of loading, the experimental reactions of all slabs tested were very similar to the elastic prediction at the end support. At higher applied loads, many cracks occurred and, consequently, the measured reactions were slightly different from that obtained from elastic analysis.
- Although the experimental bending moment distribution at failure was different from that obtained by elastic analysis for all continuous BFRP reinforced concrete slabs, the experimental bending moments at failure for both the middle support and mid span sections were lower than the corresponding moment capacities.
- The BFRP continuous slab with over reinforcement at both the middle support and mid span regions exhibited the highest load capacity and lowest deflection of all BFRP slabs tested.
- Combined shear and flexural failure was the dominant mode of failure for all continuous BFRP reinforced concrete slabs tested.

CHAPTER FOUR

EXPERIMENTAL INVESTIGATION OF CFRP CONCRETE SLABS

4.1 Introduction

The use of basalt fibre reinforced polymer (BFRP) in concrete slabs was investigated in the previous chapter, owing to importance of its properties. Therefore, it was necessary to study another type of FRP reinforcement in the present experimental tests. The main objective of the experimental investigation explained in the current chapter is to investigate the behaviour of concrete slabs reinforced with carbon fibre reinforced polymer (CFRP) bars. In particular, the influence of different reinforcement arrangements on the flexural behaviour of CFRP reinforced concrete continuous slabs was investigated via the test program. Moreover, these experimental results including the deflection and ultimate load would be used in chapters five and six to validate the design codes and proposed numerical technique, respectively.

4.1 Test Specimens

Four continuously and two simply supported CFRP reinforced concrete slabs were constructed and tested in flexure. In addition, one steel reinforced continuous slab was also tested for comparison purposes. All slabs tested had a rectangular cross-cross of 500 mm in width and 150 mm in depth. The continuous slabs had two equal clear spans, each of 2000 mm, whereas the simple slabs had a span of 2000 mm as shown in Figures 4–1 and 4–2 below. The CFRP reinforcing bars were selected to investigate two different modes of failure, namely CFRP bar rupture and concrete crushing. The former was achieved by using a reinforcement ratio ρ_f less than the balanced reinforcement ratio ρ_{fb}, whereas the latter by using a reinforcement ratio greater than ρ_{fb}, as

recommended by the ACI 440.1R–06 guidelines. The combination and number of top and bottom reinforcing bars were the main parameters studied, as given in Table 4–1 below. The CFRP reinforced concrete continuous slabs were reinforced with three different reinforcement arrangements at the top and bottom layers. Slab C–C–OU was reinforced with five CFRP longitudinal bars of 12 mm diameter (over reinforcement) at the bottom side and three 8 mm diameter CFRP bars (under reinforcement) at the top side, whereas slab C–C–UO was reinforced with an opposite combinations of CFRP longitudinal bars as presented in Table 4–1. Moreover, the bottom reinforcement of slabs C–C–OO and C–C–UU was the same as the top reinforcement; each consisting of five CFRP bars of 12 mm diameter (over reinforcement) in slab C–C–OO and three CFRP bars of 8 mm diameter (under reinforcement) in slab C–C–UU. The simply supported slabs, S–C–O and S–C–U, were reinforced with five CFRP bars of 12 mm diameter (over reinforcement) and three CFRP bars of 8mm diameter (under reinforced), respectively, at the bottom side. The bottom steel reinforcement of the continuous slab C–S_2–UU was the same as the top reinforcement, each consisting of six 10-mm diameter steel bars. This slab reinforcement was selected to have similar tensile strength as the three CFRP bars of 8-mm diameter used at the bottom layer of slabs C–C–UU, C–C–UO and S–C–U and top layer of slabs C–C–OU and C–C–UU.

Table 4–1: Designation of slabs and characteristics of reinforcement and concrete

Slab no.	Longitudinal reinforcing bars								Concrete properties	
	Bottom bars at mid-span				Top bars at central support					
	No.	Diameter: Mm	ρ_f%	$\frac{\rho_f}{\rho_{fb}}$	No.	Diameter: mm	ρ_f%	$\frac{\rho_f}{\rho_{fb}}$	f_{cu}, MPa	f_{ct}, MPa
C–C–OU	5 CFRP	12	0.9	1.58	3 CFRP	8	0.24	0.66	47.2	3.6
C–C–UO	3 CFRP	8	0.24	0.66	5 CFRP	12	0.9	1.58	51.6	4.2
C–C–OO	5 CFRP	12	0.9	1.58	5 CFRP	8	0.9	1.58	50.3	3.9
C–C–UU	3 CFRP	8	0.24	0.66	3 CFRP	8	0.24	0.66	52.5	3.7
S–C–O	5 CFRP	12	0.9	1.58	N/A	N/A	N/A	N/A	53.7	4.2
S–C–U	3 CFRP	8	0.24	0.66	N/A	N/A	N/A	N/A	54.3	4.5
C–S_2–UU	6 steel	10	0.75	0.26	6 steel	10	0.75	0.26	50.8	4.0

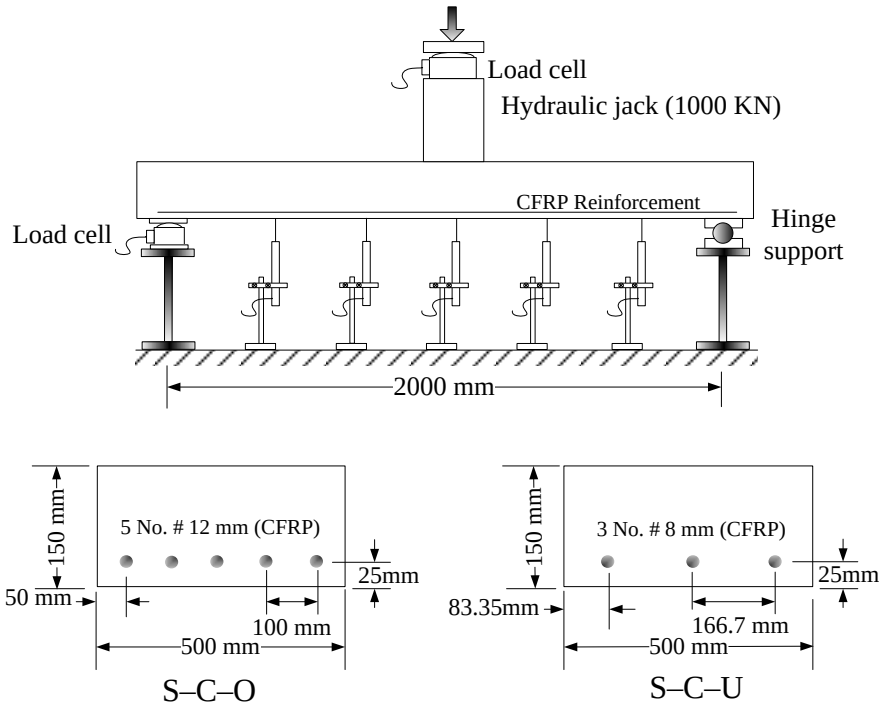

Figure 4–1: Experimental setup and details of CFRP simple slabs

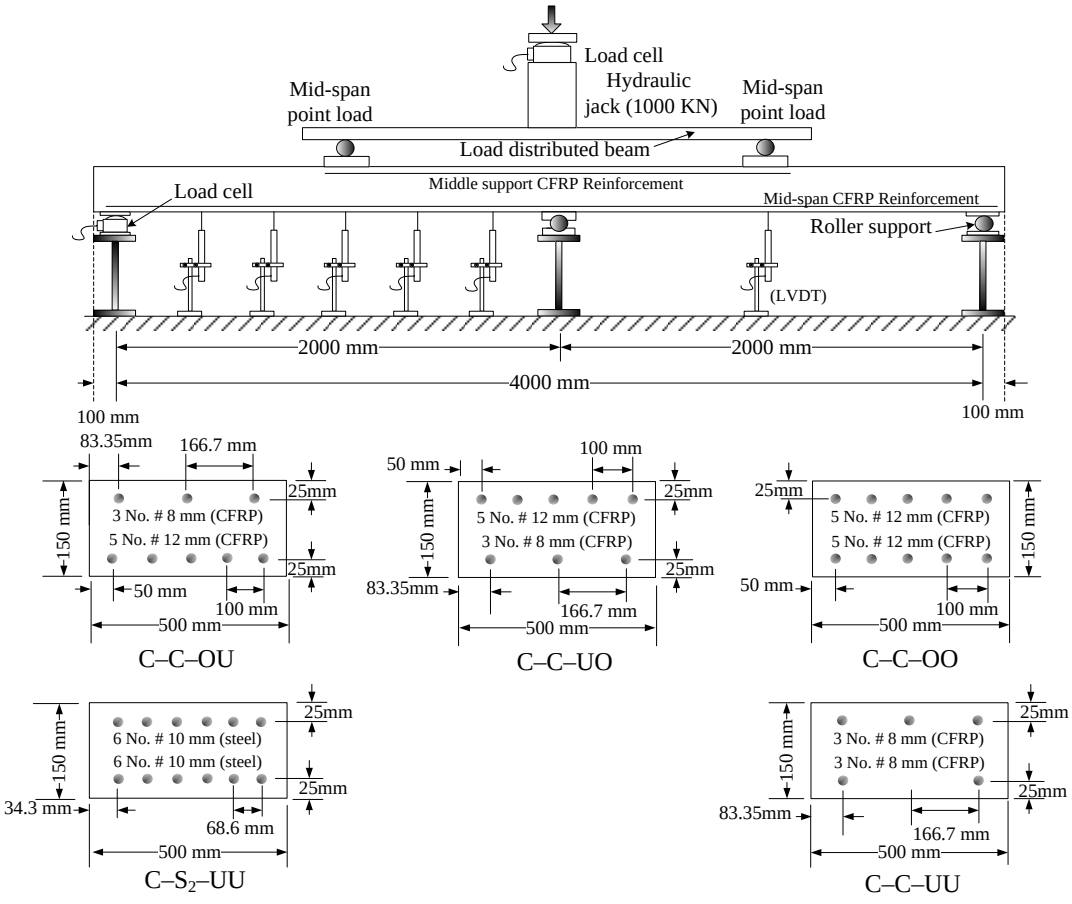

Figure 4–2: Experimental setup and details of CFRP continuous slabs

4.2 Material Properties

The slabs were constructed using ready-mixed, normal weight concrete with a target compressive strength of 50 MPa at 28 days. Five cubes (100 mm) and three cylinders (150 mm-diameter×300 mm-high) were made and tested immediately after testing of each slab to provide the average values of cube compressive strength, f_{cu}, and splitting tensile strength, f_{ct}, respectively as listed in Table 4–1. Three prisms 100×100×500 mm were also tested for this group of slabs to obtain the modulus of rupture, f_r, (average value = 4.0 MPa). After concrete casting, all specimens were covered with polyethylene sheets to keep down moisture loss at all times during the period of curing and stored in the laboratory under the same condition until the day of testing.

The CFRP bars used in this study are manufactured by the pultrusion process and the surface is eventually treated to improve the bond characteristics. The mechanical properties of CFRP reinforcing bars were obtained by carrying out tensile tests on three specimens of each bar diameter. Specimens were initially prepared by embedding the ends of the CFRP bar into steel pipes filled with expansive grout to avoid premature failure of CFRP bars at the steel jaws of the testing machine. All prepared specimens were tested using a 500 kN capacity, universal testing machine. Table 4–2 lists the mechanical properties of the used CFRP and steel bars as determined by tensile tests.

Table 4–2: Mechanical Properties of CFRP and Steel Reinforcing Bars

Type of bars	Diameter: Mm	Modulus of elasticity: GPa	Tensile strength: MPa	Ultimate strain	Yield strength: MPa
CFRP	8	137	1773	0.0129	N/A
CFRP	12	137	1375	0.01	N/A
Steel	10	200	645	0.003	575

4.3 Slabs Notations

The slab notation was defined based on the type of reinforcement, support system and identification of reinforcement ratio. The first letter in the notation corresponds to the

type of supporting system, 'C' for continuously supported slabs and 'S' for simply supported slabs. The second letter indicates the type of reinforcement, either 'C' or 'S_2' for CFRP and steel reinforcement, respectively. The third letter reflects the reinforcement ratio on the bottom mid-span region of the simply or continuously supported slab, 'U' for under-reinforcement or 'O' for over-reinforcement ratio. The forth letter, 'U' or 'O', is used only for the continuously supported slabs, illustrating the over middle-support reinforcement ratio. As an example, the slab notation C–C–UO illustrates a continuously supported CFRP reinforced slab having under and over reinforcement ratios of CFRP bars at mid-span and over middle-support layers, respectively.

4.4 Test Setup and Instrumentations

Figures 4–1 and 4–2 above present the experimental setup of the simply and continuously supported slabs tested, respectively. Each span of the continuous slabs was loaded at its mid-point and supported on two end rollers and a middle hinge support. All details of test setup and instruments were similar to that used for BFRP slabs described and explained in the previous chapter.

4.5 Test Results and Discussion

4.5.1 Crack propagation and failure modes

Table 4–3 presents the first visible cracking load of all slabs tested. The CFRP reinforced concrete slab C–C–OO experienced the largest first cracking load than other slabs due to the fact that slab C–C–OO had higher flexural stiffness. However, for the CFRP continuous slabs, the earliest crack initiation, at the middle support regions, was observed in slab C–C–UO reinforced with over CFRP reinforcement ratio in the hogging moment zone. It can be also seen that the first crack in slab C–C–OU was

noticed in the hogging moment zone at the middle support (under reinforcement), followed immediately by another crack in the sagging moment zone at the mid-span (over reinforcement). Slab C–C–UU demonstrated a lower first cracking load than steel-reinforced slab C–S_2–UU as both were designed to have similar tensile strength.

The crack patterns of the CFRP continuously supported slabs are sketched in Figure 4–3. Slab C–C–OO demonstrated lower crack spacing at mid-span and middle support regions than these of other CFRP continuously supported slabs due to the fact that slab C–C–OO had higher flexural reinforcement ratio at mid-span and middle support regions. In general, all CFRP continuous slabs demonstrated deeper cracks compared with the slab reinforced with steel due to the lower elastic modulus of CFRP bars.

Figures 4–4 and 4–5 present the main crack width at both middle support and mid-span regions for all slabs tested, respectively. The control slab C–S_2–UU had considerably less crack width at both mid-span and middle support regions among all slabs tested due to the higher axial stiffness of steel reinforcement than that of CFRP reinforcement. For the CFRP continuous slabs tested, wider cracks at the mid-span region were observed in slabs C–C–UU and C–C–UO with under reinforcement ratio than the over reinforced CFRP slabs, C–C–OO and C–C–OU, at their mid-span regions.

Table 4–3: First cracking loads and total experimental failure loads of slabs tested

Slabs no.	First cracking loads, P_{cr}: kN		Total experimental failure load, 2*P*: kN	Observed failure mode (see Fig. 2)
	sagging	*hogging*		
C–C–OO	29	28	232	Flexure-shear failure at middle support
C–C–OU	24	22.5	200	Flexure-shear failure at middle support
C–C–UO	15	11.5	179	Flexure-shear failure at middle support
C–C–UU	18	21	165	Flexure-shear failure at middle support
S–C–O	17	N/A	115[a]	Flexure-shear failure at end support
S–C–U	13	N/A	59[a]	CFRP bar rupture at mid-span
C–S_2–UU	22.5	22.5	210	Flexural-Tension Failure at both mid-span and middle support

[a]Just *P* for the simply supported slabs

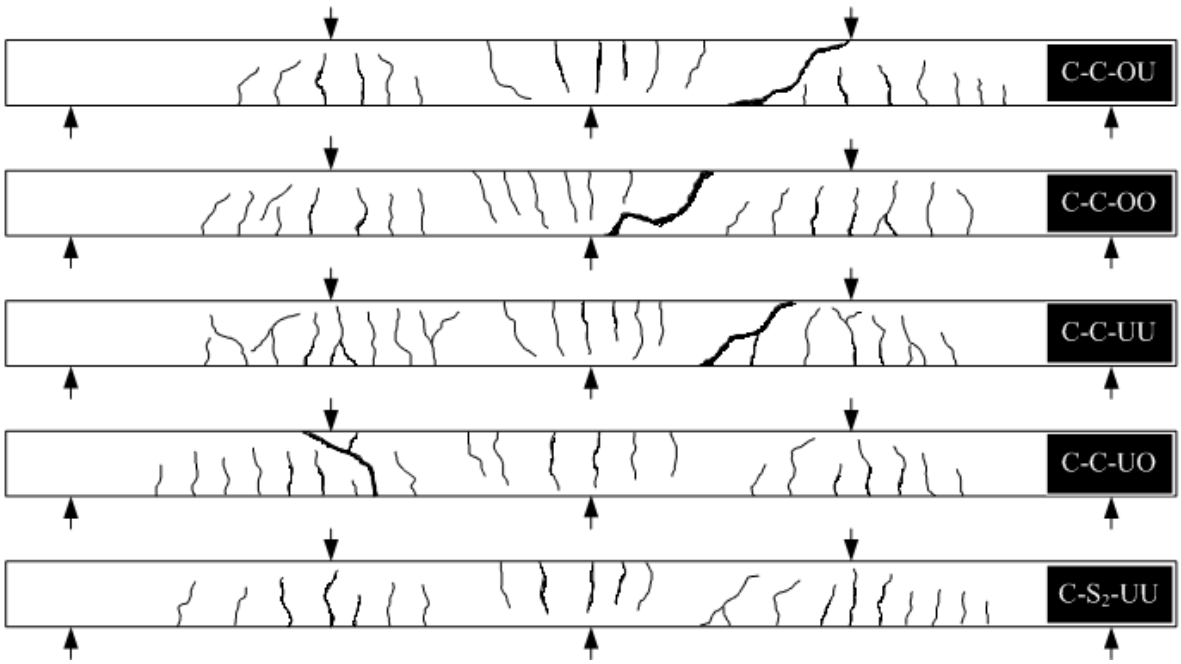

Figure 4–3: Typical cracking patterns and failure shape of CFRP RC slabs

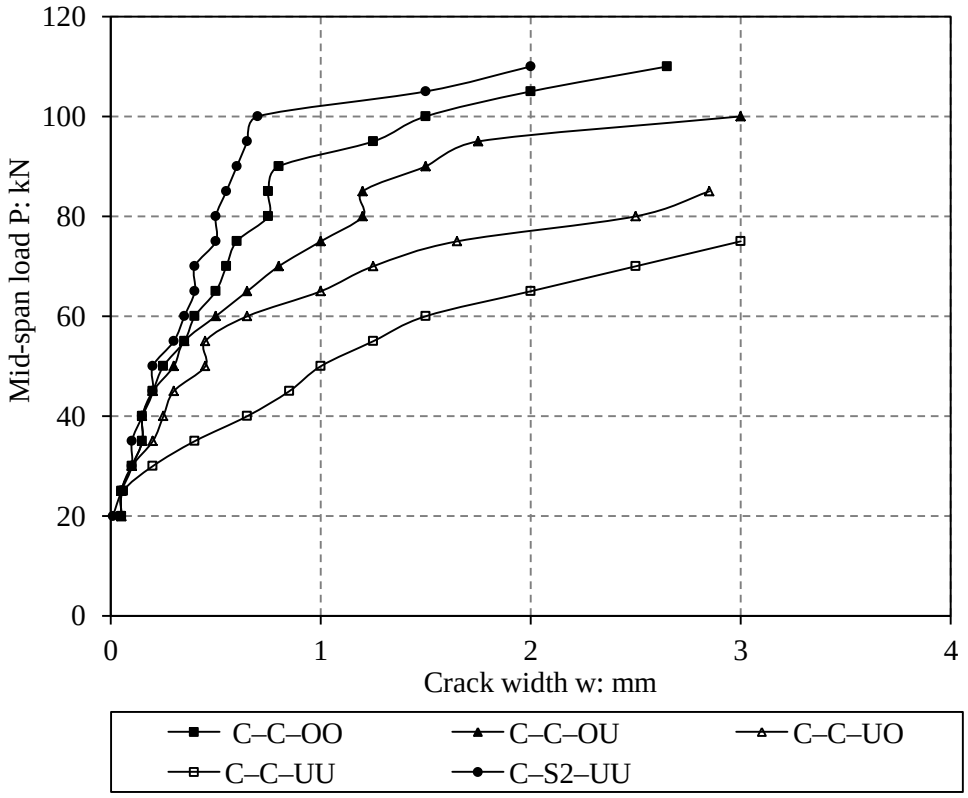

Figure 4–4: Middle support crack width of slabs tested

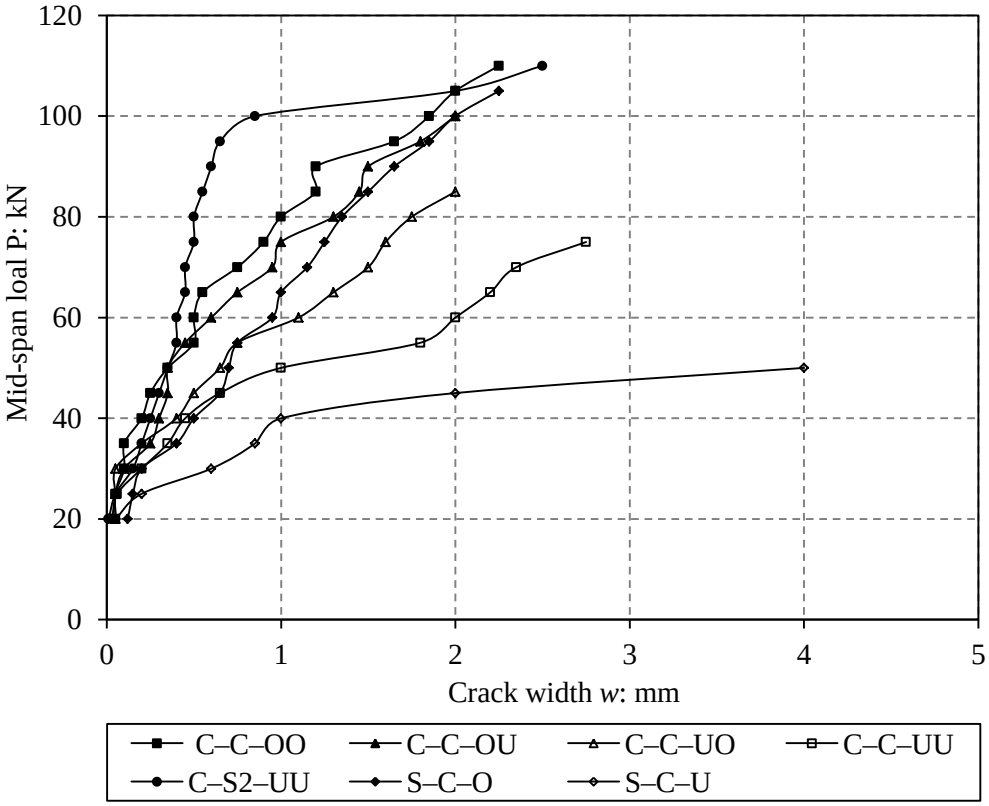

Figure 4–5: Mid-span crack width of slabs tested

Three different failure modes were observed in the experimental tests as shown in Figures 4–6 to 4–8 and explained below.

Mode 1: Combined flexural-shear failure–This mode was illustrated by CFRP slabs C–C–OO, C–C–UU, C–C–UO, C–C–OU and S–C–O. In the slab C–C–OO, the failure started at the compression side of the middle support region, followed by a major, sudden diagonal shear crack at the same location as shown in Figure 4–6a. However, the diagonal flexural-shear cracks near the mid-span region propagated towards the loading point, causing failure in case of slabs C–C–UU, C–C–UO, C–C–OU and S–C–O as presented in Figures 4–6b, 4–6c, 4–6d and 4–6e, respectively.

(a) Flexural–shear failure at middle support of slab C–C–OO

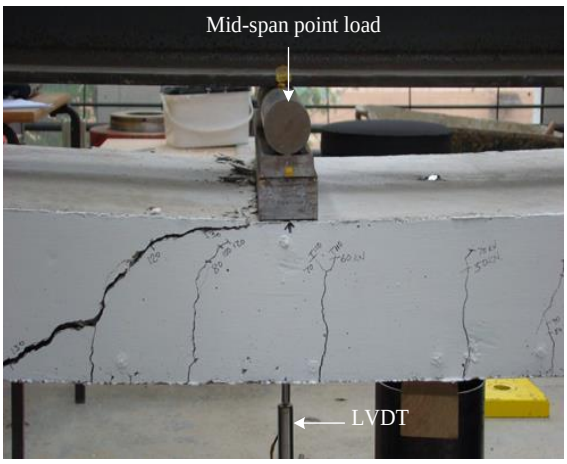

(b) Flexural–shear failure at mid-span of slab C–C–UU

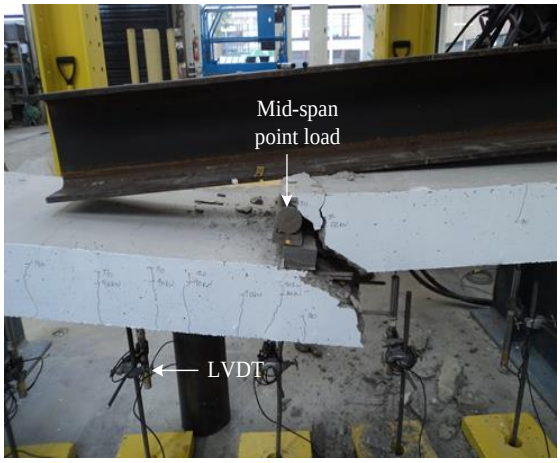

(c) Flexure–shear failure at mid-span of slab C–C–UO

(d) Flexure–shear failure at mid-span of slab C–C–OU

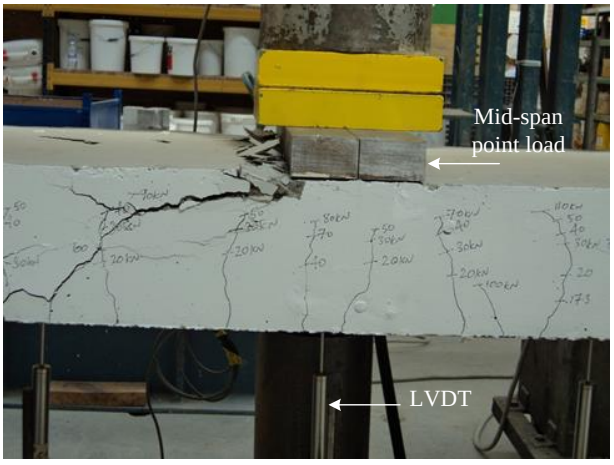

(e) Flexure–shear failure at mid-span of slab S–C–O

Figure 4–6: Flexure–shear failure mode of different slabs

Mode 2: CFRP Bar rupture–This mode was demonstrated by slab S–C–U, which was provided with an under reinforcement ratio of CFRP bars at the bottom layer. Such reinforcement was the reason behind the CFRP rupture at the bottom layer before reaching the ultimate crushing strain of concrete as revealed in Figure 4–7. It was also noticed that rupture of CFRP bars was sudden and accompanied by a loud noise indicating a rapid release of energy and a complete loss of load capacity.

Figure 4–7: CFRP bar rupture failure at mid-span of slab S–C–U

Mode 3: Conventional ductile flexural failure–This mode was experienced by the steel reinforced concrete slab C–S_2–UU as shown in Figures 4–8a and 4–8b. It occurred due to yielding of tensile steel reinforcement followed by concrete crushing at mid-span region (see Fig. 4–8b). Hogging flexural failure was observed as a result of the yielding of the tensile steel reinforcement at the central support earlier than that at the slab mid-span as depicted in Figure 4–8a.

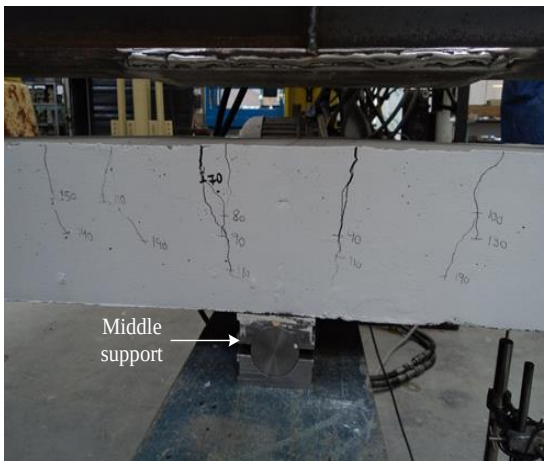

(a) Flexural–tension failure at middle support of slab C–S_2–UU

(b) Flexural–tension failure at mid-span of slab C–S_2–UU

Figure 4–8: Conventional ductile flexural failure mode of steel slab C–S_2–UU

4.5.2 Load capacity

Failure loads of the tested slabs are plotted in Figure 4–9. The failure load of simply supported slab S–C–O, which had high reinforcement ratio at mid-span region, was around 50% and 57% of the total failure load of slabs C–C–OO and C–C–OU, respectively. On the other hand, the failure load of under reinforced simply supported slab S–C–U was nearly 35% and 33% of the failure load of slabs C–C–UO and C–C–UU, respectively. Likewise slab S–C–U failed at 51% of the failure load of beam S–C–O. Slab C–C–OO that was over reinforced at both the mid-span and middle support regions tolerated more load than slab C–C–OU or C–C–UO that is reinforced with over reinforcement ratio in only one region. In spite of the under-reinforcement ratio used at the middle support and mid-span regions of steel reinforced concrete continuous slab C–S_2–UU; this slab resisted a failure load similar to that of slab C–C–OU and exhibited a higher load capacity than that of slabs C–C–UU and C–C–UO. Slab C–C–OU have tolerated more loads than slab C–C–UO, which was provided with CFRP longitudinal reinforcement configuration opposite to that used in C–C–OU. Even though the fact that the reinforcement ratio in slab C–C–UO was around 3.75 times that in slab C–C–UU at

middle support, slab C–C–UO accomplished a failure load close to that of slab C–C–UU. This concludes that top reinforcement ratio of CFRP bars at middle support region had a small influence in enhancing the slab load carrying capacity, agreeing with previous investigations on continuous FRP reinforced concrete beams (Ashour and Habeeb 2008 and El-mogy et al. 2010).

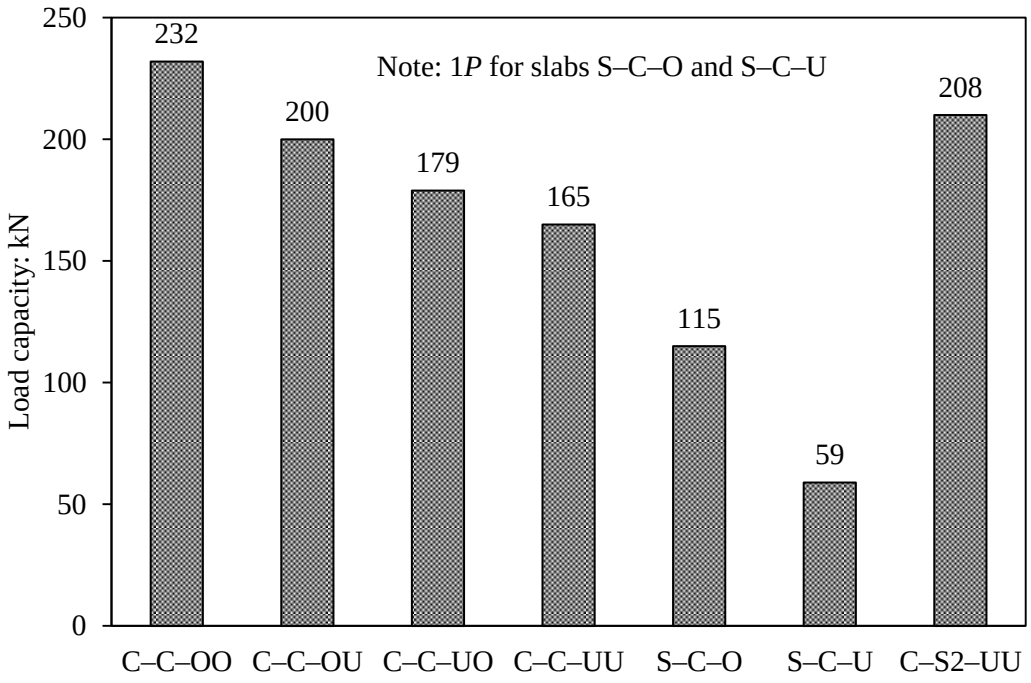

Figure 4–9: Experimental load capacities of CFRP slabs

4.5.3 Redistribution of load and bending moment

The measured end support reaction versus the total applied load for each continuous slab tested is presented in Figure 4–10. The elastic reaction at the end support, considering uniform flexural stiffness throughout the entire length of slabs, was also illustrated in Figure 4–10 to assess the amount of load redistribution. At the initial stages of loading before concrete cracking, the measured end support reaction of continuous slabs was very close to that obtained from the elastic analysis due to the linear elastic characteristics of concrete, CFRP bars and steel bars before reaching the cracking load. Slabs C–C–OO and C–C–UU demonstrated similar unremarkable load

redistribution behaviour until failure owing to the uniform flexural stiffness throughout the slab length. On the other hand, the end support reaction of slab C–C–OU was slightly larger than the elastic reaction, indicating signs of load redistribution from the middle support region to the mid-span region due to the higher stiffness at mid-span region. Conversely, slab C–C–UO demonstrated an opposite reaction response to slab C–C–OU, that is attributed to the reverse reinforcement arrangement of slab C–C–UO in comparison with slab C–C–OU.

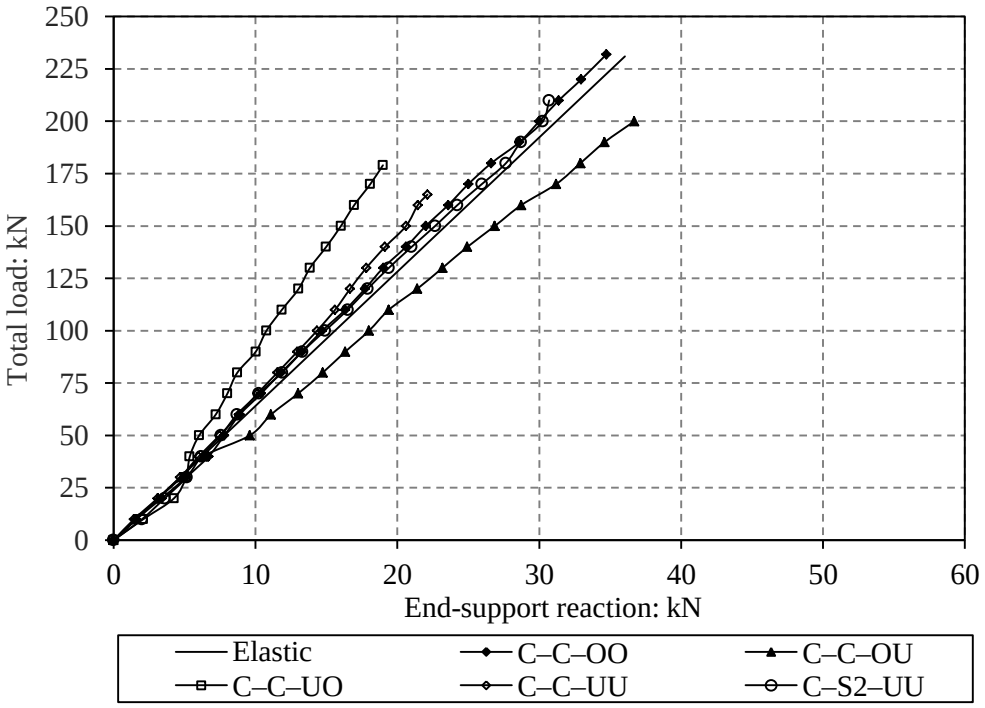

Figure 4–10: Total applied load versus end support reaction of continuous slabs tested

Figures 4–11 to 4–14 present the experimental and elastic bending moment distributions at failure for continuous CFRP slabs. The predicted moment capacities at both mid-span and over support sections calculated from the ACI 440.1R–06 are also presented in these figures. The amount of moment redistribution, β, can be calculated (see Eq. 3–4) by comparing the experimental and elastic bending moments. The amounts of moment redistribution, β, for the mid-span and over support sections are given in Figures 4–11 to 4–14. Unlike the rest of the tested slabs, slab C–C–OO exhibited no moment

redistribution between the middle support and mid-span sections as presented in Figure 4–11. This might be attributed to the same stiffness of the slab cross-section at middle support and mid-span regions. Redistribution of moment from the middle support section to the mid-span section occurred for C–C–UU and C–C–OU slabs. In slab C–C–UO, however, it was observed that redistribution of hogging bending moment from mid-span to middle support sections as shown in Figure 4–14. This is due to the higher stiffness at the middle support section provided by the higher reinforcement ratio as compared to the mid-span section. Slab C–C–UO exhibited the largest moment redistribution at middle support (53.5%) and mid-span section (32.2%). For all slabs but C–C–OU at middle support section, neither the middle support nor mid-span section reached the corresponding predicted moment capacity as depicted in Figures 4–11 to 4–14. In general, this indicates that the moment redistribution occurred is likely to be attributed to cracks at different locations or slight debonding of CFRP reinforcement.

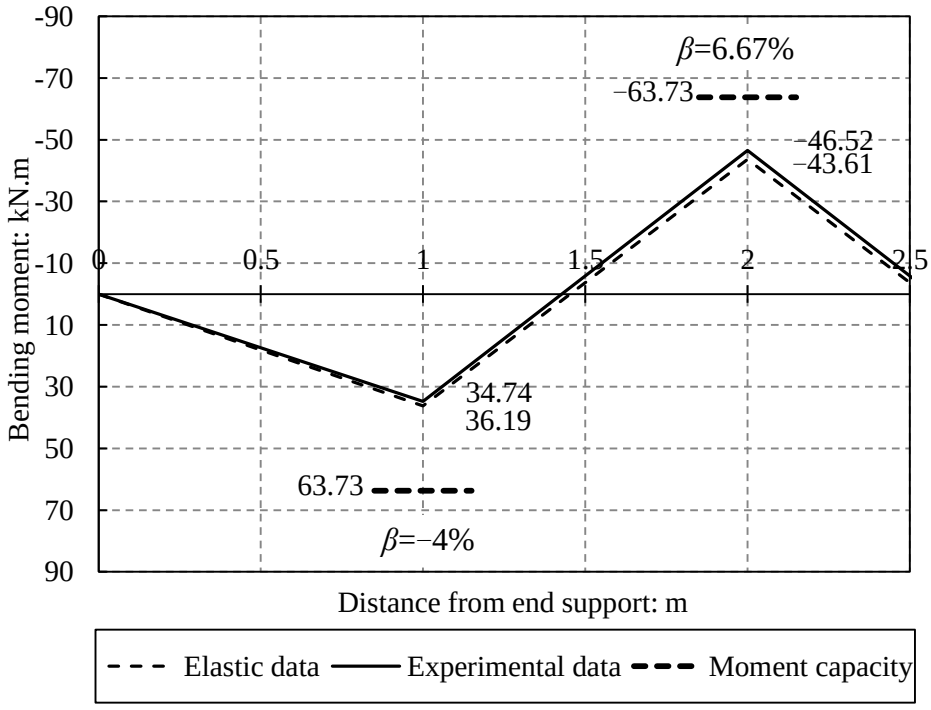

Figure 4–11: Elastic and experimental bending moments relations at failure for slab C–C–OO

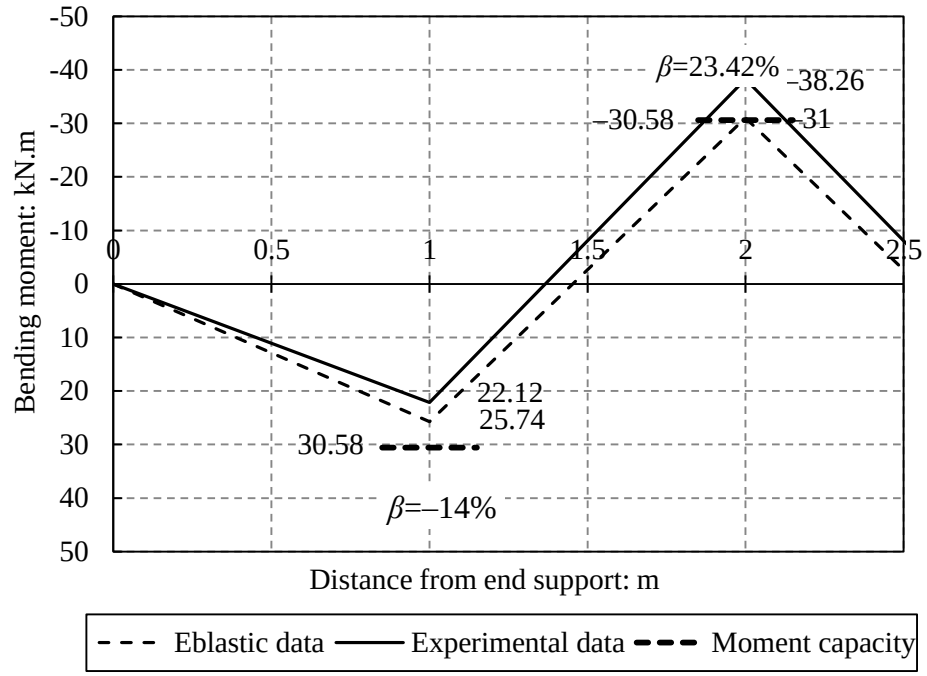

Figure 4–12: Elastic and experimental bending moments relations at failure for slab C–C–UU

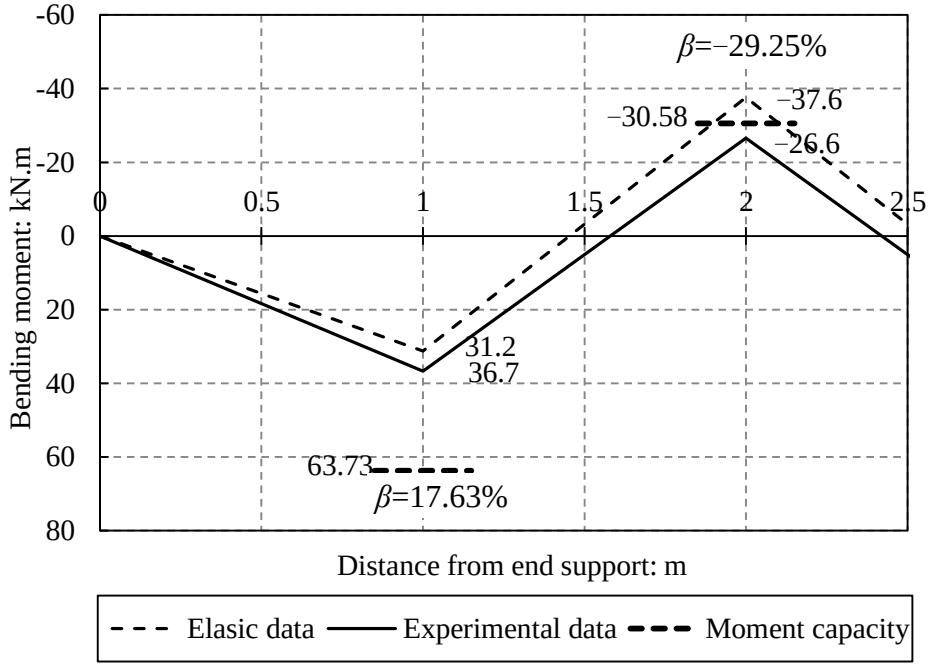

Figure 4–13: Elastic and experimental bending moments relations at failure for slab C–C–OU

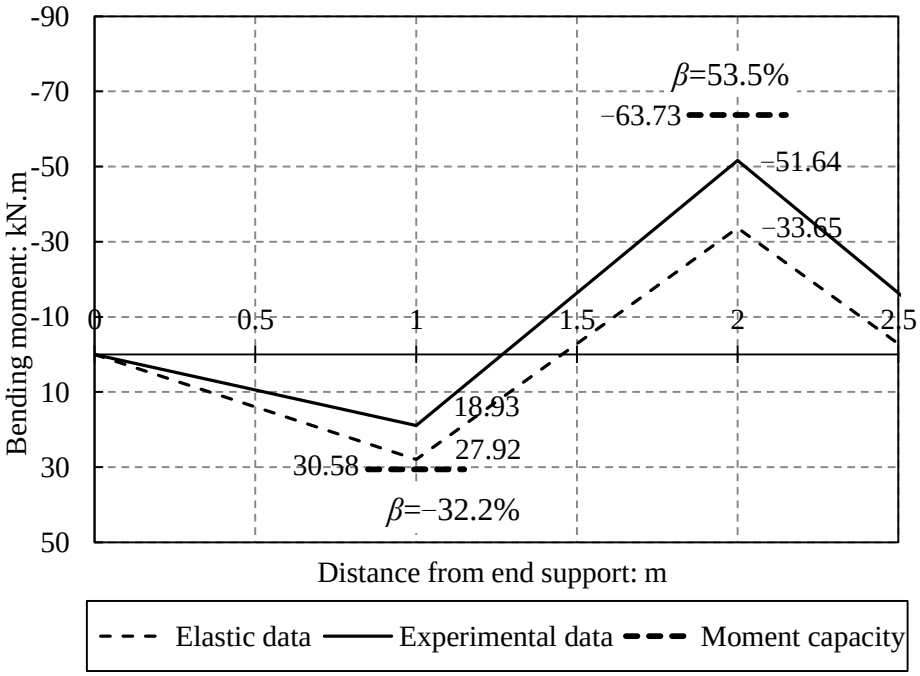

Figure 4–14: Elastic and experimental bending moments relations at failure for slab C–C–UO

4.5.4 Load-Deflection Response

The mid-span point load versus the recorded mid-span deflections of all slabs tested are shown in Figure 4-15. The LVDTs at the end and middle supports did not record any noticeable movement; therefore not presented. At initial stages of loading, all slabs were un-cracked and, therefore, demonstrated linear load-deflection behaviour owing to the linear elastic characteristics of concrete and CFRP bars. After concrete cracking, there is a clear reduction in the flexural stiffness; as the load increased, the stiffness of slabs is further reduced due to the occurrence of more cracks. Generally, the amount of CFRP reinforcement is a key factor in enhancing the flexural stiffness and, consequently, reducing deflections of the slabs tested. As expected, due to the higher axial stiffness of steel bars, C–S_2–UU slab exhibited the lowest deflection of all slabs tested before yielding of steel. Slab C–C–OO demonstrated the lowest deflection among the CFRP continuous slabs, followed by C–C–OU, S–C–O, C–C–UO, C–C–UU and S–C–U, which is attributed to the relative flexural stiffness at the mid-support region of the slabs tested.

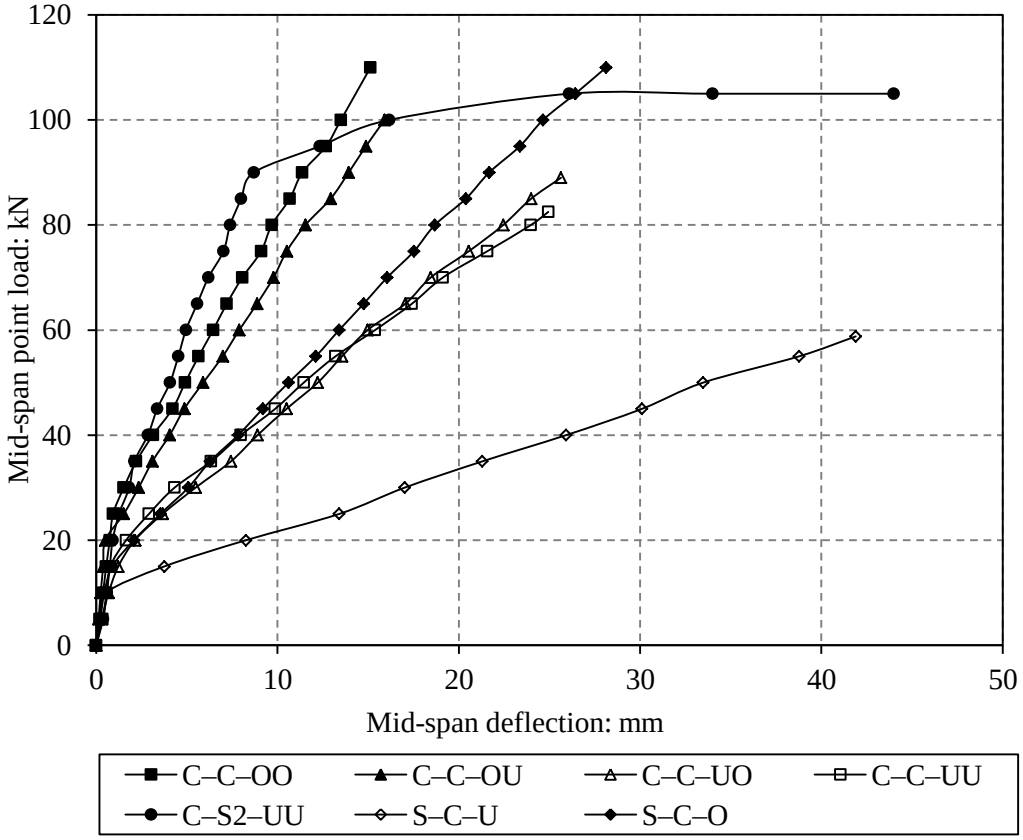

Figure 4–15: Load-deflection at mid-span for continuous slabs tested

Figure 4–16 illustrates the deflection curve of slabs tested, measured at 5 points along the slab span at a mid-span point load of 50kN. The test results illustrate that the largest deflection of all continuous slabs tested belongs to slab S–C–U with the smallest amount of CFRP reinforcement at the mid-span region. However, the lowest deflection exhibited by the steel reinforced concrete slab C–S_2–UU due to the higher axial stiffness of steel reinforcement used.

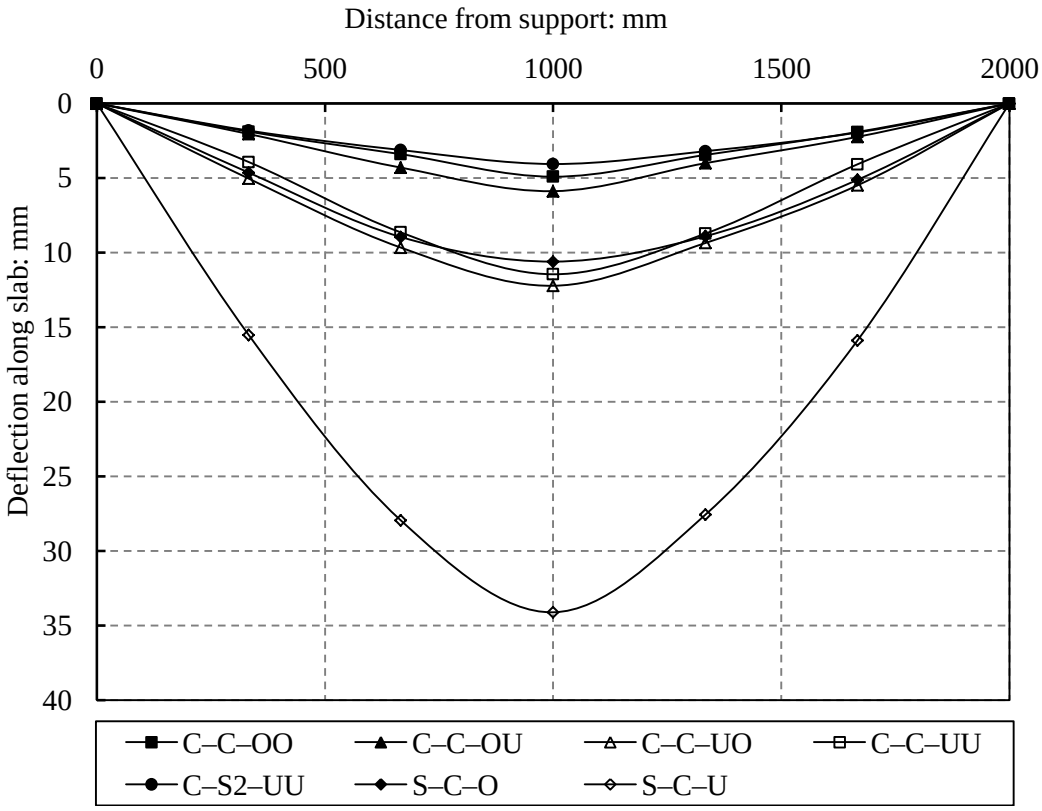

Figure 4–16: Typical experimental profile of deflections along slabs tested at a mid-span load of 50 kN

4.6 Conclusions

The principal findings drawn from the present investigation are presented below:

- Continuously supported CFRP reinforced concrete slabs illustrated wider cracks and larger deflections than the control steel reinforced concrete slab, owing to the lower elastic modulus of CFRP bars compared with steel.
- At early stages of loading before the onset of concrete cracking, the measured end support reactions of all slabs tested were very similar and close to that obtained from elastic analysis. After concrete cracking, the measured reactions were slightly different from that obtained from elastic analysis, depending on the relative flexural stiffness at mid-span and over middle support regions.
- Combined shear and flexural failure was the dominant mode of failure for all continuous CFRP reinforced concrete slabs tested.
- Increasing the bottom mid-span CFRP reinforcement of continuous slabs is more effective than the top over middle support CFRP reinforcement in improving the load capacity and reducing mid-span deflections

CHAPTER FIVE

DESIGN CODES EVALUATION AGAINST EXPERIMENTAL RESULTS OF BFRP AND CFRP CONCRETE SLABS

5.1 Introduction

In chapters three and four, the experimental investigation of BFRP and CFRP concrete slabs, respectively have been studied. The principal aim of the work presented in this chapter is to evaluate the design codes (ACI 440.1R–06, ISIS–07, CSA S806–02) equations for moment capacity, deflection as well as shear capacity. This evaluation was carried out by comparing the results from design codes equations with those obtained from the experimental tests described in chapters three and four.

5.2 Moment capacity predictions

The moment capacity, M_{pre}, of FRP-reinforced concrete members is predicted based on ACI 440.1R–06 design code using equations 5–1 and 5–2 when the reinforcement ratio ρ_f is greater than ρ_{fb} (concrete compression failure), and equations 5–3 and 5–4 when the reinforcement ratio ρ_f is less than ρ_{fb} (FRP rupture failure):

$$M_{pre} = \rho_f f_f \left(1 - 0.59 \frac{\rho_f}{f'_c}\right) bd^2 \quad (5\text{–}1)$$

$$f_f = \sqrt{\frac{(E_f \varepsilon_{cu})^2}{4} + \frac{0.85\beta_1 f'_c}{\rho_f} E_f} - 0.5 E_f \varepsilon_{cu} \leq f_{fu} \quad (5\text{–}2)$$

$$M_{pre} = A_f f_{fu} \left(d - \frac{\beta_1 c_b}{2}\right) \quad (5\text{–}3)$$

$$c_b = \left(\frac{\varepsilon_{cu}}{\varepsilon_{cu} + \varepsilon_{fu}}\right) d \quad (5\text{–}4)$$

where ρ_f (=A_f/bd) is the FRP reinforcement ratio, ρ_{fb} is the balanced FRP reinforcement ratio (see Eq. 3–1 in chapter three), f'_c is the cylinder compressive strength of concrete, f_f is the FRP stress at which concrete crushing failure occurs, f_{fu} is the ultimate tensile strength of FRP bars, ε_{cu} is the ultimate concrete strain, E_f is the modulus of elasticity of FRP bars, β_1 is the strength reduction factor, which can be determined based on the ACI 440.1R-06 (see Eq. 3–3 in chapter three) and c_b is the neutral axis depth for balanced failure as defined by Eq. (5–4).

The ISIS design code, according to the balanced FRP reinforcement ratio ρ_{fb}, calculates the moment capacity of FRP reinforced concrete members using Eqs. 5–5, 5–6 and 5–7 when flexural failure is induced by crushing of concrete without rupture of FRP reinforcement (over-reinforced) and Eqs. 5–8 when a section is under-reinforced.

$$f_f = 0.5 E_f \varepsilon_{cu} \left[\left(1 + \frac{4\alpha_1 \beta_1 \varnothing_c f'_c}{\rho_f \varnothing_f E_f \varepsilon_{cu}} \right)^{1/2} - 1 \right] \tag{5–5}$$

$$M_{pre} = A_f \varnothing_f f_f \left(d - \frac{\beta_1 c_b}{2} \right) \tag{5–6}$$

$$c_b = \left(\frac{0.0035}{0.0035 + \varepsilon_{fu}} \right) d \tag{5–7}$$

$$M_{pre} = A_f \varnothing_f f_{fu} \left(d - \frac{\beta_1 c_b}{2} \right) \tag{5–8}$$

According to the ISIS design code the equivalent stress block parameters α_1 and β_1 are tabulated in Figure A–1, respectively (see Appendix A); $\varnothing_c$ (=0.65) is material resistance factor for concrete and $\varnothing_f$ (=0.75) is material resistance factor for FRP bars. However, CSA S806–02 design code recommended that the uniform equivalent compressive strength of $\alpha_1 \varnothing_c f'_c$ is assumed to be distributed over distance $a = \beta_1 c_b$. where

$\beta_1 = 0.85 - 0.0015 f'_c \quad \geq 0.67$

$\alpha_1 = 0.97 - 0.0025 f'_c \quad \geq 0.67$

The CSA S806–02 design code recommended also that the ratio c_b/d calculated from:

$$c_b/d \geq \frac{7}{7+2000\,\varepsilon_{fu}} \tag{5–9}$$

According to CSA–02 design code the moment capacity, M_{pre}, of FRP reinforced concrete section is calculated as follows:

$$M_{pre} = A_f f_f \left(d - \frac{a}{2}\right) \tag{5–10}$$

5.2.1 Moment predictions for the FRP Reinforced concrete slabs

Tables 5–1, 5–2 and 5–3 compare the moment capacity predictions obtained from design codes (ACI 440–06, CSA–02 and ISIS–07) against the experimental moment capacity of BFRP and CFRP reinforced concrete slabs described in chapters three and four, respectively. These tables clearly indicate that there is a discrepancy among the predictions of the three design codes for continuously supported slabs. The design code equations reasonably predicted the failure moments of the CFRP simply supported slabs S–C–O and S–C–U, but for the BFRP simply supported slabs S–B–O and S–B–U, the CSA–02 and ISIS–07 equations were immoderate. However, for the continuously supported BFRP and CFRP reinforced concrete slabs, the design code equations have mostly overestimated the moment capacity of the slabs C–C–OO, C–B–OU, C–C–OU, C–C–UO, C–B–UO and C–C–UU as it is adversely affected by shear failure. Unlike the other continuous slabs the CSA–02 and ISIS–07 equations provided the closet prediction to the experimental moment capacity of the slabs C–B–OO at both the mid-span and middle support sections and C–B–UU at the mid-span section (see Tables 5–2 and 5–3).

Table 5–1: Details of experimental and ACI 440–06 moment capacity results

Slab notation	Experimental Failure moment, M_{exp}: kN.m		ACI 440.1R–06 Failure moment, M_{pre}: kN.m		$\frac{M_{exp}}{M_{pre}}$	
	Sagging	*Hogging*	*Sagging*	*hogging*	*sagging*	*Hogging*
C–B–OO	34.17	29.16	38.10	38.10	0.89	0.76
C–B–OU	27.25	15.56	38.10	22.33	0.71	0.69
C–B–UO	15.76	33.48	22.33	38.10	0.70	0.88
C–B–UU	22.81	18.41	22.33	22.33	1.02	0.82
S–B–O	41.97	N/A	38.86	N/A	1.10	N/A
S–B–U	20.22	N/A	22.55	N/A	0.90	N/A
C–C–OO	34.74	46.52	63.73	63.73	0.54	0.73
C–C–OU	36.70	26.60	63.73	30.58	0.57	0.87
C–C–UO	18.93	51.64	30.58	63.73	0.62	0.81
C–C–UU	22.12	38.26	30.58	30.58	0.72	1.25
S–C–O	57.50	N/A	63.73	N/A	0.90	N/A
S–C–U	29.50	N/A	30.58	N/A	0.96	N/A
Average					0.80	0.85

Table 5–2: Details of experimental and ISIS–07 moment capacity results

Slab notation	Experimental Failure moment, M_{exp}: kN.m		ISIS–07 Failure moment, M_{pre}: kN.m		$\frac{M_{exp}}{M_{pre}}$	
	Sagging	*Hogging*	*Sagging*	*hogging*	*sagging*	*Hogging*
C–B–OO	34.17	29.16	29.69	29.69	1.15	0.98
C–B–OU	27.25	15.56	29.69	24.37	0.91	0.63
C–B–UO	15.76	33.48	24.37	29.69	0.64	1.12
C–B–UU	22.81	18.41	24.37	24.37	0.93	0.75
S–B–O	41.97	N/A	29.69	N/A	1.41	N/A
S–B–U	20.22	N/A	24.37	N/A	0.82	N/A
C–C–OO	34.74	46.52	53.96	53.96	0.64	0.86
C–C–OU	36.70	26.60	53.96	30.81	0.68	0.86
C–C–UO	18.93	51.64	30.81	53.96	0.61	0.95
C–C–UU	22.12	38.26	30.81	30.81	0.71	1.24
S–C–O	57.50	N/A	53.96	N/A	1.06	N/A
S–C–U	29.50	N/A	30.81	N/A	0.95	N/A
Average					0.87	0.92

Table 5–3: Details of experimental and CSA S806–02 moment capacity results

Slab notation	Experimental Failure moment, M_{exp}: kN.m		CSA S806–02 Failure moment, M_{pre}: kN.m		$\frac{M_{exp}}{M_{pre}}$	
	Sagging	*Hogging*	*Sagging*	*Hogging*	*sagging*	*Hogging*
C–B–OO	34.17	29.16	32.36	32.36	1.05	0.90
C–B–OU	27.25	15.56	32.36	23.24	0.84	0.66
C–B–UO	15.76	33.48	23.24	32.36	0.67	1.03
C–B–UU	22.81	18.41	23.24	23.24	0.98	0.79
S–B–O	41.97	N/A	32.36	N/A	1.29	N/A
S–B–U	20.22	N/A	23.24	N/A	0.87	N/A
C–C–OO	34.74	46.52	59.54	59.54	0.58	0.78
C–C–OU	36.70	26.60	59.54	30.16	0.61	0.88
C–C–UO	18.93	51.64	30.16	59.54	0.62	0.86
C–C–UU	22.12	38.26	30.16	30.16	0.73	1.26
S–C–O	57.50	N/A	59.54	N/A	0.96	N/A
S–C–U	29.50	N/A	30.16	N/A	0.97	N/A
Average					0.85	0.89

5.3 Failure load predictions

Based on the brittle nature of FRP bars and concrete, the predicted mid-span failure load P of the continuous FRP reinforced concrete slabs would be obtained from the lower load that causes the achievement of the moment capacity at either middle support (M_h=0.188PL) or mid-span (M_s=0.156PL) section. While, the predicted failure load P of the simple FRP reinforced concrete slabs is calculated from the load that causes the accomplishment of the moment capacity at mid-span section (P=4M_s/L), where M_s and M_h are the moment capacities at mid-span and middle support sections calculated using design codes equations and L is the slab span.

5.3.1 Failure load predictions for the FRP Reinforced concrete slabs

Comparisons between the load capacity calculated from the three different design codes and experimental results of the slabs tested are listed in Table 5–4. The ratio of the experimental to predicted failure loads ranged between 0.91 to 1.18 for BFRP slabs

using ACI 440–06 equations. Overall, load predictions were in far much better agreement with the measured failure loads of all slabs tested than the moment capacity predictions of the mid-span and over support sections. This may be attributed to the brittle failure of BFRP reinforced concrete slabs in such a way that as soon as one section reaches its moment capacity, the whole slab fails without any moment redistribution. Conversely, for CFRP reinforced concrete slabs C–C–OO, C–C–UO and S–C–O was much less in comparison to load predictions and that of slab C–C–OU was, however, much higher. On the other hand, load predictions of slabs C–C–UU and S–C–U reasonably compared with the measured failure loads. The CSA–02 and ISIS–07 equations for estimating the load capacity of slabs S–C–U, S–C–O, C–B–UU and C–C–UU were very good, while for other slabs, these equations give reasonable predictions as shown in Table 5–4.

Table 5–4: Details of experimental and design codes results

Slab notation	Experimental failure load, P_{exp}: kN	ACI 440.1R–06		ISIS–07		CSA S806–02	
		Prediction failure load, P_{pre}: kN	$\frac{P_{exp}}{P_{pre}}$	Prediction failure load, P_{pre}: kN	$\frac{P_{exp}}{P_{pre}}$	Prediction failure load, P_{pre}: kN	$\frac{P_{exp}}{P_{pre}}$
C–B–OO	97.5	101	0.96	78.96	1.23	86.06	1.13
C–B–OU	70	59.4	1.18	64.81	1.08	61.81	1.13
C–B–UO	65	71.5	0.91	78.10	0.83	74.49	0.87
C–B–UU	64	59.4	1.07	64.81	0.98	61.81	1.03
S–B–O	84.8	83.9	1.01	59.38	1.42	64.72	1.31
S–B–U	42.0	40.4	1.04	48.74	0.86	46.48	0.90
C–C–OO	116	169.5	0.68	143.51	0.80	158.35	0.73
C–C–OU	100	81.33	1.23	81.94	1.22	80.21	1.24
C–C–UO	89.5	98.01	0.91	98.75	0.90	96.66	0.92
C–C–UU	82.5	81.33	1.01	81.94	1.00	80.21	1.02
S–C–O	115	127.5	0.90	107.92	1.06	119.08	0.96
S–C–U	59	61.16	0.96	61.62	0.95	60.32	0.97
Average			0.98		1.03		1.01

5.4 Deflection models

In this section, three design guidelines, namely ACI 440.1R–06, ISIS–M03–07, CSA S806–02, are employed to predict the mid-span deflections of slabs tested. ACI 440 1R–06 provided an expression for the effective moment of inertia, I_e, to be used for calculating the mid-span deflection of FRP reinforced concrete elements as in Eq. (5–11) below:

$$I_e=\left(\frac{M_{cr}}{M_a}\right)^3 \beta_d I_g+\left(1-\left(\frac{M_{cr}}{M_a}\right)^3\right) I_{cr} \leq I_g \tag{5–11}$$

where M_{cr} is the cracking moment of the member cross-section, M_a is the applied moment, $\beta_d\left(=0.2\rho_f/\rho_{fb}\leq 1\right)$ is a reduction factor, $I_g\left(=bh^3/12\right)$ is the gross section moment of inertia, b and h are the width and overall depth of the slab, respectively, $I_{cr}\left(=\left(bd^3/3\right)k^3+n_f A_f d^2\left(1-k\right)^2\right)$ is the transformed cracked moment of inertia, where $k\left(=\sqrt{(\rho_f n_f)^2+\rho_f n_f}-\rho_f n_f\right)$ is the ratio of the neutral axis depth to reinforcement depth, n_f $(=E_f/E_c)$ is the modular ratio of FRP reinforcement with respect to concrete and $E_c\left(=4750\sqrt{f_c'}\text{, in N/mm}^2\right)$ is the concrete modulus of elasticity. Eq. (5–11) is a modified version of Branson's equation developed for steel reinforced concrete elements. On the other hand, ISIS Canadian network design manual introduced a method for predicting the member effective moment of inertia, I_e, for immediate deflection of FRP reinforced concrete elements and slabs as follows:

$$I_e=\frac{I_g I_{cr}}{I_{cr}+\left[1-0.5\left(\frac{M_{cr}}{M_a}\right)^2\right]\left[I_g-I_{cr}\right]} \tag{5–12}$$

Canadian Standards Association recommended the use of Eq. (5–13) below to calculate the effective moment of inertia, I_e, for FRP reinforced concrete members:

$$I_e = \frac{I_{cr}}{1-\left(1-\frac{I_{cr}}{I_g}\right)\left(\frac{M_{cr}}{M_a}\right)^3} \quad (5\text{–}13)$$

The immediate mid-span deflection, Δ, of simple and continuous members under a mid-span point load could be calculated using Eqs. (5–14) and (5–15), respectively, below:

$$\Delta = \frac{1}{48}\left(\frac{PL^3}{E_c I_e}\right) \quad (5\text{–}14)$$

$$\Delta = \frac{7}{768}\left(\frac{PL^3}{E_c I_e}\right) \quad (5\text{–}15)$$

where P is the applied load at mid-span, L is the span length of concrete member and I_e is the effective moment of inertia of the member as calculated from Eqs. (5–11), (5–12) and (5–13) for each code modelling.

5.4.1 Deflection Prediction for BFRP Reinforced concrete slabs

The recommendations ruling the design of FRP reinforced concrete structures currently available are mainly given in the form of modifications to existing steel reinforced concrete codes of practice. Such modifications consist of basic principles, strongly influenced by the mechanical properties of FRP reinforcement, and empirical equations based on experimental investigations on FRP reinforced concrete elements. The experimental deflections of BFRP reinforced concrete slabs tested in the present study are compared against the predictions obtained from the design codes (ACI 440–1R–06, ISIS–M03–07 and CSA S806–06) as shown in Figures 5–1 to 5–6. The deflection predictions obtained from ISIS–M03–07 and CSA S806-06 are in good agreement with the measured mid-span deflections of simple slabs S–B–O and S–B–U for the applied loads up to failure; however, ACI 440 1R–06 predicted slightly stiffer behaviour for the two slabs. Meanwhile, the ISIS–M03–07 and CSA S806–06 codes reasonably predicted the deflection of BFRP continuous slabs C–B–OO, C–B–OU and C–B–UU, with a

steady underestimation of the deflection for loads higher than 70% of each slab's failure load, and accurately predicted the deflection of slab C–B–UO for all stages of loading. On the other hand, it can be seen from Figures 5–3 to 5–6 that ACI 440.1R–06 progressively underestimated the deflections of BFRP reinforced concrete continuous slabs at loads higher than the cracking load.

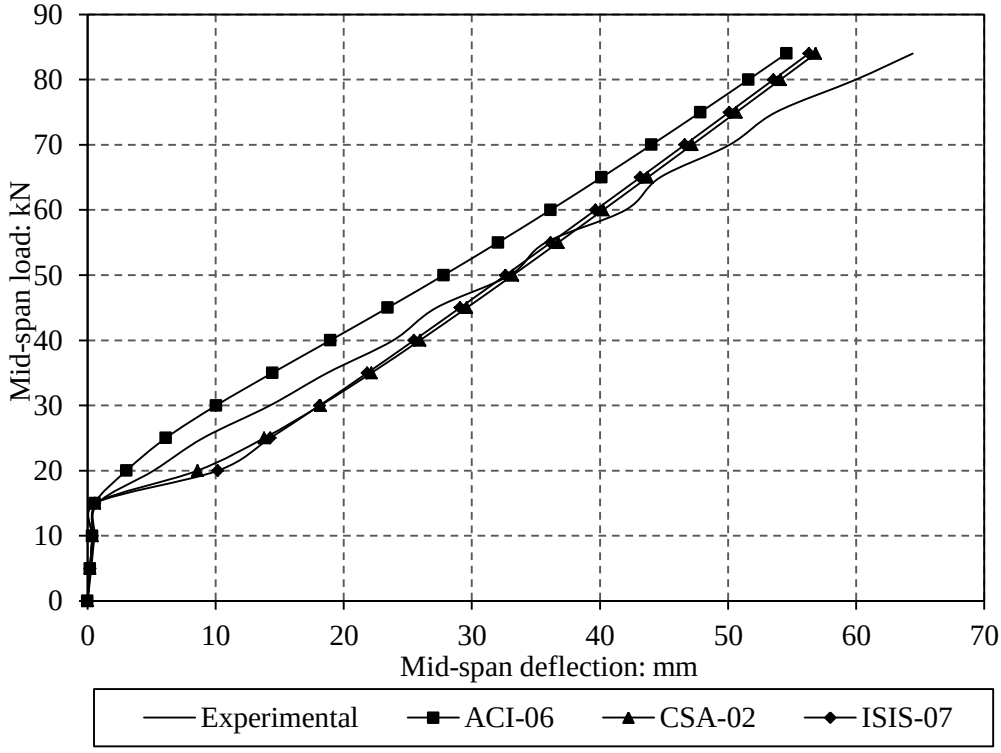

Figure 5–1: Experimental and predicted deflections for slab S–B–O

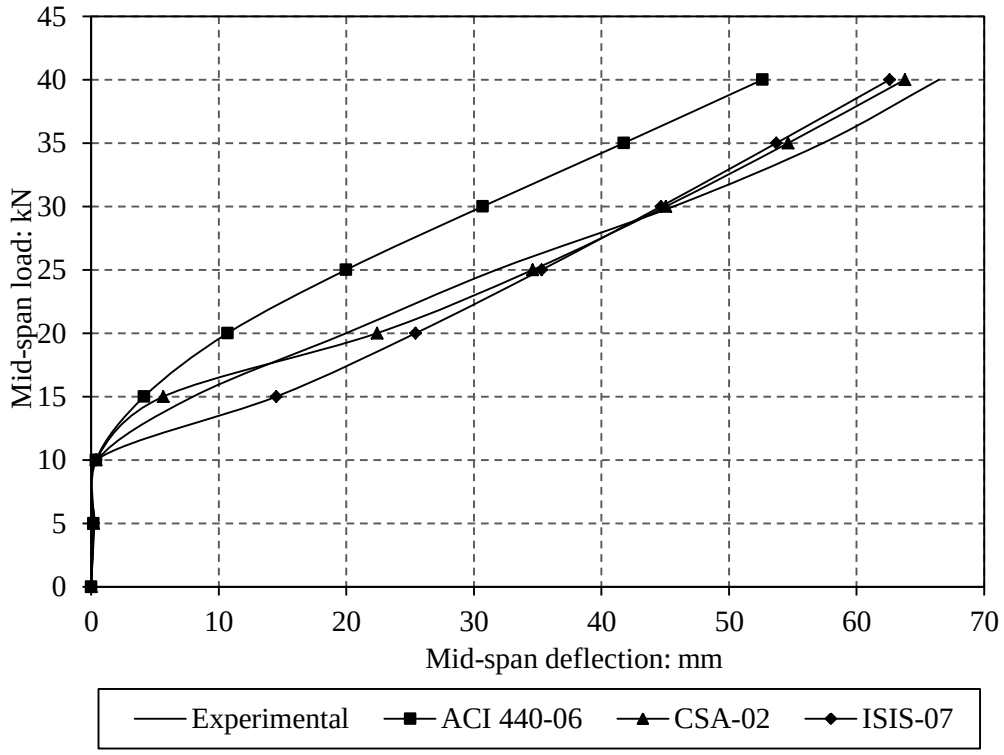

Figure 5–2: Experimental and predicted deflections for slab S–B–U

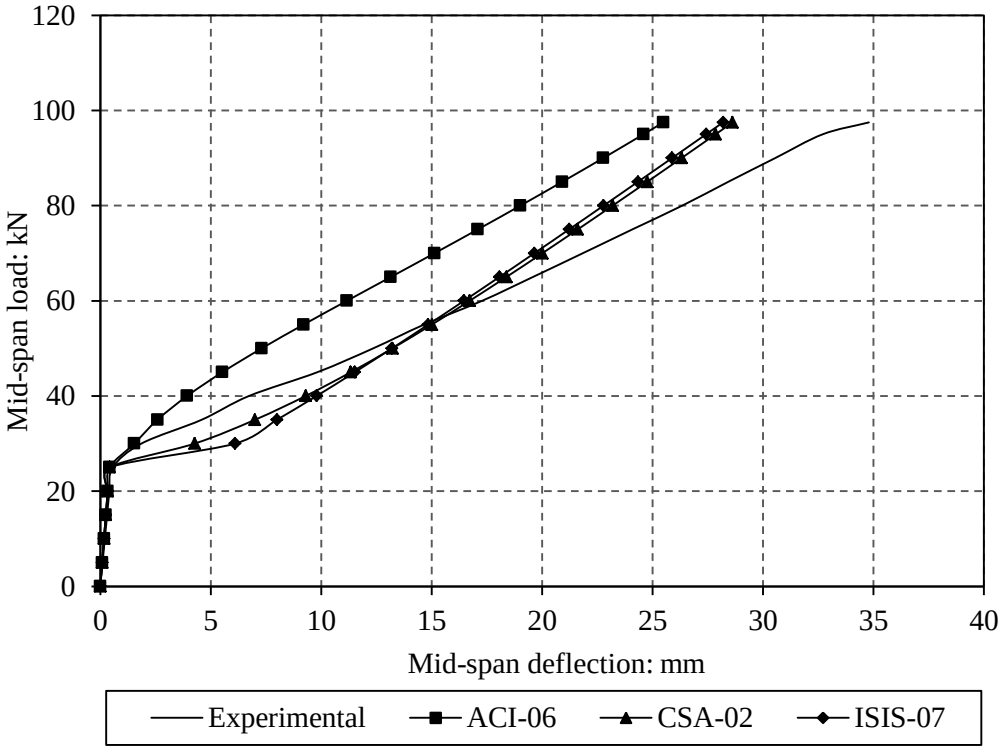

Figure 5–3: Experimental and predicted deflections for slab C–B–OO

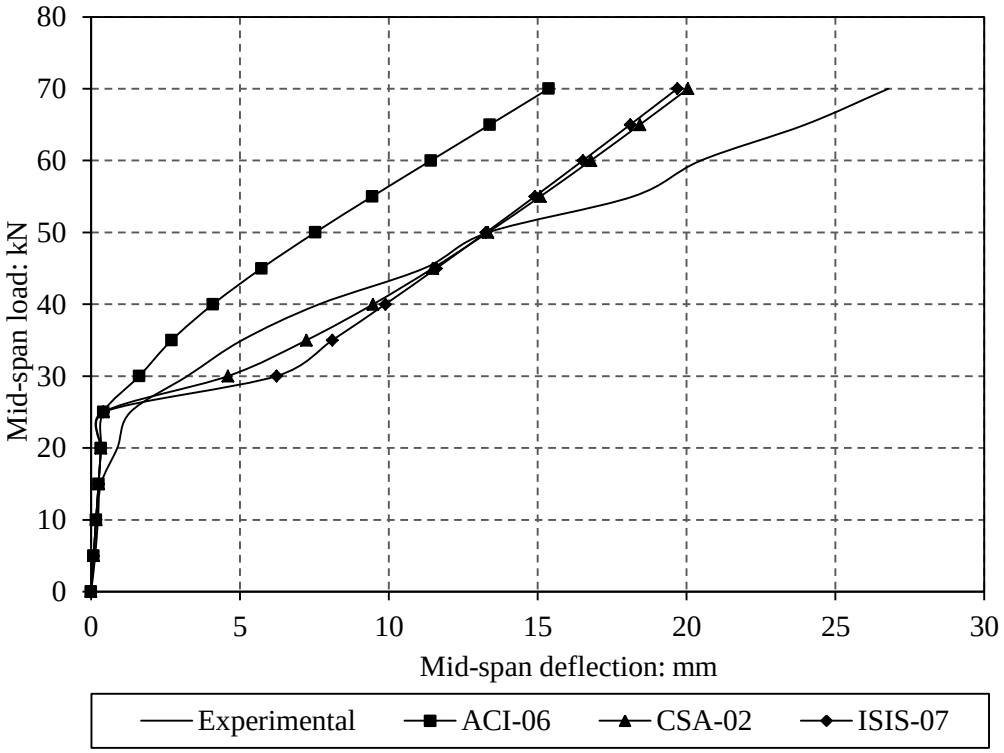

Figure 5–4: Experimental and predicted deflections for slab C–B–OU

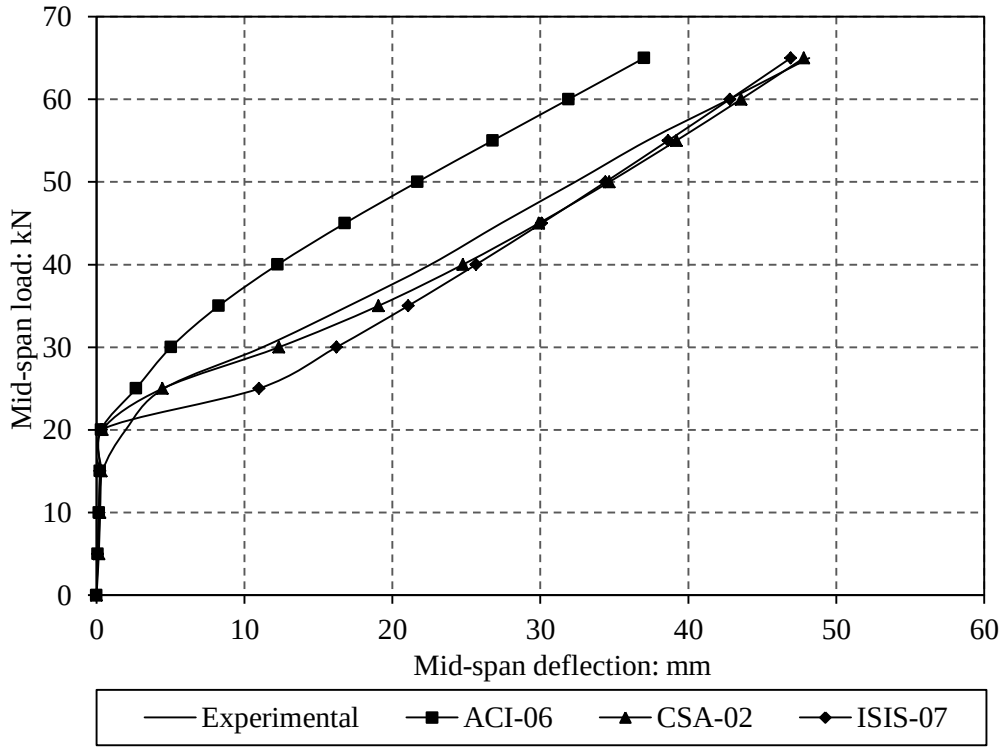

Figure 5–5: Experimental and predicted deflections for slab C–B–UO

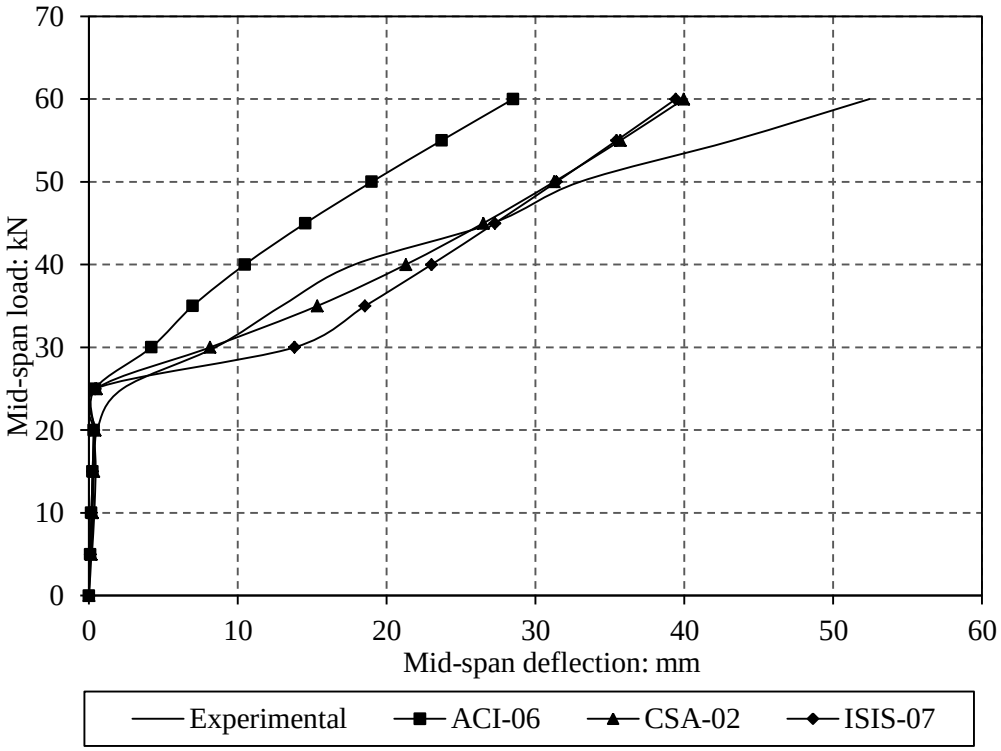

Figure 5–6: Experimental and predicted deflections for slab C–B–UU

5.4.2 Deflection Prediction for the CFRP Reinforced concrete slabs

The deflection results obtained from the design codes are in good agreement with the measured mid-span deflections of simply supported slabs S–C–O and S–C–U, with a steady underestimation of the deflection at high loads (see Figures 5–7 and 5–8). Meanwhile, using the same codes for CFRP continuous slabs C–C–OO and C–C–OU, give a closer deflection to that experimentally measured at early stages of loading, but as the load increased, the prediction process for these slabs has shown a stiffer trend as presented in Figures 5–9 and 5–10. Such discrepancies could be referred to wide cracks that were developed over the middle support of both continuous slabs due to the loss of bond between CFRP top reinforcement and concrete as reported in (Ashour and Habeeb 2008, Habeeb and Ashour 2008, El–Mogy et al. 2010). On the other hand, these codes give a better prediction of deflections for under-reinforcing the bottom layer of CFRP continuous slabs C–C–UO and C–C–UU as shown in Figures 5–11 and 5–12.

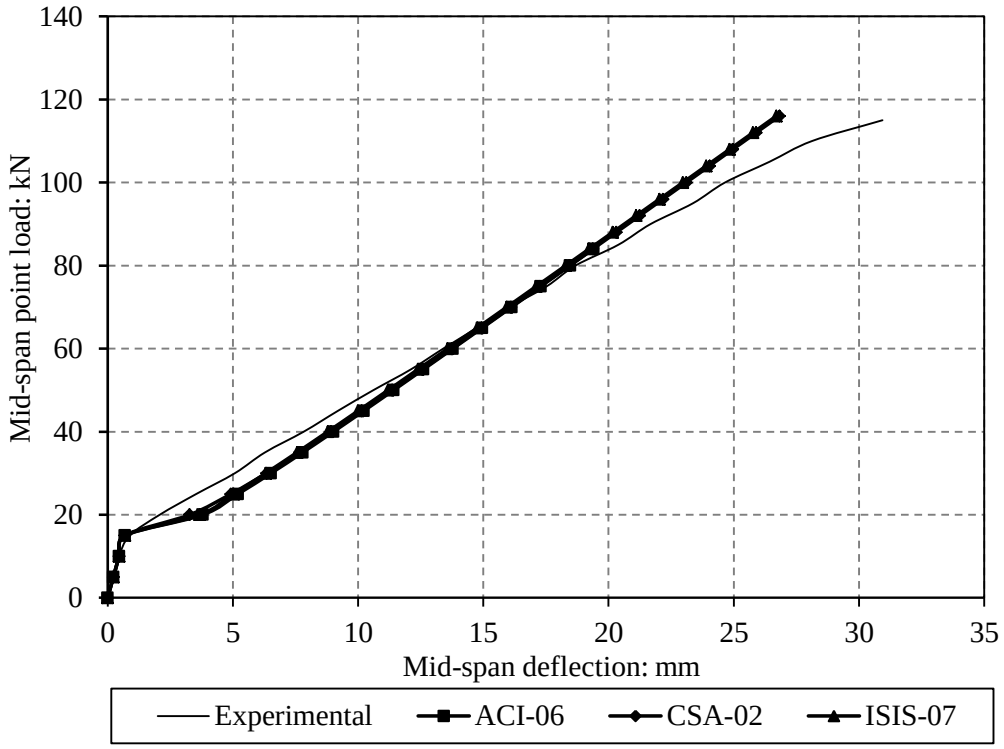

Figure 5–7: Experimental and predicted deflections for slab S–C–O

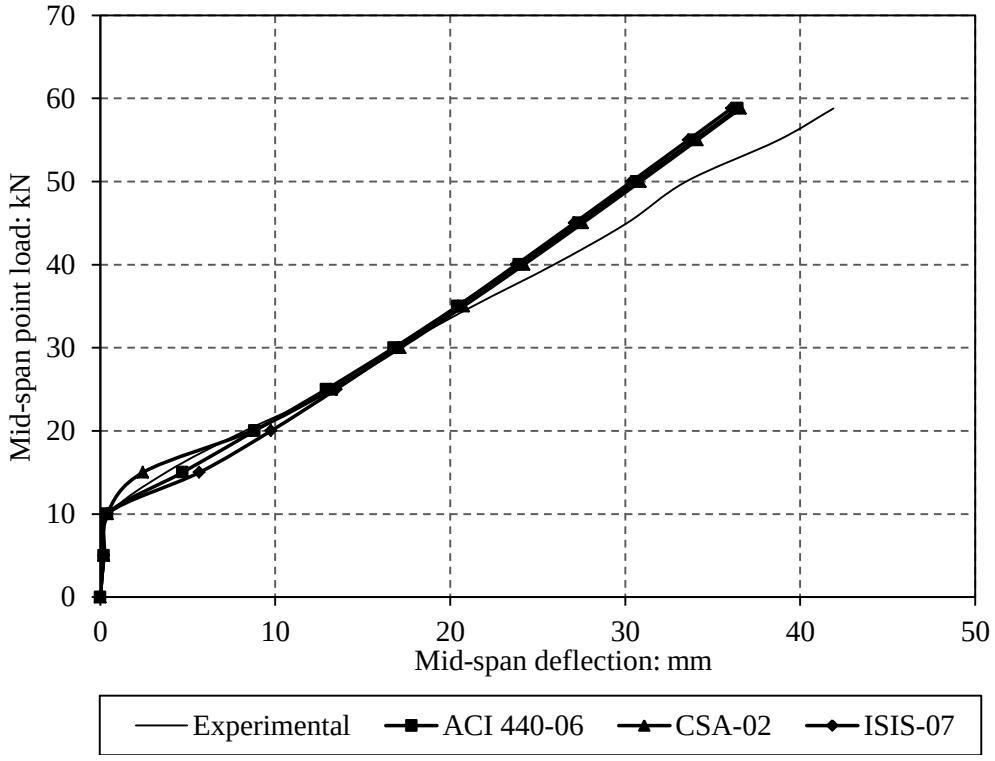

Figure 5–8: Experimental and predicted deflections for slab S–C–U

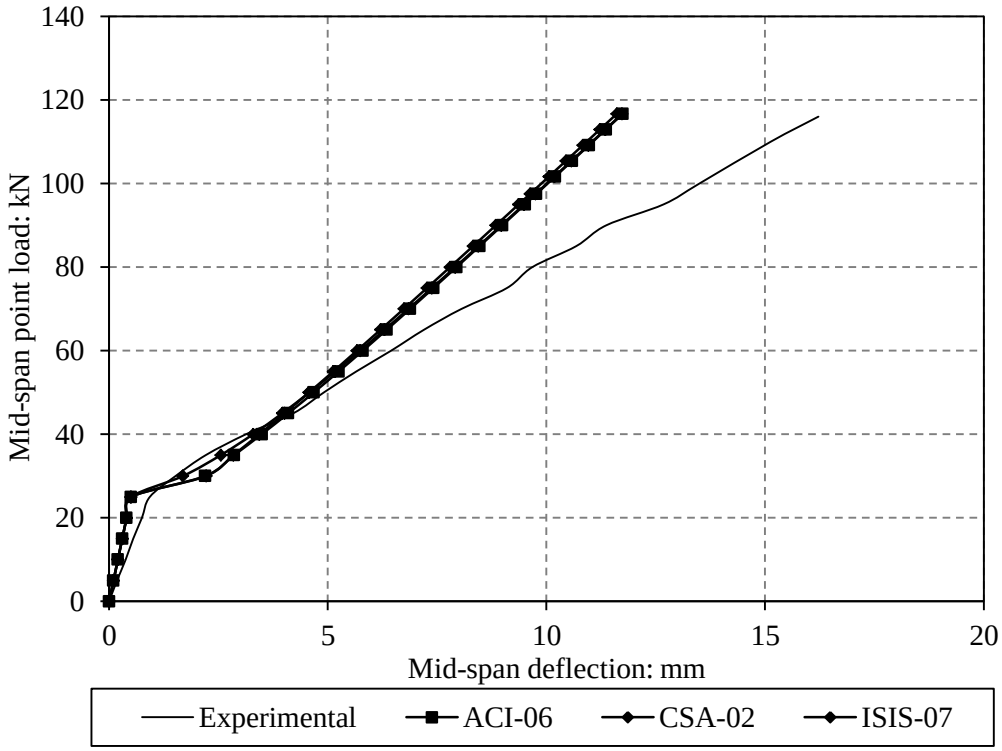

Figure 5–9: Experimental and predicted deflections for slab C–C–OO

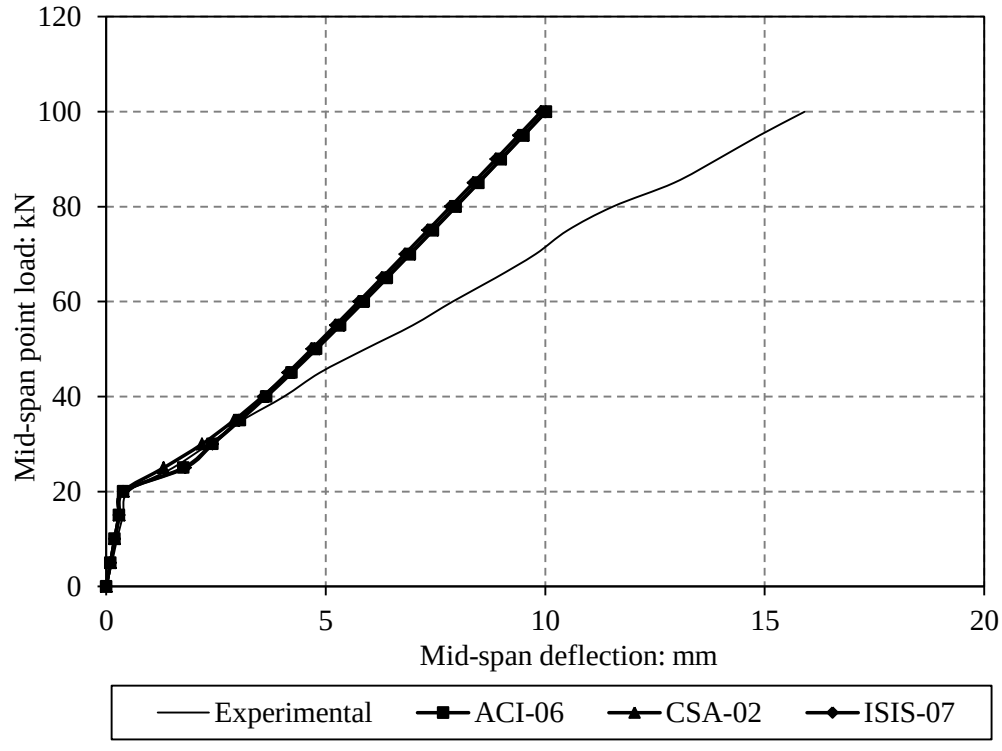

Figure 5–10: Experimental and predicted deflections for slab C–C–OU

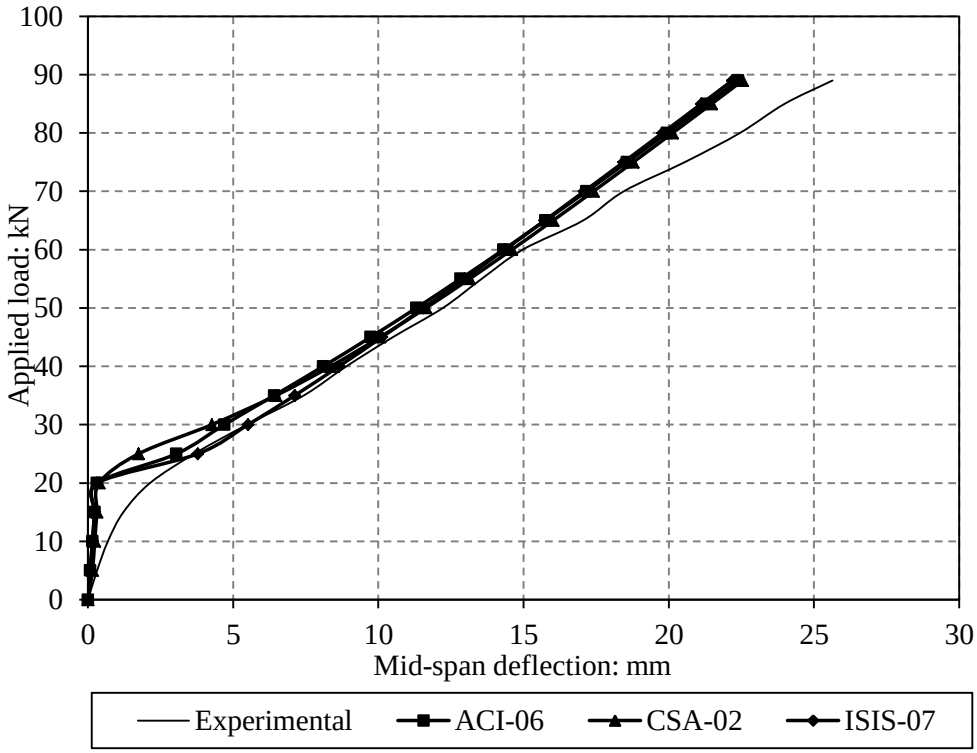

Figure 5–11: Experimental and predicted deflections for slab C–C–UO

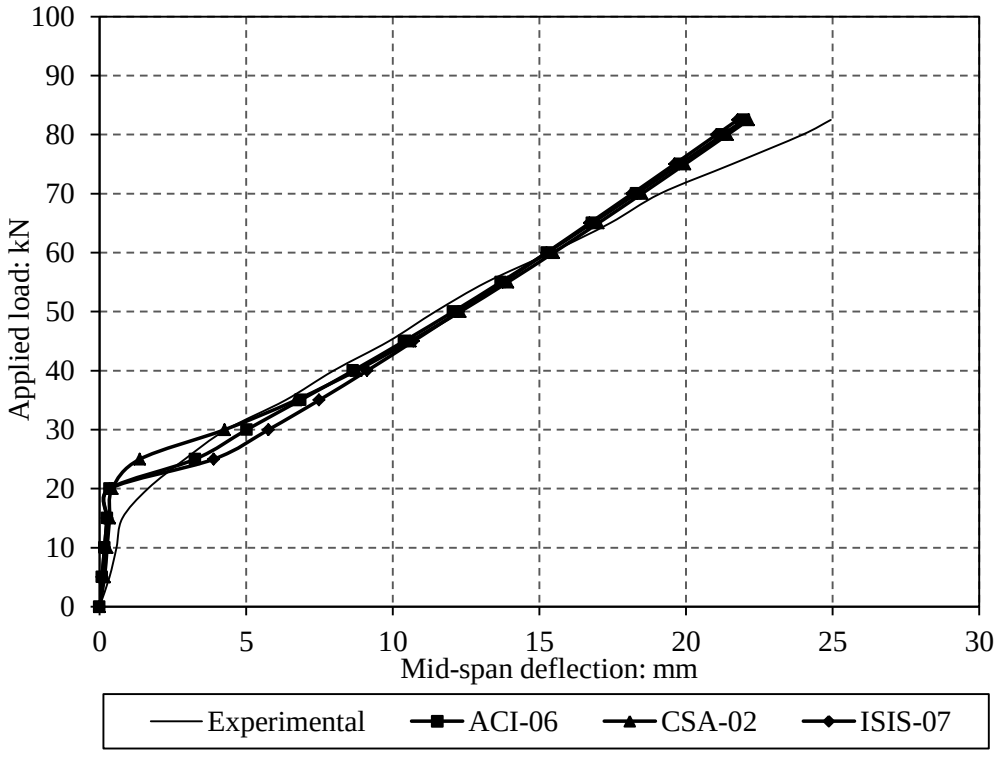

Figure 5–12: Experimental and predicted deflections for slab C–C–UU

5.5 Theoretical predictions of shear capacity

FRP-reinforced concrete elements demonstrate reduced shear strength compared with the shear strength of those reinforced with the same amounts of steel reinforcement owing to the relatively low modulus of elasticity of FRP bars as supported by several studies in the literature (Tottori and Wakui 1993, Yost and Dinehart 2001, and El-sayed et al. 2006). A number of design code (ACI 440.1R-06, ISIS 2007, CSA S806-02) formulas have been developed for shear capacity of FRP-reinforced concrete members. Some investigations concluded that shear design codes are conservative in predicting the shear capacity of simply supported FRP-reinforced concrete members (Ashour 2006, Machial et al. 2010, El-Sayed et al. 2004, 2005a, b, c, Razaqpur et al. 2004, Gross et al. 2004, Tureyen and Frosch 2002 and Wegian and Abdalla 2005).

The ACI 440.1R–06 design code formula for shear capacity of FRP-reinforced concrete members without stirrups is based on the model of Tureyen and Frosch (2002, 2003). According to this model, the axial stiffness of the longitudinal FRP reinforcement is taken into account through the depth of the concrete in compression. The concrete shear strength, $V_{c,f}$, of flexural members with FRP reinforcement is then evaluated according to the following formula:

$$V_{c,f} = \frac{2}{5}\sqrt{f_c'}\, b_w C \tag{5–16}$$

where

$$C = kd \tag{5–17}$$

$$k = \sqrt{\left(2\rho_f n_f + (\rho_f n_f)^2\right)} - \rho_f n_f \tag{5–18}$$

$$n_f = \frac{E_f}{E_s} \tag{5–19}$$

The shear strength of reinforced concrete members without stirrups, such as slabs and beams with the effective depth lower than 300 mm are predicted based on ISIS design code formula below:

$$V_{c,f} = 0.2 b_w d \sqrt{f'_c \frac{E_f}{E_s}} \qquad for\ d \le 300\ mm \qquad (5\text{–}20)$$

On the other hand, the concrete shear strength presented by CSA-S806-02 code is given by the following equation:

$$V_{c,f} = 0.035 b_w d \left(f'_c \rho_f E_f \frac{V_f d}{M_f} \right)^{1/3} \qquad for\ d \le 300\ mm \qquad (5\text{–}21)$$

such that:

$$0.1\ b_w d \sqrt{f'_c} \le V_{c,f} \ge 0.2 b_w d \sqrt{f'_c} \qquad (5\text{–}22)$$

5.5.1 Theoretical predictions of shear capacity of BFRP Reinforced Concrete Slabs

The experimental shear capacities of BFRP-reinforced continuous concrete slabs measured in the current investigation are compared against the predictions from the previous design codes as shown in Figure 5–13. The ACI 440–06 formula significantly underestimates the shear capacity of all BFRP slabs as shown in Figure 5–13. These findings are in general agreement with numerous other studies (Yost et al. 2001, Tureyan and Frosch 2002 and Ashour 2006). The same figure also shows that the CSA–02 steady underestimate of the shear capacities of these slabs tested in the existing study. However, the experimental shear capacities are much less than those calculated from the ISIS–07 formula for slabs C–B–OO and C–B–UO, while the experimental shear capacities of slabs C–B–OU and C–B–UU agreed with those calculated from the ISIS–07 equation (see Figure 5–13).

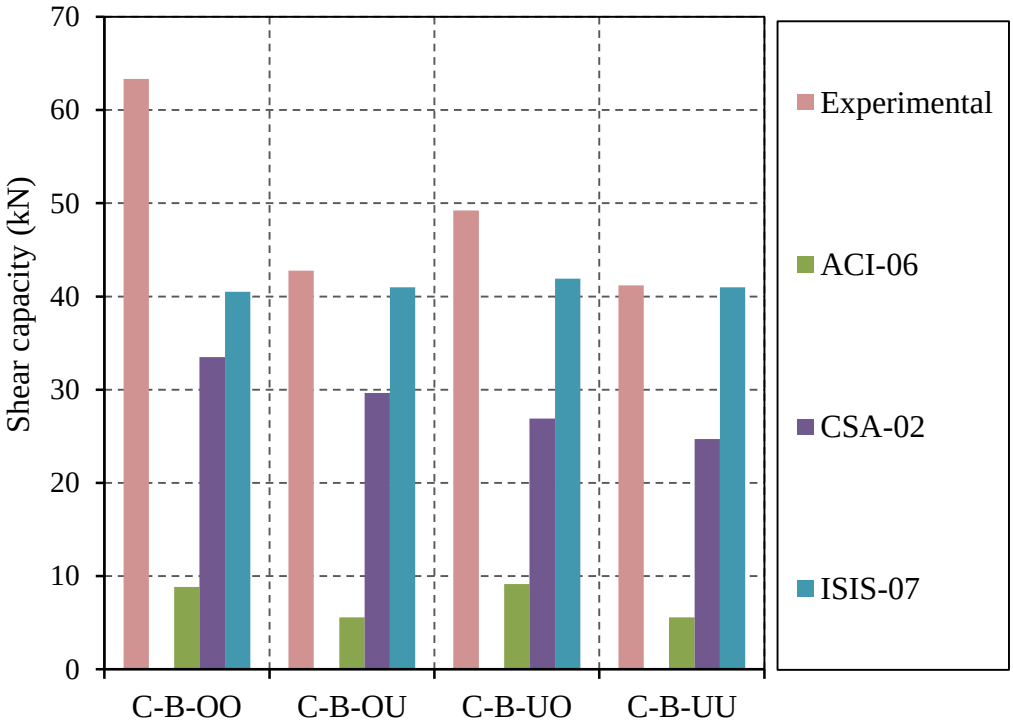

Figure 5–13: Comparisons between shear resistance obtained from experimental and different design equations for BFRP-reinforced concrete slabs

5.5.2 Theoretical predictions of shear capacity of CFRP Reinforced Concrete Slabs

Figure 5–14 presents comparisons between experimental shear capacities of CFRP reinforced concrete continuous slabs tested and those predicted by the previous design codes as given in Eqs. 5–16, 5–20 and 5–21. The ACI 440–06 and CSA-02 equations are clearly underestimate the shear capacity of all CFRP slabs as given in Figure 5–14. However, the ISIS–07 equations seem to be effective in calculating the shear capacity of slabs C–C–UO and C–C–OU, with underestimation of shear capacity of slab C–C–OO. These equations give a slight steady overestimation for predicting the shear capacity of continuous CFRP reinforced concrete slab C–C–UU. Finally, ACI 440–06 provided the lowest prediction to the experimental shear capacity of all the methods, whereas, ISIS–07 equations could reasonably predict the shear capacity of continuous slabs.

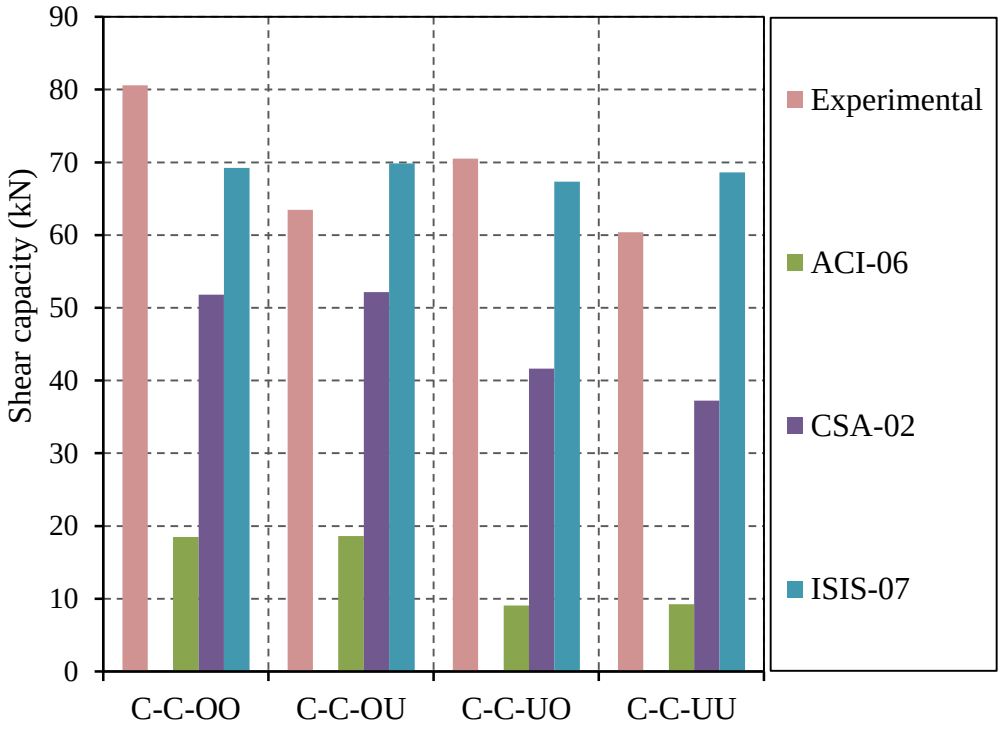

Figure 5–14: Comparisons between shear resistance obtained from experimental and different design equations for CFRP-reinforced concrete slabs

5.6 Conclusion

The main conclusions drawn from the work discussed in this chapter are summarised below:

- The ACI 440.1R–06 equations overestimated the experimental failure moment in most continuous CFRP and BFRP reinforced concrete slabs tested. This may be attributed to the shear effect combined with flexure at failure.
- ISIS–M03–07 and CSA S806-06 reasonably predicted the deflections of BFRP and CFRP simple slabs tested, whereas ACI 440–1R-06 showed slight under-estimation of the deflections of BFRP simple slabs.
- The ACI 440.1R–06, ISIS–M03–07 and CSA S806-06 design code equations seem to be effective in predicting the deflection of BFRP continuously supported concrete

slabs before the occurrence of excessive cracks over the middle support. Further to that, the prediction process has been negatively affected.

- The ACI 440.1R–06, ISIS–M03–07 and CSA S806-06 design code equations reasonably predicted the deflections of the under-reinforced at the bottom layer CFRP continuously supported slabs. However, for the over-reinforced at the bottom layer CFRP continuously supported concrete slabs, the prediction process has been unconstructively affected by the excessive cracks occurred over the middle support of these slabs, especially at higher loading stages.
- The ACI 440-06 and CSA-02 equations significantly underestimate the shear capacity of all BFRP and CFRP slabs. On the other hand, ISIS-07 formulas could mostly reasonably predict the shear capacity of BFRP and CFRP reinforced continuous slabs with a slight under-estimation for over-reinforced at both the bottom and top layers BFRP and CFRP concrete slabs.

CHAPTER SIX

NUMERICAL MODELLING OF FRP CONCRETE REINFORCED MEMBERS

6.1 Introduction

In this chapter, the analytical modelling program is developed to investigate the behaviour of simply and continuously supported FRP reinforced concrete members. The constitutive laws of materials including stress-strain relationships of concrete and FRP reinforcing bars are first discussed. The numerical technique proposed in this research consists of two parts, namely a sectional analysis and a longitudinal analysis. The first part of the program is devoted to producing the moment-curvature relationship of sections reinforced with FRP bars. In addition, the second part of the program is employed to producing the longitudinal analysis of reinforced concrete simple and continuous slabs reinforced with FRP bars. Hence, the influence of design parameters such as the type of FRP reinforcing bars, the tensile FRP reinforcement ratio and the concrete compressive strength on the flexural performance of FRP reinforced concrete slabs could be studied.

Finally, the moment capacities and mid-span deflections predicted by the proposed numerical technique will be compared with the experimental results presented in chapters three and four and test results of FRP concrete members collected from previous experimental studies.

6.2 Moment-Curvature of FRP Reinforced Concrete Sections

6.2.1 Constitutive Models of Materials

6.2.1.1 Constitutive Model for Concrete in Compression

Figure 6–1 shows a typical stress-strain relationship used by Park and Paulay (1975), which is adopted for concrete in uniaxial compression. In the early stages of loading (*A*–*B*), the stress-strain relationship of the concrete can essentially be considered linear. After this stage, the curve becomes no-linear and increases gradually up to the maximum compressive strength (*C*). Immediately after reaching the mentioned peak point (*C*), the slope of the curve reverses as the stress linearly decreasing while the strain continues to increase up to failure load (*D*). This fact has been reported by Bangash (2001).

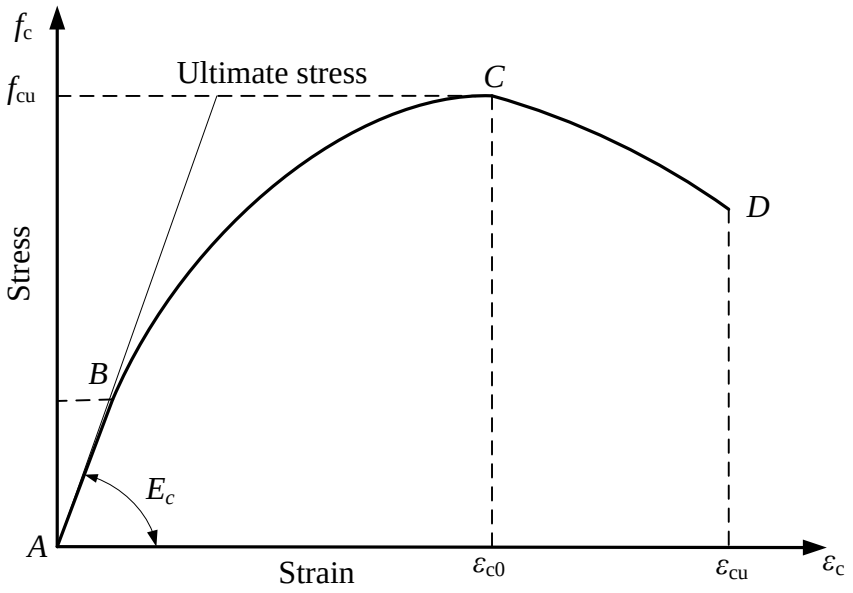

Figure 6–1: Stress–strain relationship for concrete in compression (Park & Paulay, 1975)

The mentioned stress-strain relationship, which has been originally developed by Hognestad (1955), could be written mathematically as below:

Region (A–C) $$\frac{f_c}{f_{cu}} = \left(2\frac{\varepsilon_c}{\varepsilon_{c0}} - \left(\frac{\varepsilon_c}{\varepsilon_{c0}}\right)^2\right) \qquad 0 \le \varepsilon_c \le \varepsilon_{c0} \qquad (6\text{–}1)$$

Region (C–D) $$\frac{f_c}{f_{cu}} = \left(1 - 0.15\left(\frac{\varepsilon_c - \varepsilon_{c0}}{\varepsilon_{cu} - \varepsilon_{c0}}\right)\right) \qquad \varepsilon_{c0} < \varepsilon_c \le \varepsilon_{cu} \qquad (6\text{–}2)$$

where f_c and ε_c are the stress and strain in compressive concrete, respectively, f_{cu} is the cube compressive strength of concrete, ε_{c0} $\left(=2.4 \times 10^{-4}\sqrt{f_{cu}}\right)$ is the strain of concrete corresponding to maximum stress, where E_c is the elasticity modulus of concrete and $\varepsilon_{cu}(=0.0035)$ is the ultimate strain of concrete.

6.2.1.2 Constitutive Model for Concrete in Tension

The relative weakness of concrete in tension and the resulting cracking is a fundamental factor affecting the non-linear behaviour of reinforced concrete structures. Before the initiation of the first crack, it is assumed that when concrete is subjected to a tensile stress it behaves like an elastic-brittle material. After cracking, where the average gross strain, ε_t, exceeds the cracking strain, ε_r, the formation of cracks is a brittle process and the concrete strength in the tension-loading direction reduces abruptly after such cracks have formed (Ferreira et al. 2001).

The stress-strain relationship in the initial stages of loading (A'–B') and after cracking (B'–C') is adopted to model concrete in tension as shown in Figure 6–2 and calculated in Eqs. (6–3) and (6–4) respectively, as follows (Belarbi and Hsu, 1994):

Region (A'–B') $$f_t = E_c \times \varepsilon_t \qquad (6\text{–}3)$$

Region (B'–C') $$f_t = f_r\left(\frac{\varepsilon_r}{\varepsilon_t}\right)^{0.4} \qquad (6\text{–}4)$$

where f_t and ε_t are the tensile stress and strain in concrete, respectively, f_r $(=0.62\sqrt{f_c'})$ and ε_r are the ultimate tensile strength and corresponding tensile strain of concrete, respectively.

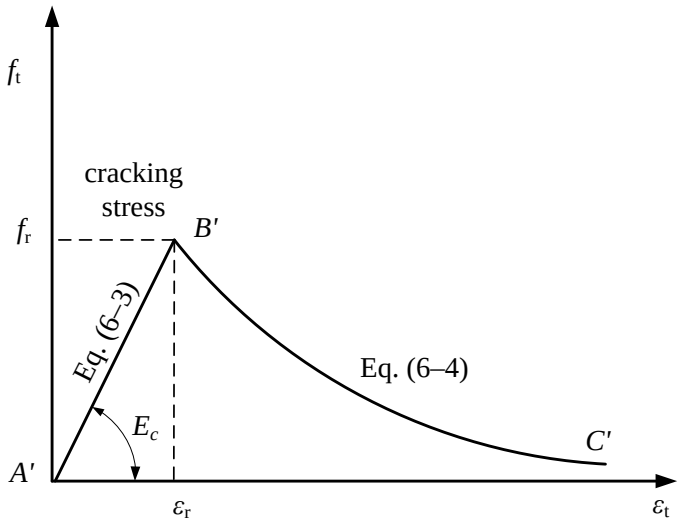

Figure 6–2: Stress-strain curve of tensile concrete

6.2.1.3 Constitutive Model for FRP Reinforcing Bars

FRP re-bars in tension rupture without any yielding due to the non-plastic behaviour of FRP re-bars. FRP re-bars have an almost linear behaviour for the whole regime of loading as shown in Figure (6–3). The stress of FRP composite in tension is given as follows (Benjamin 2002):

$$\text{Region } (A''\text{–}B'') \qquad f_f = E_f \times \varepsilon_f \qquad \varepsilon_f \leq \varepsilon_{fu} \qquad (6\text{–}5)$$

where f_f and ε_f are the stress and strain in FRP bars, respectively, E_f is the modulus of elasticity of FRP bars, and f_{fu} and ε_{fu} are the ultimate strength and strain of FRP bars, respectively, as shown graphically in Figure 6–3.

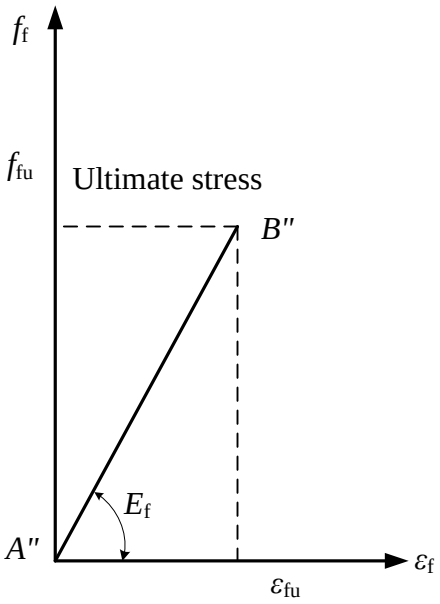

Figure 6–3: Typical stress-strain in tension for FRP reinforcing bars

6.2.2 Moment–Curvature Relationship

The numerical technique is presented to derive the moment-curvature relationship for the rectangular concrete cross-section reinforced with bottom FRP or steel that is divided into a number of segments, *n* as shown in Figure 6–4a. The moment-curvature calculation procedure is summarised as below.

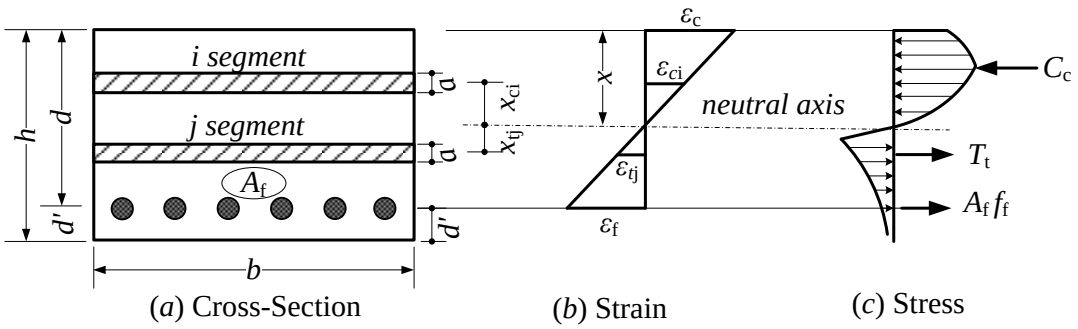

Figure 6–4: Strain and stress distribution in a reinforced section

- The computer model has been developed based on the previous material modelling. A very small proportion of concrete strain, ε_c (or tensile FRP bars, ε_f) and the value of the neutral axis depth (x) are initially assumed as depicted in Figure 6-4b above. According to the equilibrium of internal forces, the correct

value of the neutral axis depth is iteratively obtained. Based on the assumptions that plane section before bending remains plane after bending and bond between FRP bars and surrounding concrete is perfect, the strain in each concrete segment ε_{ci} can be calculated by triangle similarity (see Figure 6–4b) as expressed below:

$$\varepsilon_{ci}=\left(\frac{x_{ci}}{x}\right)\varepsilon_c \tag{6–6}$$

$$\varepsilon_{tj}=\left(\frac{x_{tj}}{d-x}\right)\varepsilon_f \tag{6–7}$$

where ε_c is the top fibre concrete compressive strain of the reinforced concrete section, ε_{ci} is the concrete compressive strain at mid-depth of i segments and ε_{tj} is the concrete tensile strain at mid-depth of j segments.

- According to the previous assumptions, strain in tensile FRP bars can also be obtained from:

$$\varepsilon_f=\left(\frac{d-x}{x}\right)\varepsilon_c \tag{6–8}$$

where ε_f indicates the strain in bottom FRP bars, and d is the FRP reinforcement depth.

- The stresses in concrete segments and FRP reinforcing bars are obtained from the corresponding stress-strain relationship. The summation of the internal forces is:

$$Q=C_c-A_f f_f-T_t\approx 0 \tag{6–9}$$

$$C_c=ab\sum_{i=1}^{n_c} f_{ci} \tag{6–10}$$

$$T_t=ab\sum_{j=1}^{n_t} f_{tj} \tag{6–11}$$

where C_c and T_t are the overall compressive and tensile forces in concrete, respectively as depicted in Figure 6–4c, a ($=h/n$) is the depth of each concrete segment in compression or tension as shown in Figure 6–4a; n_c and n_t are the

number of concrete segment in compression and tension, respectively; *b* and *h* are the width and depth of member, respectively; f_{ci} and f_{tj} are the concrete compressive stress in segment *i*, and concrete tensile stress in segment *j*.

- The value of the neutral axis depth, *x* is iteratively adjusted using the bi-section method and the procedure is repeated until the equilibrium condition of internal forces is satisfied as given below:

$$\frac{\left|C_c - A_f f_f - T_t\right|}{|C_c|} \leq 10^{-4} \qquad (6\text{–}12)$$

The developed numerical technique sets three limits for the neutral axis depth, upper limit, x_1(=0), average limit, x_2(=$h/2$), and lower limit, x_3(=*h*) as shown in Figures 6–5 and 6–6. This technique calculates both compressive and tensile forces, and then these values will be compared. According to the results of the comparison, one of the cases will be taken as bellow:

Case 1: *Total Compressive Force*, C_c > *Total Tensile Force*, F_t

In such case the neutral axis depth is overestimated and is required to be declined according to decrease the value of the compressive force of the section. To decrease the natural axis depth the upper limit, x_1 remains unchanged and the new natural axis depth is $x_2=(x_1+x_2)/2$ but the lower limit x_3 moves to the old position of the natural axis (see Figure 6–5).

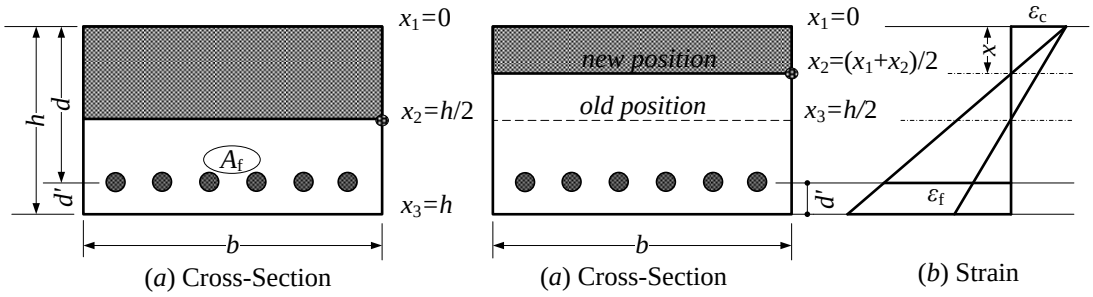

Figure 6–5: Bi-section method for adjusting the neutral axis depth in case of $C_c > F_t$

Case 2: *Total Tensile Force*, F_t>*Total Compressive Force*, C_c

The neutral axis depth is underestimated and is required to be increased according the value of the compressive force of the examined section to achieve the equilibrium condition of the internal force. In such case the new neutral axis depth x_2 is the average of the previous neutral axis depth and the lower limit x_3; (x_2=(x_2+x_3)/2). The upper limit x_1 moves to the previous position of the natural axis whereas the lower limit remains in the same position (see Figure 6–6).

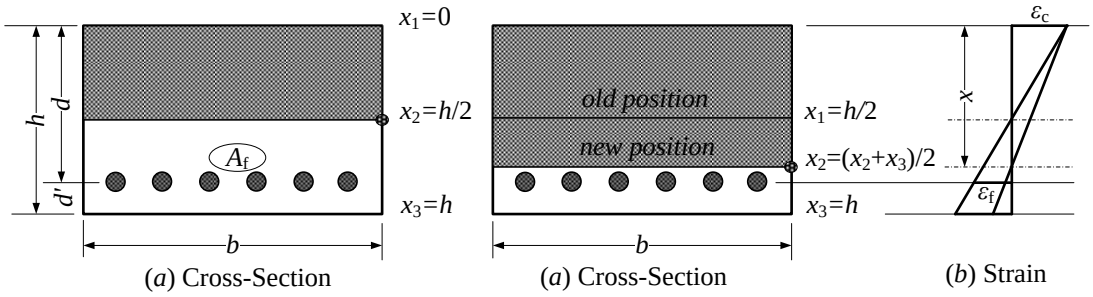

Figure 6–6: Bi-section method for adjusting the neutral axis depth in case of F_t>C_c

- The applied moment M of studied section is computed by taking moments of internal forces about FRP bar reinforcement as the following equation 6–13:

$$M = \sum_{i=1}^{nc} C_{ci} L_{ci} - \sum_{j=1}^{nt} T_{tj} L_{tj} \qquad (6\text{–}13)$$

where L_{ci} is the lever arm for concrete compressive forces C_{ci} in segment i and L_{tj} is the lever arm for concrete tensile forces T_{tj} in segment j.

- The curvature φ of the member is also calculated from the concrete strain and neutral axis depth as given below:

$$\varphi = \varepsilon_c / x \qquad (6\text{–}14)$$

Finally, in this technique, the process of incrementing ε_c and the previous calculation procedure are iteratively repeated to obtain new values of M and φ until the maximum

specified value of section under investigation reaches its ultimate failure strain, either in FRP tensile rupture strain ($\varepsilon_f=\varepsilon_{fu}$) or concrete crushing ($\varepsilon_c=\varepsilon_{cu}$). Hence, the values of moment-curvature calculated in each step will be stored (see Figure 6–7).

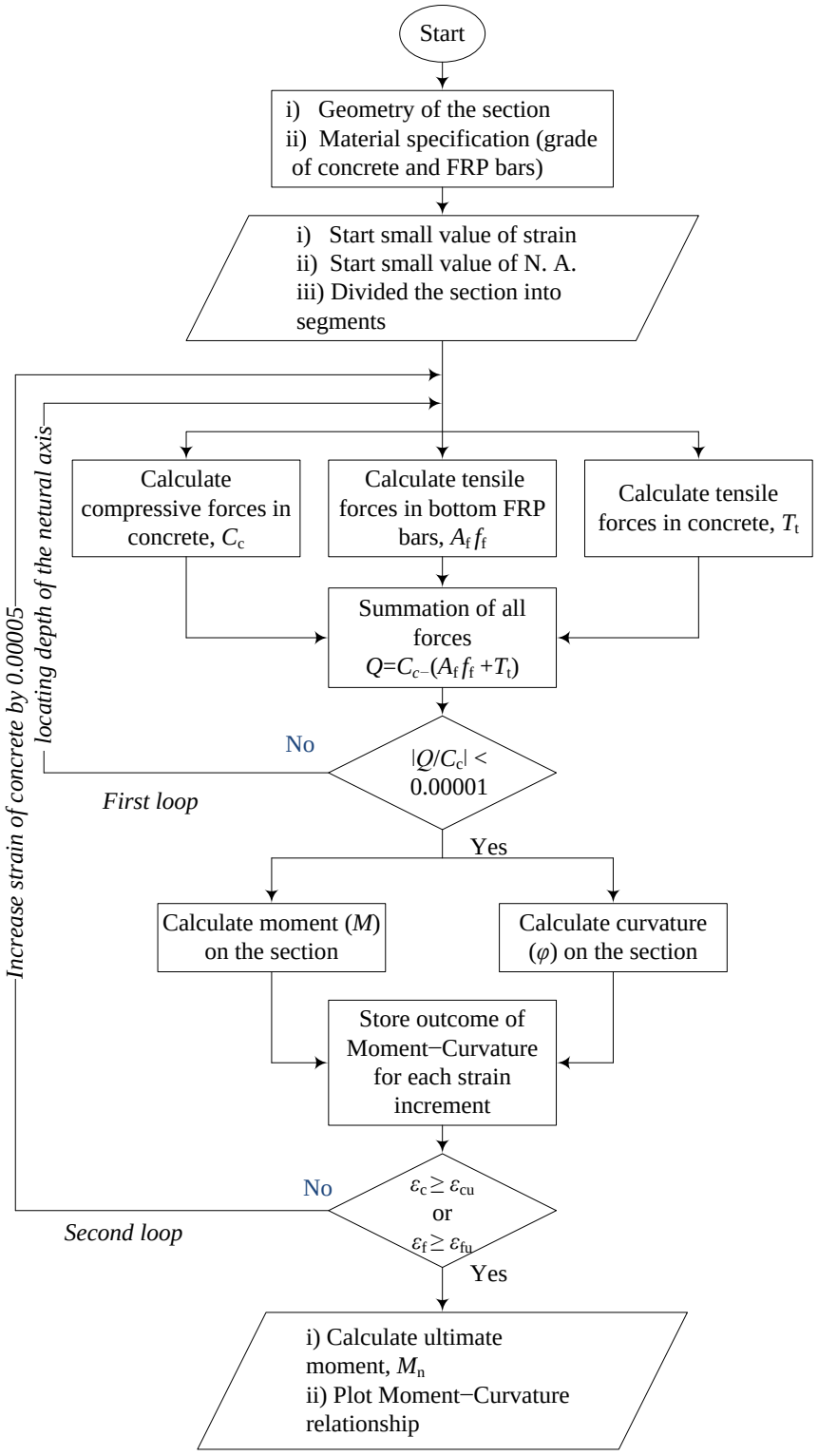

Figure 6–7: Flowchart diagram of the sectional analysis process

6.2.3 Mode of failure prediction

Depending on the type of failure, that is, FRP rupture or concrete crushing, three types of sections can be identified.

6.2.3.1 Balanced reinforcement ratio

The section is called balanced section when the maximum internal strains in the tensile reinforcement (FRP) and the compressive concrete simultaneously reach ultimate strain value. Thus tested section will fail due to concrete crushing (ε_{cu}=0.0035) and FRP reinforcement rupture ($\varepsilon_f=\varepsilon_{fu}$) at the same time. The design procedure for the FRP balanced reinforced section are shown in Figure 6–8 and described below.

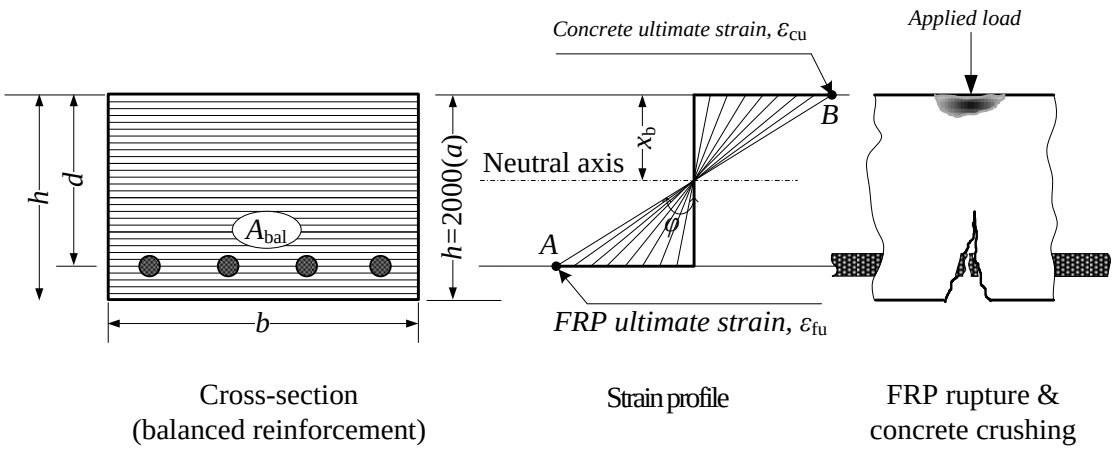

Figure 6–8: Strain and stress distribution in balanced section of slab

By referring the equilibrium status between the internal compression force C_c and the internal tension force T_t, the balanced reinforcement ratio could be then calculated as follow:

$$C_c - T_t + A_{bal} f_{fu} \approx 0 \tag{6–15}$$

$$\rho_{bal} = \frac{(C_c - T_t)}{bd f_{fu}} \tag{6–16}$$

6.2.3.2 Over reinforced section

Failure occurs by crushing of concrete, in such case, the compressive strain in concrete will reach the ultimate strain value, ε_{cu}(=0.0035), meanwhile the tensile strain in FRP reinforcement does not reach its ultimate failure condition, ε_{cu}. Such a condition is accomplished by using reinforcement ratio, $\rho_f = (A_f/bd)$ higher than that required for the balanced reinforced section, ρ_{bal} as shown in Figure 6–9.

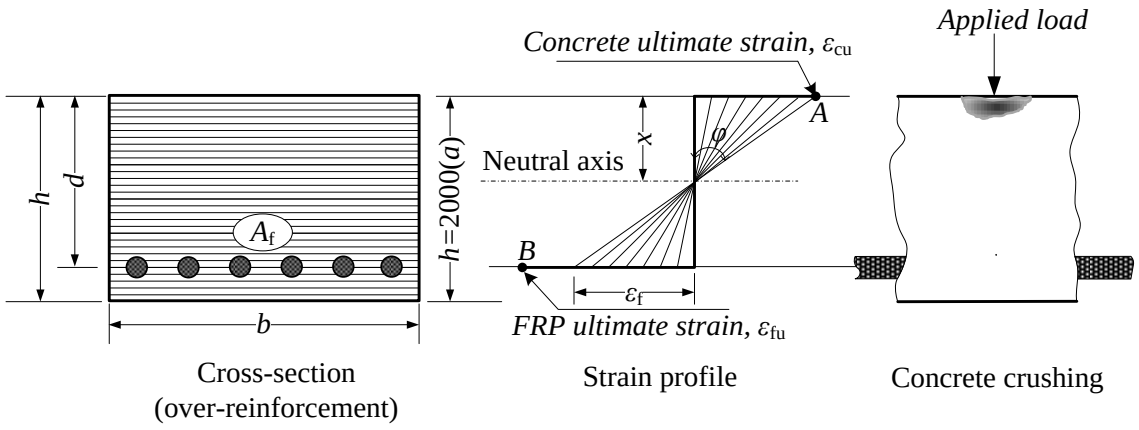

Figure 6–9: Strain and stress distribution in over reinforced section of slab

6.2.3.3 Under reinforced section

Failure occurs by initial rupture of FRP bars, in such case; the tensile strain in FRP reinforcement will reach the ultimate strain value, ε_{fu}, while the compressive strain in concrete does not reach its ultimate failure condition, ε_{cu}(=0.0035). This condition is accomplished when the reinforcement ratio of concrete section used in the slab, ρ_f (=A_f/bd) is less than required for the balanced reinforced section as shown in Figure (6–10).

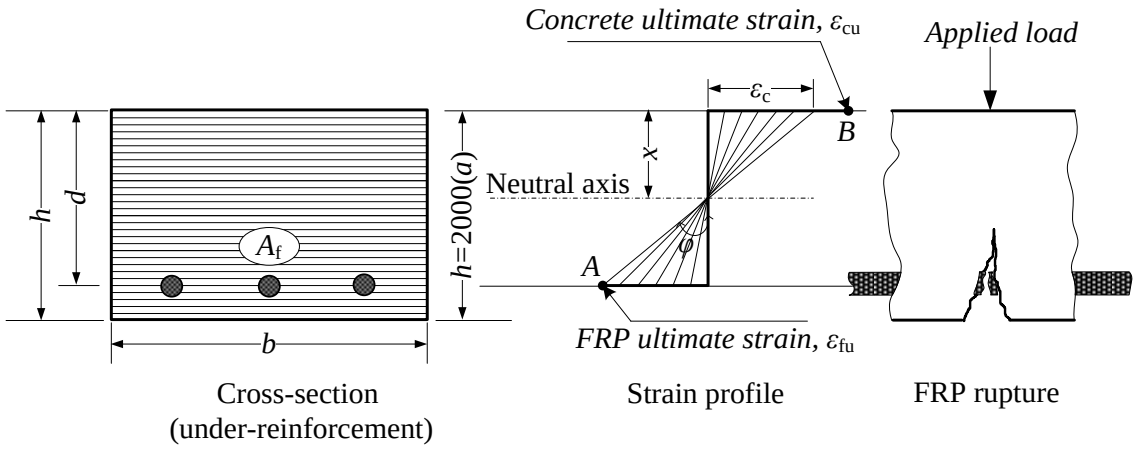

Figure 6–10: Strain and stress distribution in under reinforced section of slab

6.3 Validation of the Analytical Modelling Program against Experimental Results

The validation of current analytical modelling program has been realized by 96 reinforced concrete beams reinforced with FRP bars collected from previous experimental investigations. A comparison between the flexural capacity obtained from the current program and that measured in experiments are used to validate the proposed analytical program as shown in Table 6–1 with two modes of flexural failure were recorded in this table, either tensile rupture of the FRP bars (R) or concrete crushing (C) for all the 96 concrete beams. For all beams, the average and standard deviation of M_{exp}/M_{pre} are 0.98 and %12.6, respectively. Finally, the prediction results obtained from the present technique are in very good agreement with the experimental result.

Table 6–1: Comparisons of the flexural strength and flexural failure mode obtained experiments and the analytical

No.	Member ID	$b \times h$ (mm^2)	ρ_f (%)	f_{cu} (MPa)	M_{exp} (kN.m)	Failure Mode	M_{cur} (kN.m)	$\frac{M_{exp}}{M_{prer}}$
Current research, 2013								
1	S–C–U	500×150	0.24	40	29.50	*R*	30.0	0.98
2	S–C–O	500×150	0.90	40	57.50	*Sh*	65.0	0.88
3	S–B–U	500×150	0.24	40	20.22	*R*	22.5	0.89
4	S–B–O	500×150	0.63	40	41.97	*Sh*	45.0	0.93
Ashour and Habeeb, 2008								
1	C–S–1	300×200	0.42	31.8	64.11	*R*	60.90	1.05
2	C–S–2	300×200	0.16	31.1	44.28	*R*	42.50	1.04
3	C–S–3	300×200	0.16	31.1	44.76	*R*	42.52	1.05
4	C–S–4	300×200	0.42	31.0	60.66	*R*	54.70	1.11
Toutanji and Saafi 2000								
9	GB1–1	300×180	0.52	41.18	60.00	*C*	55.00	1.09
10	GB1–2	300×180	0.52	41.18	59.00	*C*	55.00	1.07
11	GB2–1	300×180	0.79	41.18	65.00	*C*	59.90	1.09
12	GB2–2	300×180	0.79	41.18	64.30	*C*	59.90	1.07
Al-Musallam et al. 1997								
13	COMP–00	240×200	1.33	41.65	41.40	*C*	38.70	1.07
14	COMP–25	240×200	1.33	42.82	38.50	*C*	39.80	0.96
15	COMP–50	240×200	1.33	42.94	39.70	*C*	40.67	0.98
16	COMP–75	240×200	1.33	44.12	48.90	*C*	43.65	1.12
Ashour 2006								
17	Beam2	200×150	0.23	32.56	5.89	*R*	5.96	0.98
18	Beam4	250×150	0.17	32.56	7.85	*R*	8.03	0.97
19	Beam6	300×150	0.14	32.56	10.79	*R*	10.17	1.06
20	Beam8	200×150	0.23	58.93	5.89	*R*	6.04	0.97
21	Beam10	250×150	0.17	58.93	9.48	*R*	8.55	1.10
22	Beam12	300×150	0.28	58.93	16.75	*R*	21.22	0.79
Benmokrane et al. 1996								
23	ISO2	300×200	1.13	50.59	80.40	*C*	88.5	0.90
24	ISO3	550×200	0.57	50.59	181.7	*R*	196.3	0.92
Pecce et al. 2000								
26	F2	500×185	0.7	35.29	36.8	*C*	31.4	1.17
27	F3	500×185	1.22	35.29	60.7	*C*	50.2	1.20
Brown and Bartholomew 1993								
28	1	152×152	0.38	42.24	7.04	*R*	6.43	1.09
29	2	152×152	0.38	43.41	6.64	*R*	6.82	0.97
31	4	152×152	0.38	45.76	7.23	*R*	7.64	0.95
32	5	152×152	0.38	46.94	7.35	*R*	7.85	0.94
33	6	152×152	0.38	48.12	6.75	*R*	8.18	0.82

Table 6–1 (cont.): Comparisons of the flexural strength and flexural failure mode obtained experiments and the analytical

No.	Member ID	$b \times h$ (mm^2)	ρ_f (%)	f_{cu} (MPa)	M_{exp} (kN.m)	Failure Mode	M_{pre} (kN.m)	$\frac{M_{exp}}{M_{pre}}$
Benmokrane et al. 1995								
34	ISO30–2	200×300	1.06	49.41	80.4	*C*	78.5	1.02
35	KD30–1	200×300	1.06	49.41	50.6	*C*	71.7	0.71
36	KD30–2	200×300	1.06	49.41	63.8	*C*	71.7	0.89
37	KD45–1	200×450	0.68	61.18	106.6	*C*	135.4	0.79
38	KD45–2	200×450	0.68	61.18	113	*C*	135.4	0.83
39	ISO55–1	200×550	0.55	49.41	181.5	*R*	178.2	1.02
40	ISO55–2	200×550	0.55	49.41	181.5	*R*	178.2	1.02
41	KD55–1	200×550	0.55	49.41	146.9	*R*	178.2	0.82
42	KD55–2	200×550	0.55	49.41	172.5	*R*	178.2	0.97
Duranovic et al. 1997								
43	GB5	150×250	1.36	31.2	40.3	*C*	34.8	1.16
44	GB9	150×250	1.36	39.8	39.7	*C*	37.5	1.06
45	GB10	150×250	1.36	39.8	39.5	*C*	37.5	1.05
46	GB13	150×250	0.91	43.4	34.7	*C*	29.8	1.16
Al-Sayed 1998								
47	B	200×210	3.6	36.47	36.5	*C*	33.4	1.09
48	C	200×260	1.2	36.47	48.1	*C*	42.7	1.13
49	D	200×250	2.87	48.28	53.98	*C*	48.3	1.11
Masmoudi et al. 1998								
50	CB2B–1	200×300	0.69	61.18	57.9	*C*	70.5	0.82
51	CB2B–2	200×300	0.69	61.18	59.8	*C*	70.5	0.85
52	CB3B–1	200×300	1.04	61.18	66.0	*C*	87.3	0.767
53	CB3B–2	200×300	1.04	61.18	64.8	*C*	87.3	0.74
54	CB4B–2	200×300	1.47	52.94	75.4	*C*	80.8	0.93
55	CB4B–2	200×300	1.47	52.94	71.7	*C*	80.8	0.89
56	CB6B–1	200×300	2.20	52.94	84.8	*C*	96.4	0.88
57	CB6B–2	200×300	2.20	52.94	85.4	*C*	96.4	0.89
Thériault and Benmokrane 1998								
58	BC2HA	130×180	1.24	67.29	19.7	*C*	22.6	0.87
59	BC2HB	130×180	1.24	67.29	20.6	*C*	22.6	0.91
60	BC2VA	130×180	1.24	114.59	22.7	*C*	27.1	0.84
61	BC4NB	130×180	2.70	54.35	20.6	*C*	21.0	0.98
62	BC4HA	130×180	2.70	63.41	21.0	*C*	23.4	0.90
63	BC4HB	130×180	2.70	63.41	21.4	*C*	23.4	0.91
64	BC4VA	130×180	2.70	110	28.4	*C*	32.5	0.87
65	BC4VB	130×180	2.70	110	29.5	*C*	32.5	0.91

Table 6–1 (cont.): Comparisons of the flexural strength and flexural failure mode obtained experiments and the analytical

No.	Member ID	$b \times h$ (mm^2)	ρ_f (%)	f_{cu} (MPa)	M_{exp} (kN.m)	Failure Mode	M_{cur} (kN.m)	$\frac{M_{exp}}{M_{cur}}$
Yost et al. 2001								
66	1FRP1	381×203	0.12	32.47	11.49	*R*	12.4	0.93
67	1FRP2	381×203	0.12	32.47	12.67	*R*	12.4	1.02
68	1FRP3	381×203	0.12	32.47	11.49	*R*	12.4	0.93
69	2FRP1	318×216	0.13	32.47	13.62	*R*	13.7	0.99
70	2FRP2	318×216	0.13	32.47	13.26	*R*	13.7	0.97
71	2FRP3	318×216	0.13	32.47	13.06	*R*	13.7	0.95
72	4FRP1	203×152	1.27	32.47	15.78	*C*	14.2	1.11
73	4FRP2	203×152	1.27	32.47	15.58	*C*	14.2	1.10
74	4FRP3	203×152	1.27	32.47	16.29	*C*	14.2	1.15
75	5FRP1	191×152	1.35	32.47	16.37	*C*	13.1	1.25
76	5FRP2	191×152	1.35	32.47	16.65	*C*	13.1	1.27
77	5FRP3	191×152	1.35	32.47	15.78	*C*	13.1	1.20
Kassem 2011								
78	C1–4	300×200	0.6	40.4	71.20	*C*	66.8	1.06
79	C1–6	300×200	0.9	39.3	83.13	*C*	85.9	0.97
80	C1–8	300×200	1.2	39.3	90.39	*C*	88.5	1.02
81	C2–4	300×200	0.5	39.9	78.75	*C*	64.7	1.20
82	C2–6	300×200	0.8	40.8	80.89	*C*	83.6	0.96
83	C2–8	300×200	1.1	40.8	89.39	*C*	85.8	1.04
84	G1–6	300×200	1.6	39.05	77.47	*C*	90.5	0.86
85	G1–8	300×200	2.2	39.05	86.76	*C*	97.4	0.89
86	G2–6	300×200	1.4	39.05	71.00	*C*	89.6	0.79
87	G2–8	300×200	1.9	39.05	84.54	*C*	95.7	0.88
88	AR–6	300×200	0.9	39.05	70.85	*C*	84.5	0.84
89	AR–8	300×200	1.2	39.05	71.75	*C*	86.9	0.83
Barris 2009								
91	C–212–D1	190×140	0.99	59.8	38.22	*C*	32.9	1.16
92	C–216–D1	190×140	1.78	56.3	45.06	*C*	37.4	1.20
93	C–316–D1	190×140	2.67	55.2	49.38	*C*	43.8	1.13
94	C–212–D2	190×140	0.99	39.6	27.69	*C*	22.7	1.22
95	C–216–D2	190×140	1.78	61.7	42.15	*C*	40.5	1.04
96	C–316–D2	190×140	2.67	60.1	43.20	*C*	37.3	1.15
M_{exp} and M_{pre} are the ultimate moment obtained from experimental results and numerical technique, respectively.					Average			0.98
					Standard deviation			%12.6

6.4 Different Parameters Affecting the Moment-Curvature Relationship of FRP Reinforced concrete Section

The main aim of the parametric study is to investigate the behaviour of FRP reinforced concrete sections. In particular, the influence of different parameters such as FRP reinforcement ratio, type of FRP reinforcement and concrete compressive strength on the moment capacity and moment-curvature response of FRP reinforced sections has been developed using the analytical modelling program explained previously in this chapter. Table 6–1 illustrates reinforced concrete sections with different types of FRP that represents three series, namely A, B and C based on the material properties (design parameters) of each section. All sections were 500 mm in width and 150 mm in depth. Series A was selected to achieve the first parametric study represented in type of FRP (CFRP or BFRP) bars. This group was designed to have the same reinforcement ratio (five reinforcing bars of 8mm diameter for each type). The second series, B contained the same reinforcement (four BFRP reinforcing bars) and different concrete compressive strength of 30, 40, 50 and 60 MPa. Unlikely, the series C was also selected to have the same compressive strength of 40 MPa with different reinforcement ratio as given in Table 6–4. The properties of BFRP and CFRP reinforcing bars used in the slabs tested are presented in Tables 3–2 and 4–2 in chapters three and four, respectively.

Table 6–2: Parametric studies and reinforcement of slabs tested

Series no.	Parametric study	Reinforcement of section	f'_c: MPa
A	Type of FRP reinforcement	CFRP (5#8 mm)	40
		BFRP (5#8 mm)	
B	Concrete compressive Strength	BFRP (4#8 mm)	30-60
C	FRP reinforcement ratio (%)	BFRP (3#10, 4#10 & 7#10 mm)	40

6.4.1 Effect of FRP reinforcement type

Figure 6–12 shows the moment-curvature relationship of section A with BFRP and CFRP bars. For each material type, a concrete compressive strength of 40 N/mm^2 was assumed. In all cases, five reinforcing bars of 8mm diameter were used. Section reinforced with CFRP bars exhibited higher moment compared with this reinforced with BFRP bars (Figure 6–11) after the first crack occurred. However, there is a softening in the moment-curvature relationship of slab reinforced with BFRP bars; it could be attributed to the lower modulus of elasticity of BFRP bars than that of CFRP bars.

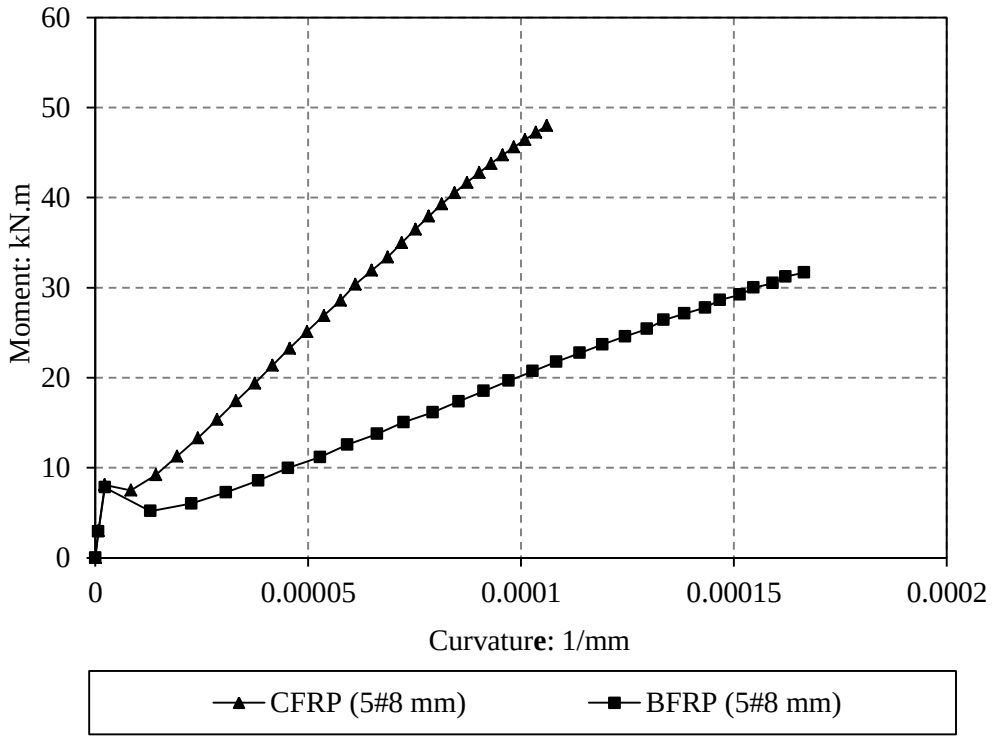

Figure 6–11: Moment-Curvature for different type of FRP bars

6.4.2 Effect of concrete compressive strength

This line of investigation will examine numerically the effect of concrete compressive strength on the moment capacity and Moment-Curvature relationship for FRP reinforced concrete sections.

6.4.2.1 Concrete compressive strength effect on moment capacity

Figure 6–12 shows the moment capacity related to concrete compressive strength of concrete section B reinforced with four BFRP bars of 8mm diameter for 30, 40, 50, and 60 MPa concrete compressive strengths. It was noticed that increasing the concrete compressive strength would increase the moment capacity of BFRP concrete section. On the other hand, increasing the concrete compressive strength had a small effect in enhancing the moment capacity after reaching the compressive strength of 45 MPa as shown in Figure 6–12.

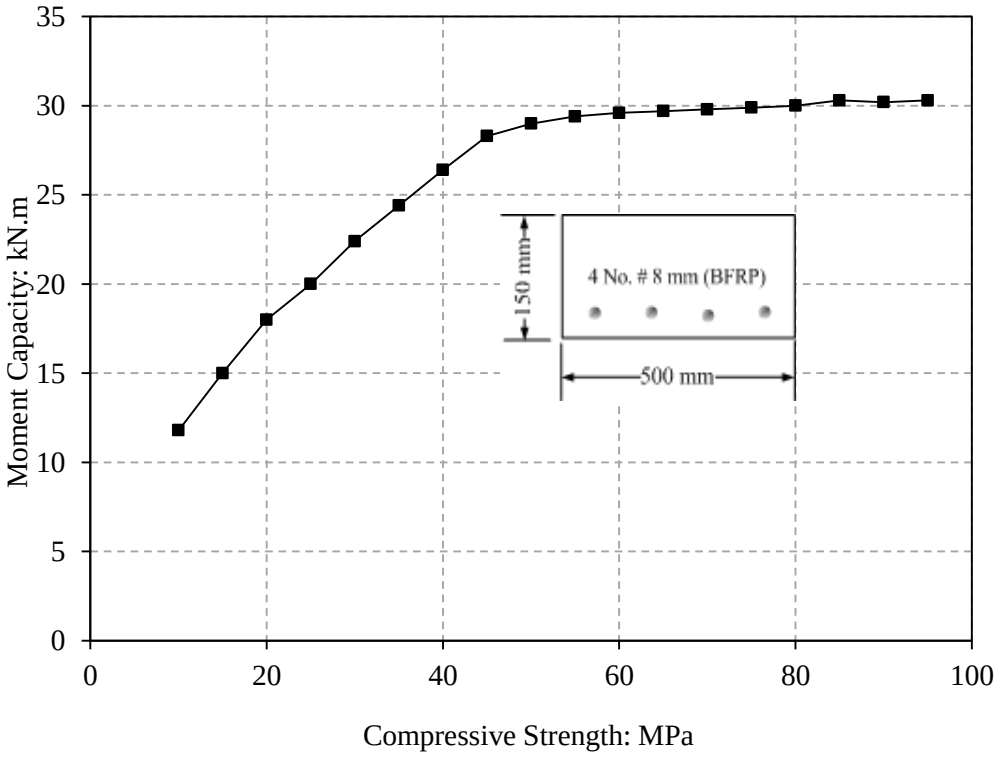

Figure 6–12: Moment capacity for BFRP bars

6.4.2.2 Concrete compressive strength effect on moment-curvature relationship

Figure 6–13 illustrates the moment-curvature relationship of BFRP reinforced concrete section B within the studied range of compressive strength (30–60 MPa with 10 MPa increment). It should be mentioned that increasing concrete compressive strength was found to decrease the curvature of the reinforced section at the same value of the

bending moment. It can be seen from Figure 6–13 that the improvement difference of the curvature for all values of compressive strength at any bending moment value, increased with a small value, as the bending moment increased. The same figure also shows that any increase in the concrete compressive strength up to the value of 40 MPa (see Figure 6–13) has a small effect on the moment-curvature response. Further to that, increasing the concrete compressive strength will generate a neglected moment-curvature enhancement.

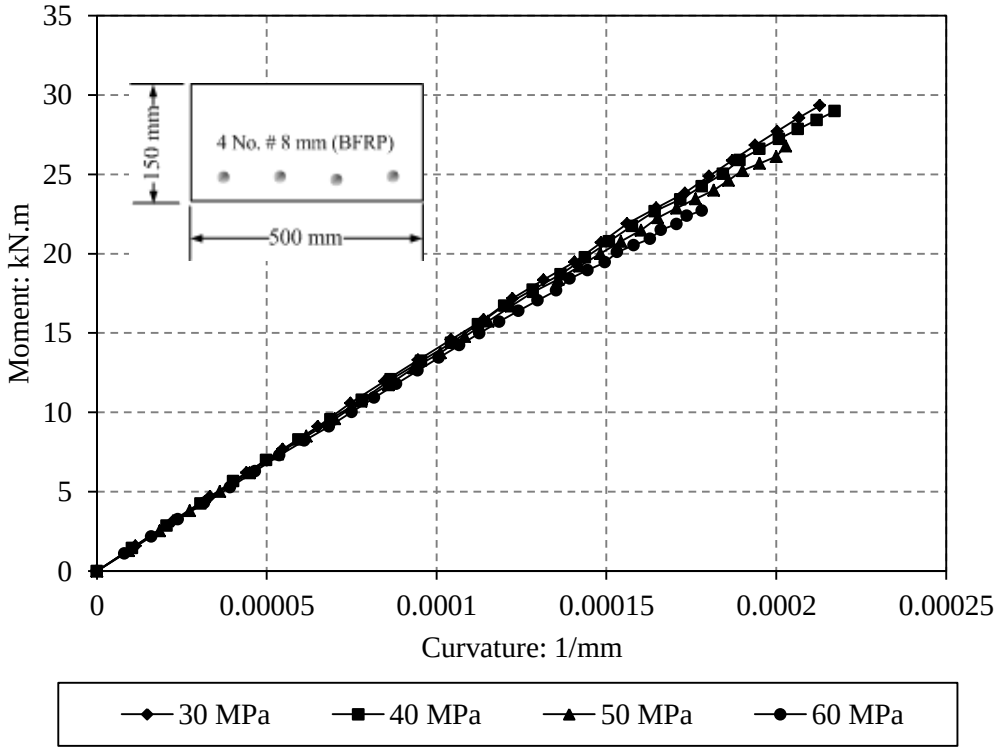

Figure 6–13: Moment-Curvature for different concrete compressive strength

6.4.3 Tensile FRP reinforcement ratio

This section will investigate the effect of FRP reinforcement ratio on the moment capacity and moment-curvature relationship of FRP concrete slabs.

6.4.3.1 Effect of tensile FRP reinforcement ratio on moment capacity

The effect of tensile FRP reinforcement ratio on the moment capacity is presented in Figure 6–14. The series C (see Table 6–1) has been investigated in this section to calculate the moment capacity related to each reinforcement ratio increase. It can be seen from Figure 6–14 that increasing the reinforcement ratio was found to increase the moment capacity of BFRP concrete reinforced section. As a result, increasing the reinforcement ratio has been proven to be effective in enhancing the moment capacity. However, increasing the reinforcement ratio becomes less effective in improving the moment capacity after reaching the balanced ratio as it could be shown in Figure 6–14.

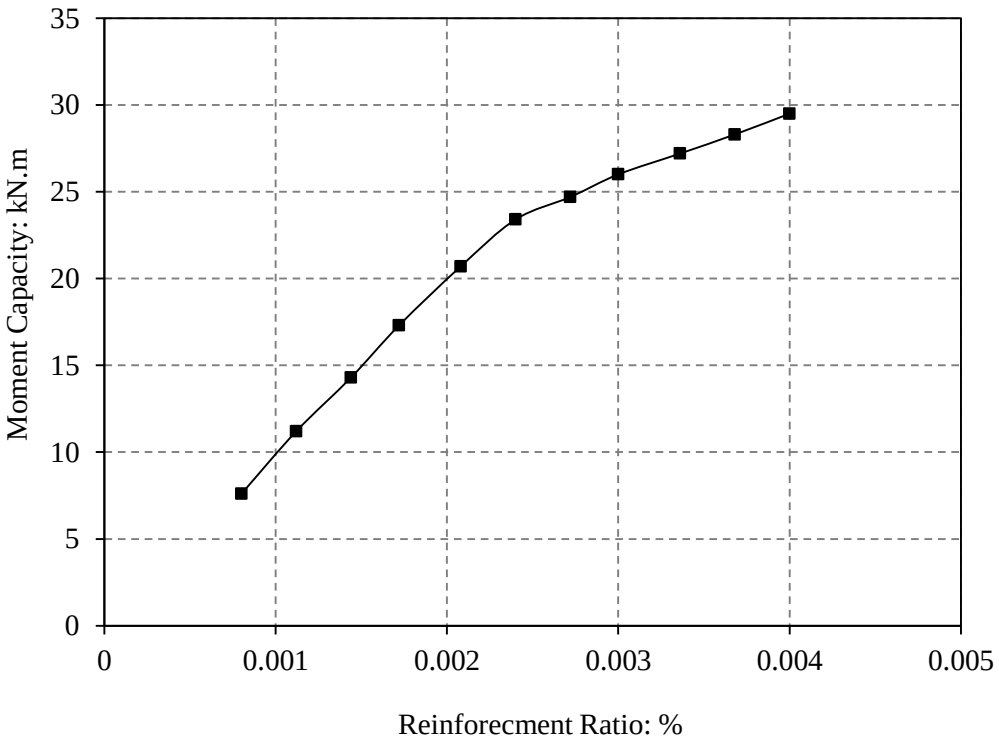

Figure 6–14: Effect of the reinforcement ratio on the moment capacity for BFRP section

6.4.3.2 Effect of tensile FRP reinforcement ratio on moment-curvature relationship

Figure 6–15 illustrates the moment-curvature relationship of investigated section C with different amount of BFRP bars. From curves of the same figure, it can be seen that

increasing the area of tensile BFRP reinforcement was found to increase the moment enhancement ratio of the reinforced section. However, decreasing the area of FRP bars decreased the flexural rigidity of the reinforced section up to reaching the flexural capacity. It was also observed that at the same value of the bending moment, increasing the reinforcement bars number decreased the curvature of BFRP sections. The figure also illustrates that the difference in curvature of BFRP sections increases as the bending moment increase.

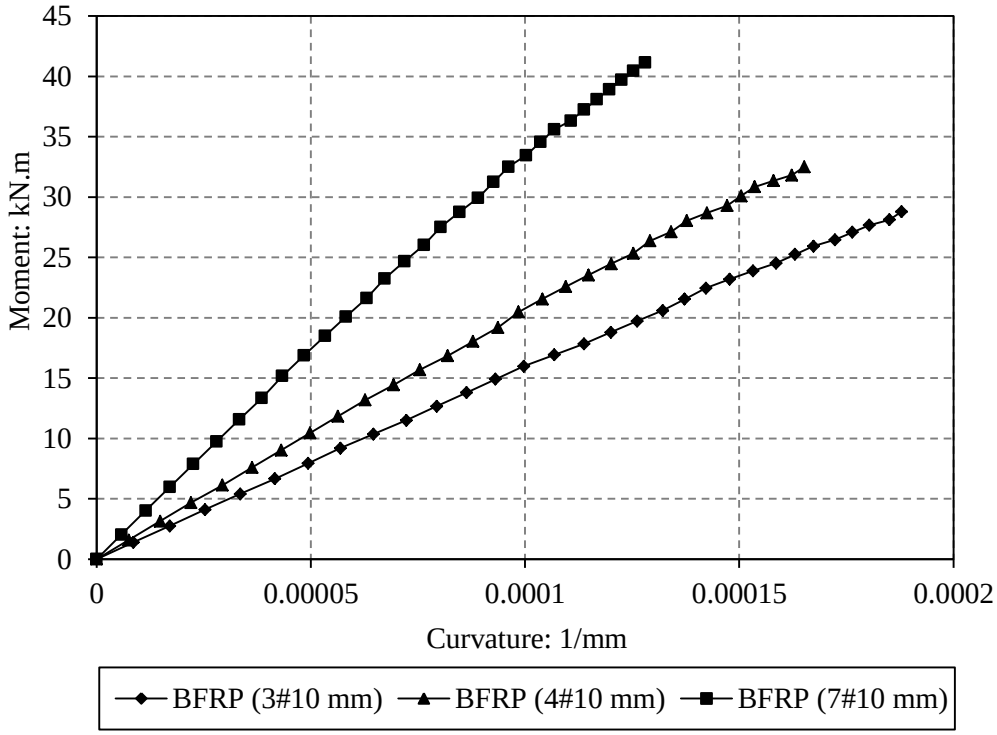

Figure 6–15: Effect of the reinforcement ratio on the moment-curvature relationship of BFRP sections

6.5 Load-Deflection of FRP Reinforced Concrete Members

In this section, the longitudinal analysis of simple and continuous slabs reinforced with FRP bars will be evaluated. This part of the program is devoted to producing the load-deflection relationship along the length of FRP reinforced concrete members. Hence, the influence of design parameters such as the type of FRP reinforcing bars, the tensile

FRP reinforcement ratio and the concrete compressive strength on the flexural performance of FRP reinforced concrete slabs could be investigated.

Based on satisfying force equilibrium and deformation compatibility conditions, the computer program has been developed using MATLAB language for investigating the deflection of member reinforced with FRP bars. The analytical modelling program can be used for analysis of both simple and continuous members reinforced with different types of reinforcing bars. This program depends on sectional analysis explained previously in this chapter and longitudinal analysis, which has been described below.

- The moment-curvature relationship is developed for different sections along the span of member, using the sectional analysis method described above (see Section 6.2). In case of a continuous member, it should be noted that each section over the central support has two moment-curvature relationship that is because the applied moment on a section could be reversed its direction, and the bottom reinforcement in a section may become in tension or compression based on the direction of the applied moment.
- The member span, L will be divided into a number of segments, m (= 500), each of length ΔL $(= L/m)$ as presented in Figure 6–16.

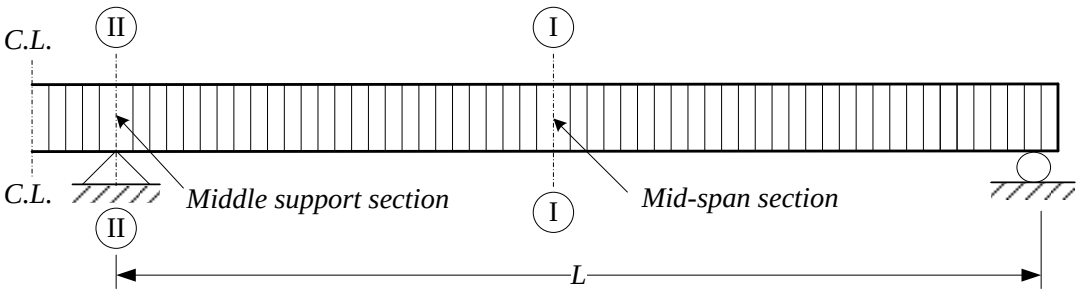

Figure 6–16: Different sections in a continuous member divided into a number of segments

- The bending moment at any point along the member length, M_r is determined by the linear interpolating using the bending moments at the mid-span M_{span} of simple and

continuous members (section I–I) and at the middle support, $M_{support}$ of continuous member (section II–II) as shown in Figures 6–17 and 6–18.

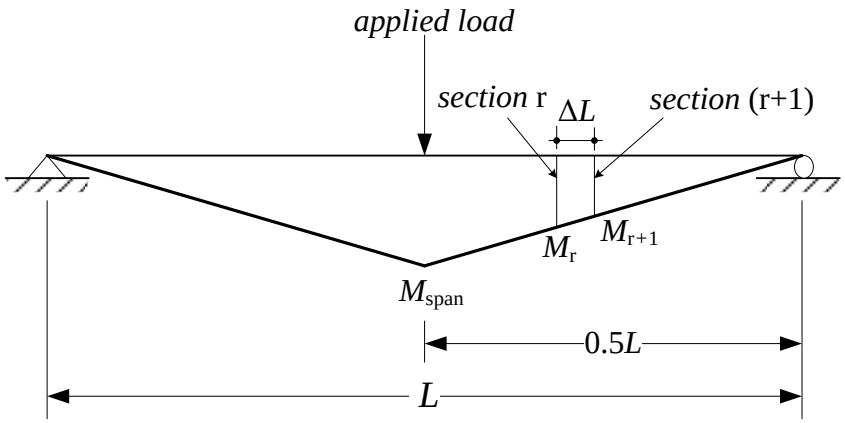

Figure 6–17: Bending moment diagram of a simple supported member

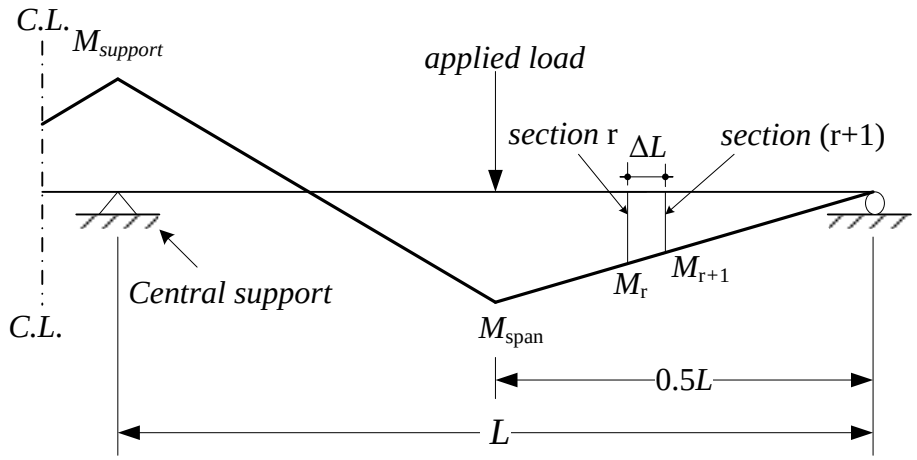

Figure 6–18: Bending moment diagram of a continuous supported member

- One of the main objectives of the computer program is to determine the curvature, φ_r at each section along the length of the simply and continuously supported concrete members, using the developed moment-curvature relationship and applied moment at each segment.
- The slope at each point throughout the length of the member is equal to the area under curvature diagram of the member up to that point (see Figures 6–19 and 6–20). The calculation for slope is started from one end support (an initial known value) to

mid-span of the member for simply supported members and to the central support for continuously supported members. The following equations Eq. (6–17) and Eq. (6–18) present the process of the calculation progress for slope at each segment θ_n along the member length:

$$A_{\varphi i}=\varphi_i \times \left(\frac{L}{m}\right) \tag{6–17}$$

$$\theta_i=\sum_{j=1}^{i} A_{\varphi i}+\theta_0 \tag{6–18}$$

where $A_{\varphi i}$ is the area below the curvature of the segment i, φ_i is the curvature of the segment i, (L/m) is the width of each segment, θ_i is the slope at segment i, and θ_0 is the boundary condition.

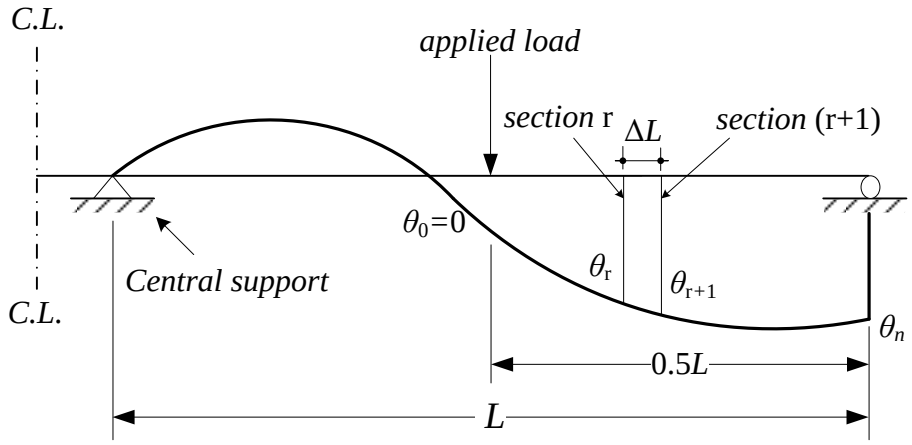

Figure 6–19: Slope along length of a continuous member

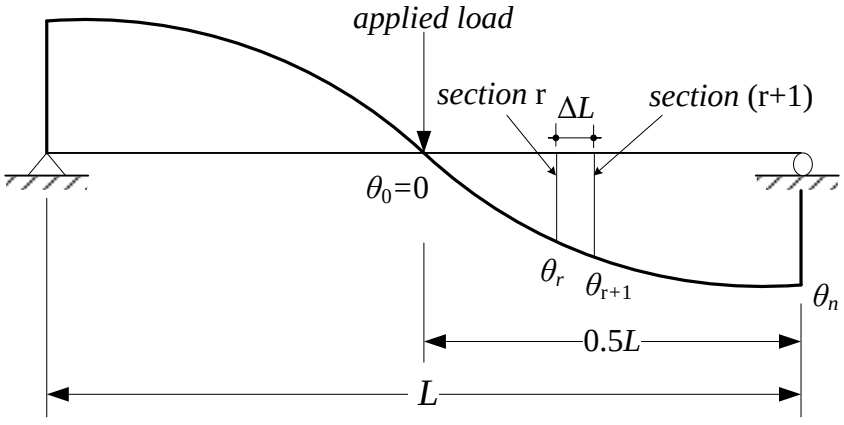

Figure 6–20: Slope along length of a simple member

- Now that the slope of the member has been calculated and located at each point within the length of the member. The next process is to calculate the deflection at each of these points, using the following equations:

$$A_{\theta i}=\theta_i\times\left(\frac{L}{m}\right) \tag{6–19}$$

$$\delta_n=\sum_{j=1}^{i}A_{\theta i}+\delta_0 \tag{6–20}$$

where $A_{\theta i}$ is the area of segment i under slope graph of the member, δ_n is the deflection of the member and $\delta_0(=0)$ is the boundary condition for deflection, which is located at each end of span of the member at supported points in case of simply supported member and that is located at end of span and over central support in case of a continuously supported member. Unlike the slope, in case of a simply supported member, the calculation of deflection will be carried out from end support to mid-span of the member (see Figure 6–21).

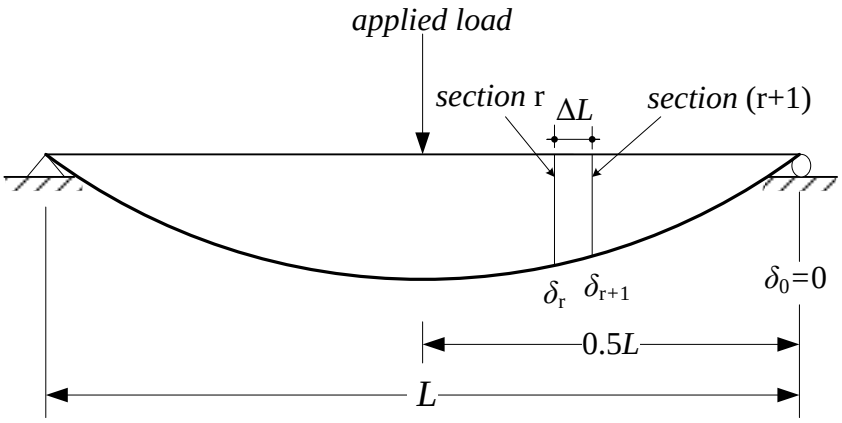

Figure 6–21: Deflection along length of a simple member

In a continuously supported member, for each reaction force increment, the bending moment at the mid-span M_{sag}, and that over the central support M_{hog} is changed until the deflection over the central support and at the end support should be zero or within an accepted tolerance ($10^{-4}\times$ slap span) (satisfy compatibility) using bisection

method which is presented in Appendix (I). Therefore, the bending moment at the mid-span will be M_{sag} (final) and that over central support will be M_{hog} (final). Hence, the reaction force R at the end of member will be R (final) as illustrated in Figure 6–22. The above stated steps are given in Figure 6–23.

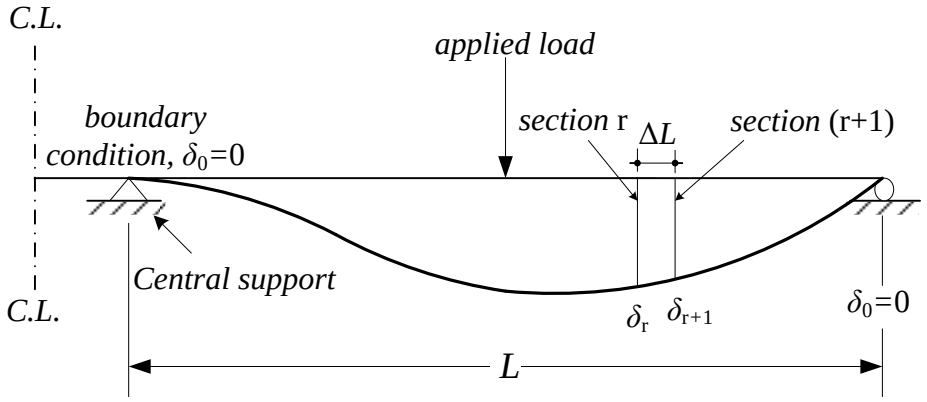

Figure 6–22: Deflection along length of a continuous member

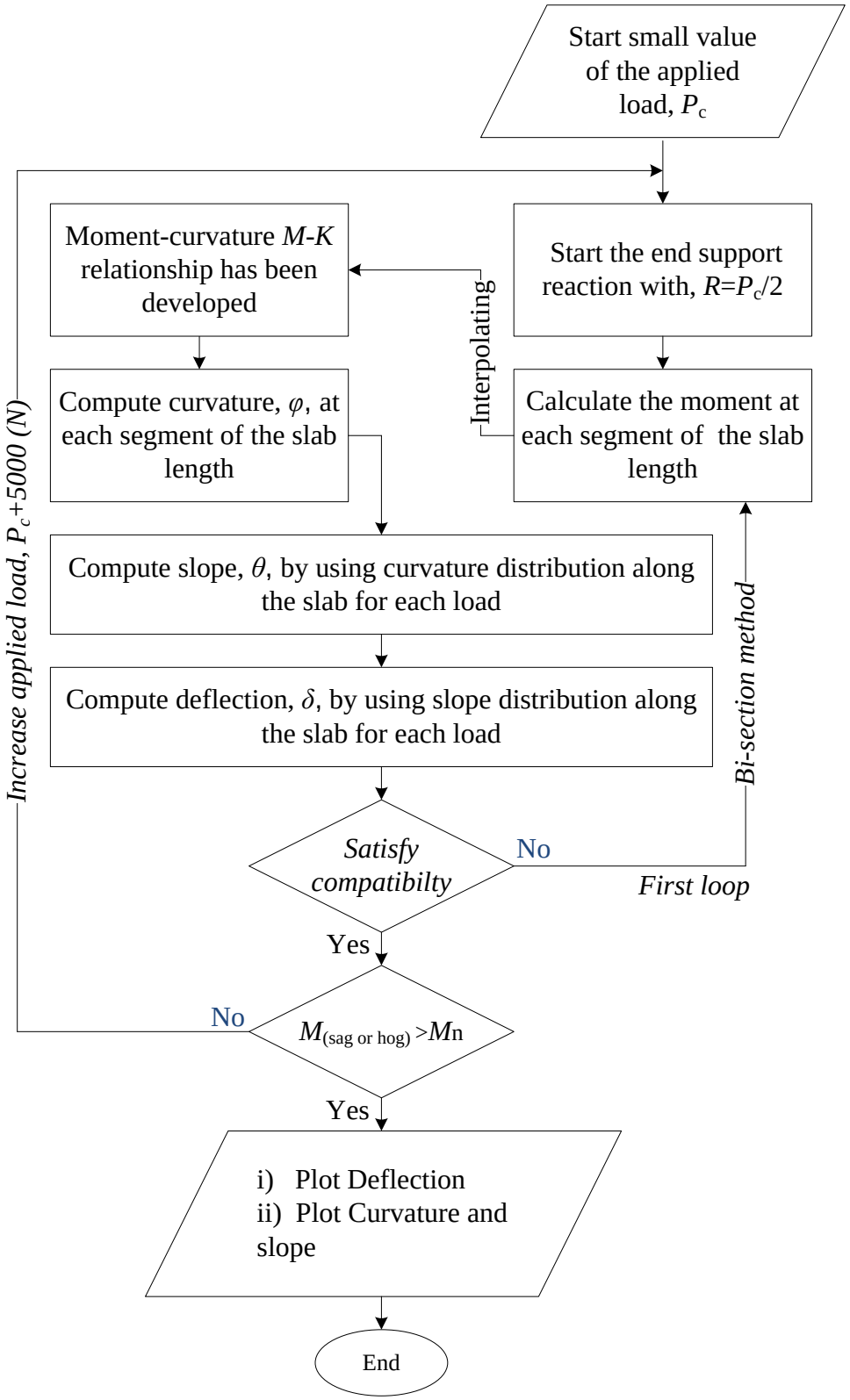

Figure 6–23: Flowchart diagram of the longitudinal analysis process employed in the program for FRP members

6.6 Verification of the Developed Numerical Technique against Experimental Results

In this section, the mid-span experimental deflections of BFRP and CFRP simply and continuously supported reinforced concrete slabs are compared with the predictions from the numerical technique as presented below.

Figure 6–24 presents the load-deflection response of slab S–C–U obtained from experimental work (chapter four) and proposed technique using different number of segments along the length of slab span. Although, just 20 segments along the slab span were used, the load-deflection relationships obtained from this numerical technique and experiments were in a reasonable agreement. However, using a number of segments higher than 500 was found to marginally affect the load-deflection as depicted in Figures 6–24 and 6–25. Thus, 250 segments were used by the author for all slabs using the numerical technique.

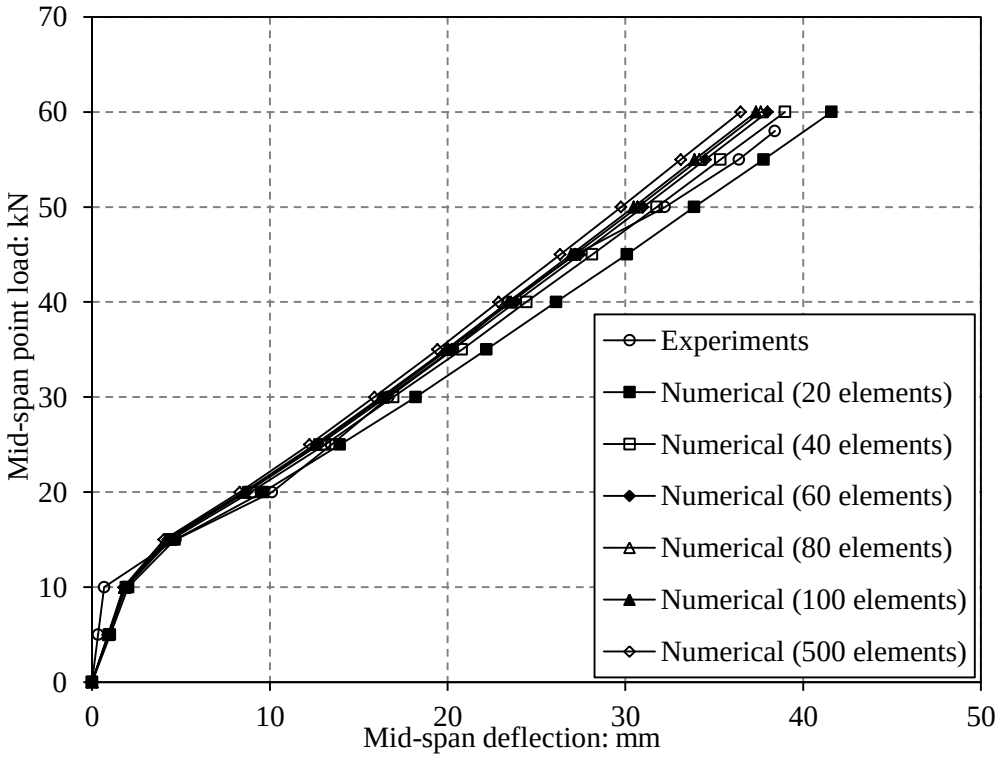

Figure 6–24: Influence of number of elements in the slab section S–C–U on deflection

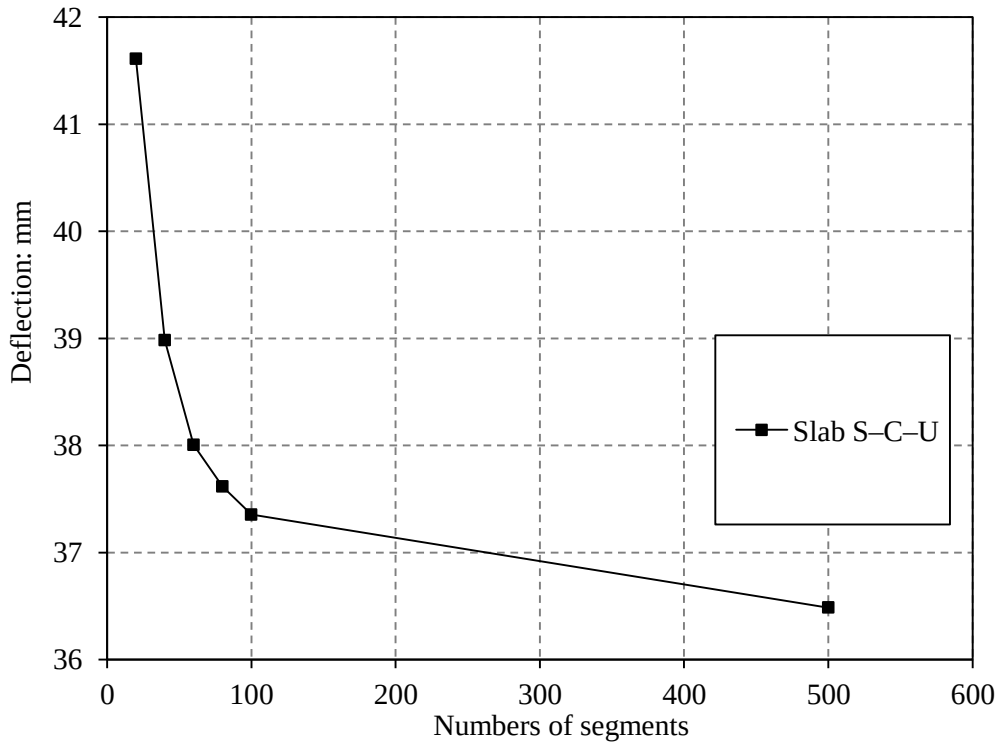

Figure 6–25: Influence of number of segments in the slab section S–C–U on the maximum deflection

6.6.1 Prediction of deflection of continuously supported slabs

The analytical modelling program described in this chapter was verified against the collected experimental results obtained from the specimens tested in this study (chapters three and four). Figure 6–26 shows the load-deflection behaviour of continuous concrete slabs C–C–OO and C–C–UU. It can be seen that the model accurately predicted the load-deflection response of the CFRP-reinforced slabs C–C–OO and C–C–UU after cracking and up to 40% and 75% of failure load, respectively. These slabs experienced a sudden increase in mid-span deflection due to significantly wide cracks over the middle support.

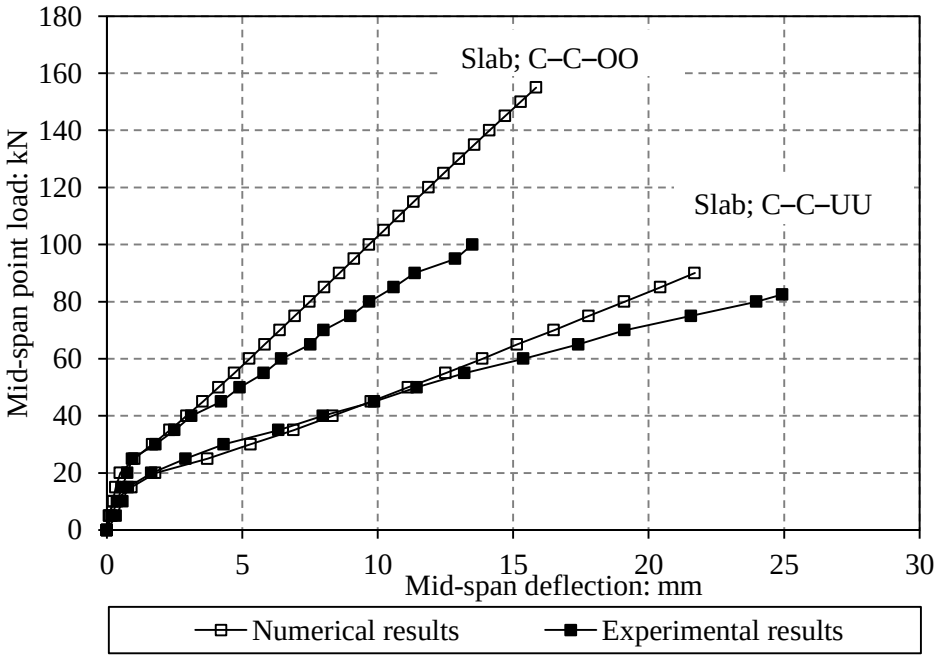

Figure 6–26: Load–Deflection relation for CFRP continuously supported slabs; C–C–OO and C–C–UU

On the other hand, further verification has been conducted by comparisons with the experimental results of slabs C–C–OU and C–C–UO as shown in Figure 6–27. The numerical model predicted the deflection response of the tested slabs C–C–OU and C–C–UO accurately up to 80% of the ultimate load. In this loading range, the difference between predicted and experimental deflection was within 20%. As load increased, the tested slab demonstrated significant increase in deflection as a result of a combination of wide cracks, which has been discussed in the earlier chapters. Figures 6–28 and 6–29 present comparisons between the load-deflection response obtained from the experimental results for BFRP concrete slabs described in chapter three and those predicted by the numerical technique. It should be mentioned that before concrete cracking, the measured deflections were similar to that predicted from the numerical technique for these slabs. However, this was not the case after cracking; where the present numerical technique may underestimate the deflection, especially at high loads.

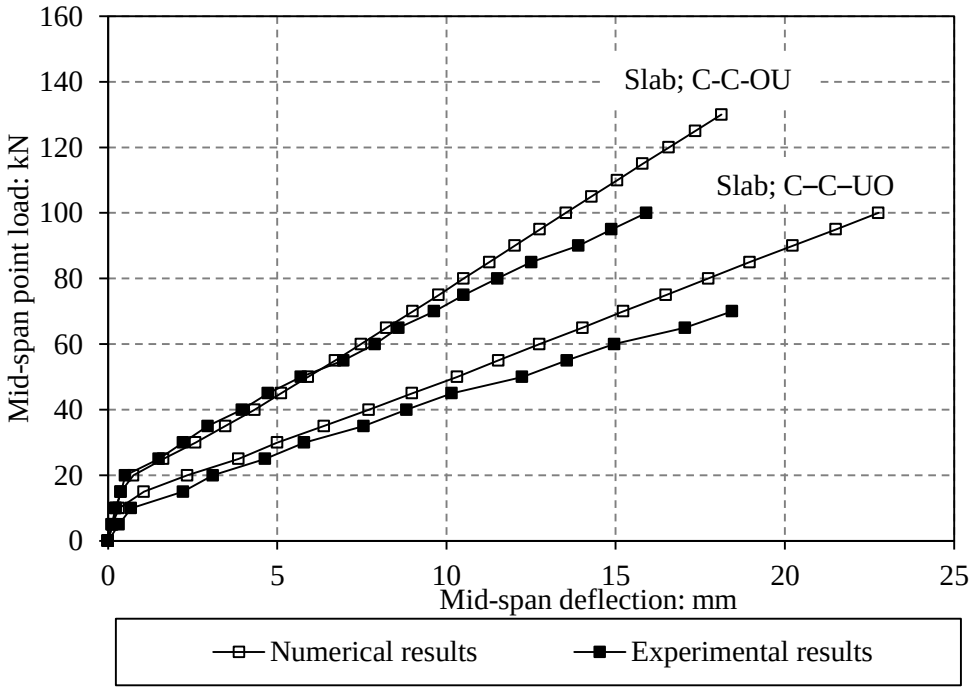

Figure 6–27: Load-Deflection relation for CFRP continuously supported slabs; C–C–OU and C–C–UO

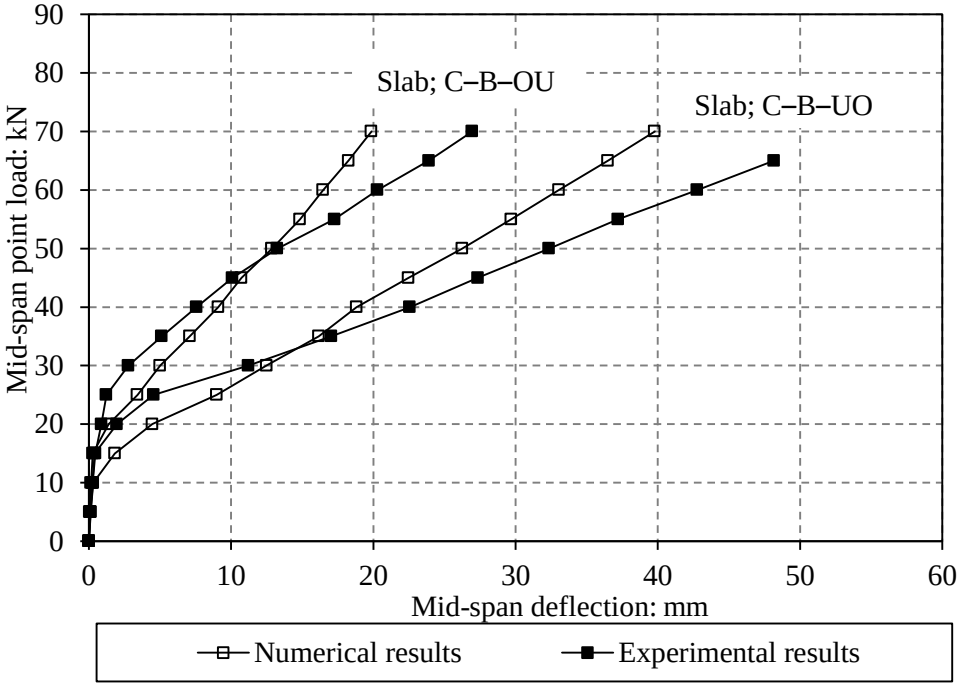

Figure 6–28: Load-Deflection relation for BFRP continuously supported Slabs; C–B–OU and C–B–UO

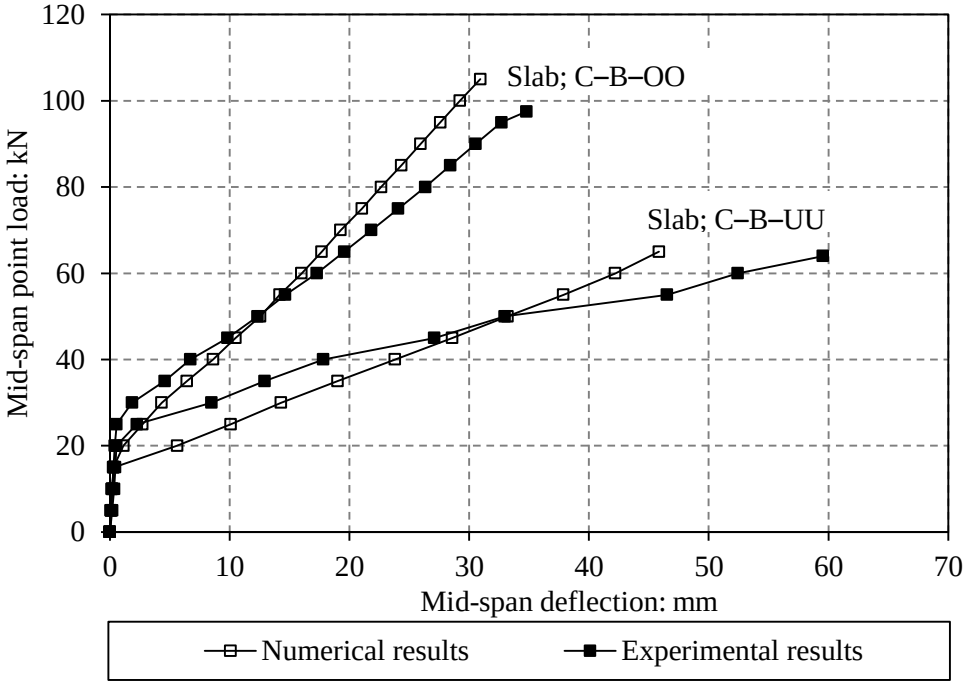

Figure 6–29: Load-Deflection relation for BFRP continuously supported slabs; C–B–OO and C–B–UU

6.6.2 Prediction of deflection of simply supported slabs

The proposed technique, as it has been displayed in Figure 6–30, gives a closer deflection to experimental results of CFRP reinforced concrete simple slabs S–C–O and S–C–U. Furthermore, this technique demonstrated a very accurate simulation to load-deflection response presented by the experimental results of the simply supported BFRP reinforced concrete slabs S–B–O and S–B–U as shown in Figure 6–31. Again, it was observed that the deflections predicted by the computer program did not match to the experimental results of slabs S–C–O and S–B–O at high stage of loading, which can be seen in Figures 6–30 and 6–31.

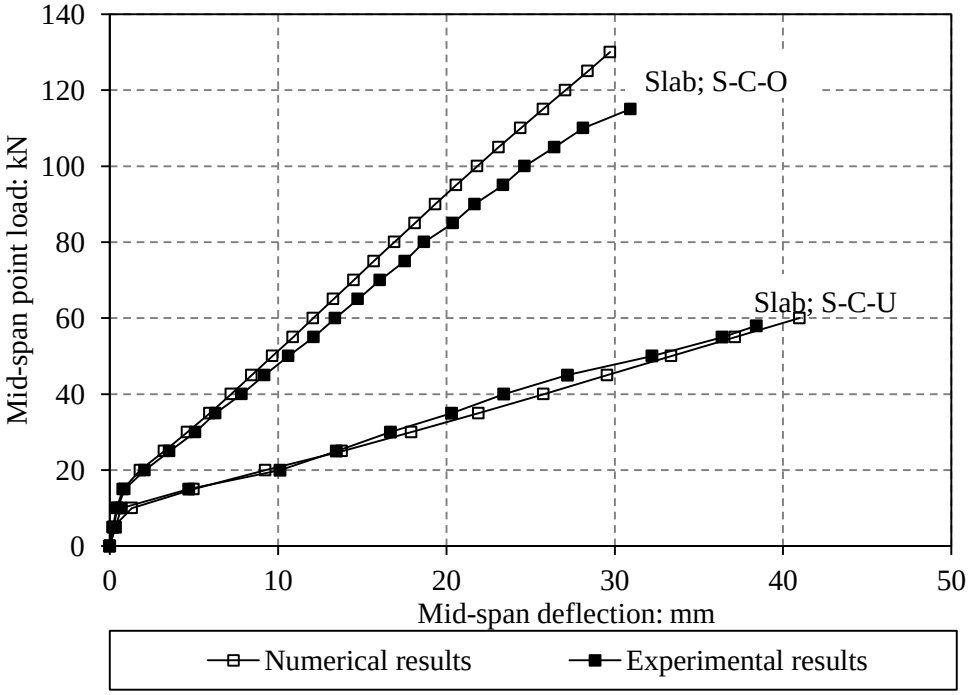

Figure 6–30: Load-Deflection relation for CFRP simply supported slabs; S–C–U and S–C–O

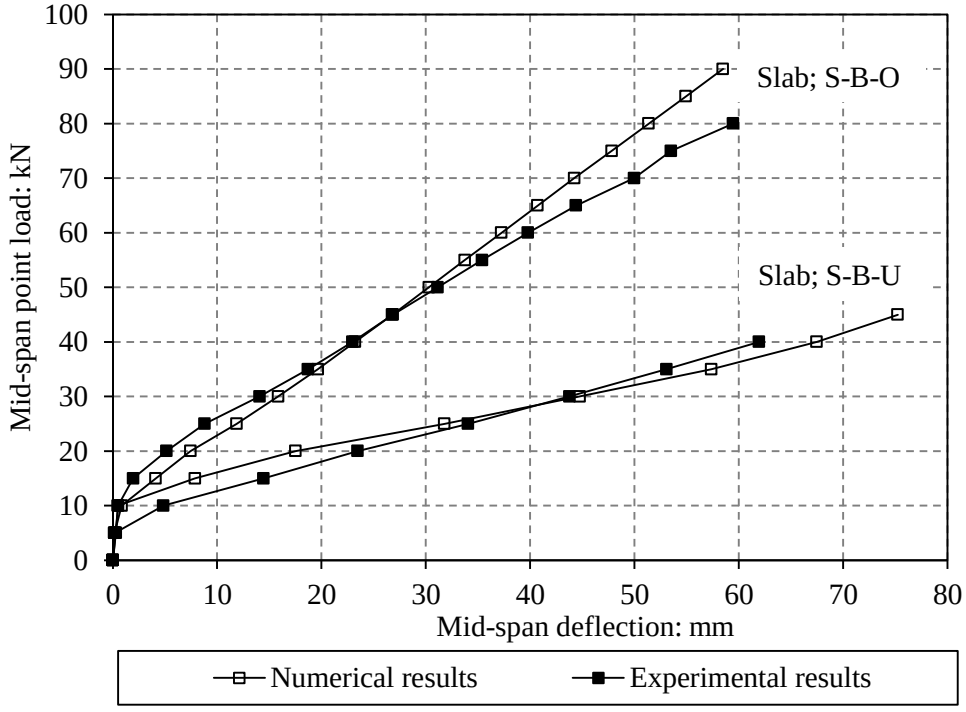

Figure 6–31: Load-Deflection Relation for BFRP Simply supported Slabs; S–B–U and S–B–O

6.7 Different Parameters Affecting Load-Deflection Relationships

6.7.1 Effect of compressive strength on load–deflection response

To assess the influence of compressive strength of concrete on the load-deflection response, this parameter was changed within 30–60 MPa with 10 MPa increment. Figure 6–32 presents the variation in the load-deflection response of slab (series B, see Table 6–1) within the investigated range of concrete compressive strength. It can be mentioned that increasing the concrete compressive strength slightly increased the cracking moment owing to the increase in concrete tensile strength as it could be seen from in Figure 6–32. The same figure also shows that for low concrete strength, the load-deflection response after cracking and up to ultimate load was mainly linear. However, considerable nonlinearity was showed in the load-deflection response for high concrete strength, especially for high concrete strength of 60 MPa. It occurred due to the fact that concrete members with higher strength need higher tensile strength in reinforcement to conserve equilibrium in the section.

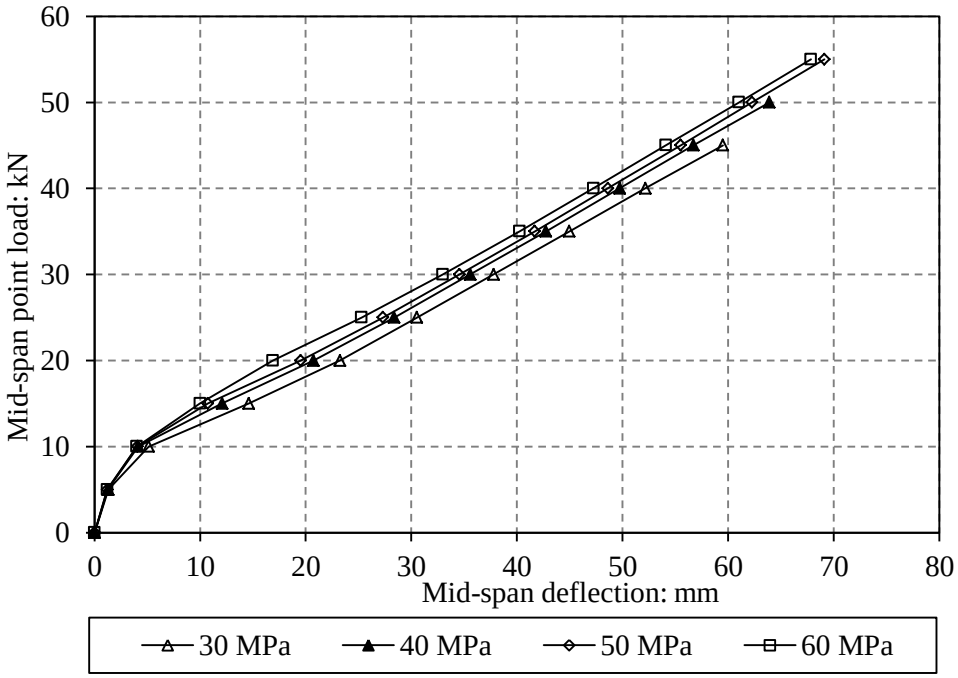

Figure 6–32: Effect of increased concrete strength on load-deflection for reinforced concrete slab (series B)

6.7.2 Effect of reinforcement ratio on load-deflection response

Figure 6–33 shows the load-deflection response of slab S–B–U obtained from experiments and numerical technique using different reinforcement ratio. It can be observed that increasing the reinforcement ratio at mid-span region of this slab had a positive impact on reducing mid-span deflection. Conversely, decreasing the reinforcement ratio by decreasing the reinforcement bars number increased the deflection of the reinforced section.

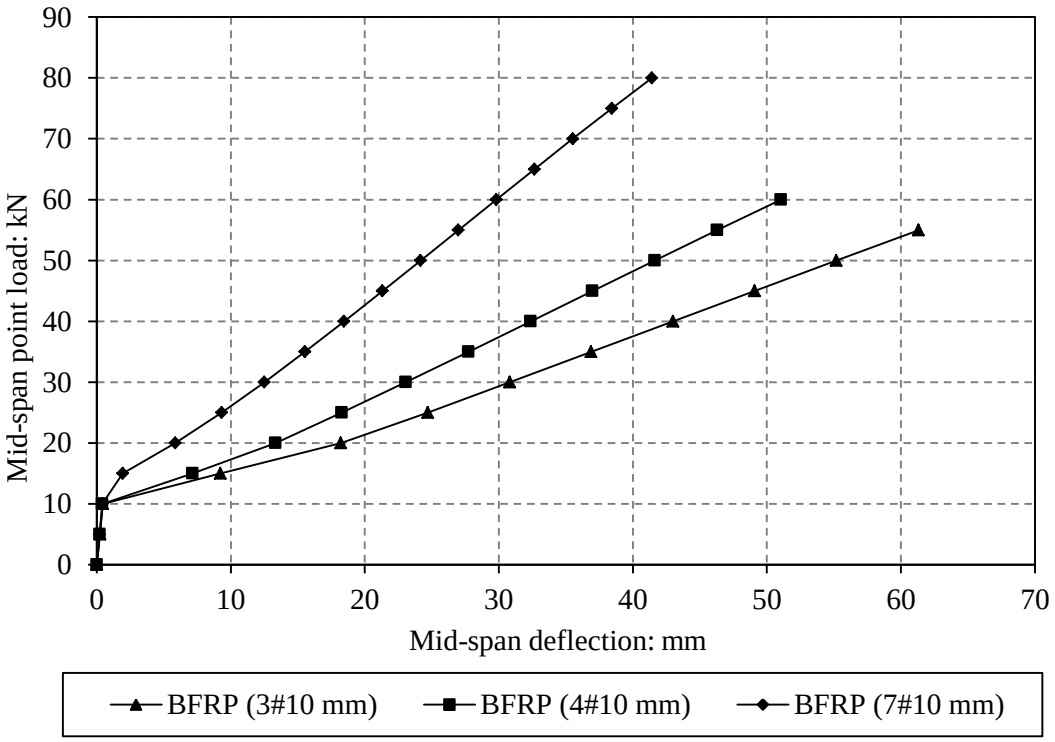

Figure 6–33: Effect of reinforcement ratio on load-deflection for BFRP reinforced concrete slabs

6.8 Conclusions

The main aim of the analytical technique was to investigate the moment-curvature relationship and moment capacity of reinforced concrete sections reinforced with FRP bars. In addition, the analytical method presented in this chapter has been employed for developing a computer model to investigate load-deflection response of FRP reinforced concrete members (beams or slabs). The processes of the analytical technique were

developed based on equilibrium and compatibility conditions of internal forces and strains, respectively.

The effect of different parameters such as amount and type of FRP reinforcement, and strength of compressive concrete on the moment capacity, failure mode and moment-curvature relationship of reinforced sections has been investigated by using the analytical modelling programme. All these variables will help to explain the flexural behaviour of FRP concrete sections of slabs.

The main conclusions drawn from the study described in this chapter are summarised as follows:

- Increasing the concrete compressive strength decreased the curvature of reinforced sections with FRP bars.
- BFRP reinforced concrete section with low modulus of elasticity exhibited a softening in the moment-curvature relationship compared with those have high modulus of elasticity (CFRP).
- The increase of tensile reinforcement ratio has a considerable influence in enhancing the moment capacity. That influence is negligible if the reinforcement ratio exceeds the balanced ratio.
- However, the reinforcement ratio has a considerable influence in decreasing the curvature of the FRP reinforced concrete sections.
- In the simply FRP RC members, the comparison between computational results obtained from the current program and experimental results obtained from this study for deflection shows good agreement. However, deflection of FRP continuously supported concrete members predicted by the analytical modelling program was slightly reasonable compared with experimental results.

CHPTER SEVEN

CONCLUSIONS AND RECOMMENDATIONS FOR FUTURE WORK

7.1 Introduction

The flexural and shear behaviour of continuously supported concrete slabs with BFRP and CFRP bars were studied in this thesis. The research consisted of three phases, an experimental investigation, evaluation of the predictability of the design codes (ACI 440.1R-06, ISIS 2007, CSA S806-02) methods against the experimental results of this research and the development of a numerical modelling program including sectional and longitudinal analyses.

The experimental phase contained the construction and testing of eight continuously and four simply supported concrete slabs reinforced with BFRP and CFRP bars. In addition, two control concrete continuous slabs reinforced with steel bars were also tested for comparison purposes. All simple and continuous reinforced concrete slabs were loaded at their midpoints up till failure. The combination and number of reinforcing bars were the main parameters investigated in this study. Hence, cracking patterns, failure modes, redistribution of support reactions, crack width, deflections and ultimate load capacity of reinforced concrete slabs were experimentally investigated.

The analytical phase included the sectional and longitudinal analyses of simply and continuously supported concrete members. The performance of the developed model was validated against the results obtained from the experimental phase in this project and elsewhere. Afterwards, the influence of design parameters such as the internal reinforcement type, longitudinal reinforcement ratio, concrete compressive strength and midspan-to-middle support reinforcement ratio could be investigated.

7.2 Conclusions

The principal findings drawn from the current investigation can be summarised below:

- The tested BFRP-reinforced continuous slabs demonstrated wider cracks and higher deflections compared to the steel-reinforced control slab due to the lower elastic modulus of BFRP bars.
- The tested CFRP and BFRP-reinforced continuous slabs demonstrated redistribution of moment from the middle support to the mid-span sections and conversely from the mid-span to the middle support due to cracks and bond slip.
- Over reinforcing the bottom layer of the BFRP and CFRP simply and continuously supported reinforced concrete slabs contribute significantly in improving the load capacity and deflection reduction.
- Over reinforcing the middle support section of continuously supported BFRP and CFRP reinforced concrete slabs slightly reduced deflections, and improved load capacity.
- Increasing the bottom layer reinforcement of continuously supported BFRP and CFRP reinforced concrete slabs does not exhibit any remarkable first visible cracking load.
- The BFRP and CFRP continuously supported concrete slabs were adversely affected by shear failure.
- ACI 440.1R-06 equations appear to be effective in predicting the load capacity of CFRP and BFRP simply supported reinforced concrete slabs. Conversely, these equations did not illustrate a good potential capability for predicting the load capacity of the tested continuous CFRP and BFRP reinforced concrete slabs.

- The ACI 440.1R–06 equations overestimated the experimental failure moment in most continuous CFRP and BFRP reinforced concrete slabs tested. This may be attributed to the shear effect combined with flexure at failure.
- The ISIS–M03–07 and CSA S806-06 design equations reasonably predicted the deflections of the CFRP simply and continuously supported slabs up to the initiation of excessive cracks. As the load was increased, the prediction process of BFRP continuously supported slabs has been negatively affected by the excessive cracks occurred over the middle support of these slabs.
- ACI 440–1R-06 equations underestimated the slab deflections of the BFRP reinforced concrete slabs tested.
- The ACI 440.1R–06, ISIS–M03–07 and CSA S806-06 design equations appear to be effective in predicting the deflections of the under-reinforced at the bottom layer CFRP continuously supported slabs. However, for the over-reinforced at the bottom layer CFRP continuously supported slabs, the prediction process has been adversely affected by the wide cracks occurred over the middle support of these slabs, especially at higher loading stages.
- The analytical modelling program could be used to investigate the several parameters such as reinforcement ratio and compressive strength that could influence the flexural behaviour of the FRP reinforced concrete members.
- Comparisons between the predicted moment capacities of FRP reinforced concrete members using the developed numerical technique and experimental results available in the literature indicate very good agreement.

7.3 Recommendations for Future Work

The following important areas are recommended for further investigations:

- As the present research was carried out using BFRP and CFRP reinforcement, it is recommended to investigate more experiments on concrete slabs reinforced with other types of fibres such as AFRP and GFRP reinforcement.
- Further research is needed to investigate the effect of high reinforcement ratio and different compressive strengths on the flexural performance of continuous concrete slabs such as crack propagation, crack width, moment redistribution and deflection.
- Further to the current research, it is recommended to investigate the effect of use of FRP reinforcing bars on the shear behaviour of continuously supported FRP reinforced concrete slabs.
- As the present experimental study was carried out using equal spans and one loading configurations, more variables need to be studied such as the effect of unequal spans and different loading configurations.
- Further experimental researches are required to validate design codes (ACI 440.1R–06, ISIS–M03–07 and CSA S806-06) for moment capacity and deflection of continuously supported FRP reinforced concrete slabs.
- Further work is needed to consider the bond characteristics between FRP bars and surrounding concrete for prediction the deflection of indeterminate FRP reinforced concrete members.

REFERENCES

Abdalla, H. (2002). “Evaluation of deflection in concrete members reinforced with fiber reinforced polymer (FRP) bars.” *Compos. Struct.*, 56(1), 63–71.

Achillides, Z., Pilakoutas, K. (2004), “Bond Behavior of Fiber Reinforced Polymer Bars under Direct Pullout Conditions”, *ASCE Journal of Composites for Construction*, Vol. 8, No. 2, March-April 2004.

ACI Committee 440. (1996). “State-of-the-Art Report on Fiber Reinforced Plastic (FRP) Reinforcement for Concrete Structures.” ACI 440R-96, *American Concrete Institute*, Detroit, MI.

ACI Committee 440. (2002) Recommended test methods for FRP rods and sheets. In: Unpublished draft specifications. Farmington Hills, MI: American Concrete Institute.

Ahmed, E. A., El-Salakawy, E. and Benmokrane, B. (2006). “Performance Evaluation of Glass Fiber-Reinforced Polymer Shear Reinforcement for Concrete Beams.” *ACI Structural Journal*, 107(1), 53-62.

Aiello, A., and Ombres, L. (2000a). “Cracking analysis of FRP-reinforced concrete flexural members.” *Mech. Compos. Mater.*, 36(5), 389–394.

Aiello, A., and Ombres, L. (2000b). “Load-deflection analysis of FRP reinforced concrete flexural members.” *J. Compos. Constr.*, 4(4), 164–170.

Almusallam, T. H. (1997). “Analytical prediction of flexure behavior of concrete beams reinforced with FRP bars.” *J. Compos. Mater.*, 31(7), 640–57.

Al-Salloum, Y. A., Alsayed, S. H., Almusallam, T. H., and Amjad, M. A. (1996). ‘‘Evaluation of service load deflection for beams reinforced by GFRP bars.’’ *Proc., 2nd Advanced Compos. Mat. in Bridge and Struct. Conf.*, Canadian Society for Civil Engineering, Montreal, 165–172.

Alsayed SH, Al-Salloum YA, Almusallam TH (2000). "Performance of glass fiber reinforced plastic bars as a reinforcing material for concrete structures", Composites Part B: Engineering, (31), 555-567.

Alsayed SH, Al-Salloum YA, Almusallam TH. (2000) “Performance of glass fiber reinforced plastic bars as a reinforcing material for concrete structures.” *Compos Part*, 31:555–67

Alsayed SH. (1998) “Flexural behaviour of concrete beams reinforced with GFRP bars.” *Cem Concr Compos*, 20(1), 1–11.

Al-Sunna, R. A. S. (2006). “Deflection Behavior of FRP Reinforced Concrete Flexural Members.” Ph.D. Dissertation, University of Sheffield, Sheffield, England, 318pp.

Alves, J., El-Ragaby, A. and El-Salakawy, E. (2011). "Durability of GFRP Bars Bond to Concrete under Different Loading and Environmental Conditions," *Journal of Composites for Construction, ASCE*, 15(3), 249-262.

American Concrete Institute (ACI). (2004). "Guide test methods for fiber reinforced polymers (FRPs) for reinforcing or strengthening concrete structures." *ACI 440.3R-04*, Farmington Hills, Mich.

American Concrete Institute (ACI). (2006). "Guide for the design and construction of concrete reinforced with FRP bars." *ACI 440.1R-06*, Farmington Hills, Mich.

American Concrete Institute (ACI). (2008). "Building code requirements for structural concrete and commentary." *ACI 318-08 and ACI 318R-08*, Farmington Hills, Mich.

Applications," *Composites: Part B*, 27B, pp. 245-252.

Ashour, A. F. (2006). "Flexural and shear capacities of concrete beams reinforced with GFRP bars." *Construction and Building Materials*, 20(10), 1005-1015.

Ashour AF, Habeeb MN, "Continuous concrete beams reinforced with CFRP bars." *Struct Build*, SB6, 349–57 (2008).

Baena M, Torres Ll, Turon A, Barris C. (2009). "Experimental study of bond behaviour between concrete and FRP bars using a pull-out test." *Compos. Part B Eng*., 40(8):784–97.

Barris, C., Torres, Ll., Turon, A., Baena, M. & Catalan, A. 2009. An experimental study of the flexural behaviour of GFRP RC beams and comparison with prediction models. *Composites Structures* 91(09): 286-295.

Benmokrane, B., Chaallal, O. and Mamoudi, R. (1996). "Flexural Response of Concrete Beams Reinforced with FRP Reinforcing Bars." *ACI Structural Journal*, 93(1), 46-55.

Benmokrane, B., El-Salakawy, E.F., Cherrak, Z., and Wiseman, A. (2004). "FRP Composite Bars for the Structural Concrete Slabs of a PWGSC Parking Garage." *Canadian Journal of Civil Engineering*, 31(5), 732-748.

Benmokrane, B., Ghao, D., and Tighiouart, B. (1998). "Investigation on the bond of fiber reinforced polymer (FRP) rebars to concrete." *Proc., 2nd Int. Conf. on Compos. in Infrastructure*, University of Arizona, Tucson.

Benmokrane, B.; Chaallal, O.; and Masmoudi, R. (1995), "Glass Fiber Reinforced Plastic (GFRP) Rebars for Concrete Structures", *Construction & Building Materials Journal*, 9(6), pp.353–364.

Bischoff, B.H., and Scanlon, A. (2007). "Effective Moment of Inertia for Calculating Deflections of Concrete Members Containing Steel Reinforcement and Fiber Reinforced Polymer Reinforcement." *ACI Struct. J.*, 104(1), 68 – 75.

Bischoff, P. H. (2005) "Reevaluation of Deflection Prediction for Concrete Beams Reinforced with Steel and Fiber Reinforced Polymer Bars." ASCE J. Struct. Eng., 131(5) 752 – 767.

Bischoff, P. H. (2007). "Deflection calculation of FRP reinforced concrete beams based on modifications to the existing Branson equation." *ASCE Journal of composites for construction*, 11(1), 4-14.

Bischoff, P. H., and Paixao, R. (2004). "Tension stiffening and cracking of concrete reinforced with glass fiber reinforced polymer (GFRP) bars." *Can. J. Civ. Eng.*, 31(4), 579 – 588.

Branson, D. E. (1968). "Design Procedures for Computing Deflections." *ACI Struct. J.*, 65(8), 730 – 742.

Branson, D.E. (1977) "Deformation of Concrete Structures," *McGraw-Hill*, New York,

Brown, V.L., and Bartholomew, C.L. (1996). "Long-term deflection of GFRP reinforced concrete beams. In: Fiber Composites in Infrastructure." *Proceedings of the 1st international conference on composites in infrastructures* (ICCI/96), 389 – 400.

Bunsell AR, Renard J (2005). "Fundamentals of fibre reinforced composite materials". *Institute of Physics Publishing*, Bristol.

Canadian Standards Association (CSA). (2002). "Design and construction of building components with fibre-reinforced polymers." *CSA Standard S806-02*, Rexdale, Ont., Canada.

Canadian Standards Association (CSA). (2004). "Design of concrete structures." *CSA Standard A23.3-04*, Rexdale, Ont., Canada.

Canadian Standards Association (CSA). (2006). "Canadian highway bridge design code." *CSA Standard S6-06*, Rexdale, Ont., Canada.

Chaallal, O. and Benmokrane, B. (1996). "Fiber-Reinforced Plastic Rebars for Concrete

Clarke, J. L., and O'Regan, D. P. (1995) ''Design of concrete structures reinforced with fibre composite rods.'' Proc., Non-Metallic (FRP) Reinforcement for Concrete Structures (FRPRCS-2), E & FN Spon, London, 646–653.

CNR-DT 203 (2006). "Guide for the Design and Construction of Concrete Structures Reinforced with Fiber-Reinforced Polymer Bars." *National Research Council*, Rome, Italy.

Cosenza, E., Manfredi, G., and Realfonzo, R. (1997). "Behavior and modelling of bond of FRP rebars to concrete." *J. Compos. for Constr.*, ASCE, 1(2), 40–51.

Deitz, D. H.; Harik, I. E.; and Gesund, H. (1999), "One-Way Slabs Reinforced with Glass Fiber Reinforced Polymer Reinforcing Bars", In ACI Proceedings, the Fourth International Symposium, Detroit, pp. 279–286.

Duranovic, N.; Pilakoutas, K.; and Waldron, P. (1997), "Tests on Concrete Beams Reinforced with Glass Fiber Reinforced Plastic Bars", Third International Symposium on Non-Metallic (FRP) Reinforcement for Concrete Structures (FRPRCS-3), Japan, vol. 2, pp. 479–486.

Ehab A. Ahmed, Ehab F. El-Salakawy, and Brahim Benmokrane. (2010) Shear Performance of RC Bridge Girders Reinforced with Carbon FRP Stirrups. Journal of Bridge Engineering 15(1), 44-54.

Ehsani, M. R-, Saadatmanesh, H. and Tao, S. (1993). "Bond of GFRP Rebars to Ordinary-Strength Concrete." Fiber-Reinforceci-Plastic Reinforcement for Concrete Structures, SP-138, Amencan Concrete uistitute, Detroit, 333-345.

El-Mogy, M., El-Ragaby, A. and El-Salakawy, E. (2010). "Flexural Behaviour of FRP-Reinforced Continuous Concrete Beams." *ASCE Journal of Composites for Construction*, 14(6), 486-497.

El-Mogy, M., El-Ragaby, A., and El-Salakawy, E. (2011). "Effect of Transverse Reinforcement on the Flexural Behavior of Continuous Concrete Beams Reinforced with FRP." J. Compos. Constr., 15(5), 672–681.

El-Salakawy, E. F., and Benmokrane, B. (2004). "Serviceability of concrete bridge deck slabs reinforced with FRP composite bars." *ACI Struct. J.*, 101(5), 727–736.

El-Sayed AK, El-Salakawy EF, Benmokrane B. (2006a) "Shear Strength of FRP-Reinforced Concrete Beams without Transverse Reinforcement." *Structural Journal*; 103(2): 235-243.

El-Sayed AK, El-Salakawy EF, Benmokrane B. (2006b) "Shear capacity of high-strength concrete beams reinforced with FRP bars." *ACI Struct J*, 103(3), 383–9.

El-Sayed, A. K., El-Salakawy, E. and Benmokrane, B. (2006). "Shear Strength of FRP-Reinforced Concrete Beams without Transverse Reinforcement." *ACI Structural Journal*, 103(2), 235-243.

Faza, S. S. (1991). "Bending and Bond Behavior and Design of Concrete Beams Reinforced with Fiber Reinforced Plastic Rebars." Ph.D. Dissertation, West Virginia University, Morgantown, WV, 200pp.

Faza, S.S. and GangaRao, H.V.S. (1992). "Pre- and post-cracking deflection behavior of concrete beams reinforced with fiber-reinforced plastic rebars." *Proceedings of the 1st international conference on the use of advanced composite materials in bridges and structures (ACMBS-I),* Ed. Neale K., Labossiere P., Montreal, Canadian, Society for Civil Engineering, 151 – 160.

Faza, S.S. and GangaRao, H.V.S., (1993), "Theoretical and Experimental Correlation of Behavior of Concrete Beams Reinforced with Fiber Reinforced Plastic Rebars," Fiber-Reinforced-Plastic Reinforcement for Concrete Structures, SP-138, *American Concrete Institute*, Detroit, Michigan, pp. 599-614.

Frosch, R. J. (1999). "Another look at cracking and crack control in reinforced concrete." *ACI Structural Journal*, May–June, pp. 437–442.

GangaRao, H. V. S., and Vijay, P. V. (1997). ''Design of concrete members reinforced with GFRP bars.'' *Proc., 3rd Int. Symp. on Fiber Reinforced Polymer for Reinforced Concrete Struct.*, Japan Concrete Institute, Tokyo, 143–150.

GangaRao, V. S. and Vijay, P. V. (2007). "Reinforced Concrete Design with FRP Composites," *CRC press*, Boca Raton, FL.

Gao, D., Benmokrane, B., and Masmoudi, R. (1998). "A calculating method of flexural properties of FRP-reinforced concrete beam: Part 1: Crack width and deflection," Technical Report, Department of Civil Engineering, University of Sherbrooke, Sherbrooke, QC, Cananda.

Gergely, P. and Lutz, L. A. (1968). "Maximum Crack Width in Reinforced Concrete Flexural Members." *ACI, Causes, Mechanism, and Control of Cracking in Concrete, SP-20*, Farmington Hills, MI, 1968, 87 – 117.

Gergely, P. and Lutz, L. A. (1968). "Maximum crack width in reinforced concrete flexural members." *Causes, Mechanism and Control of Cracking in Concrete*, SP–20, American Concrete Institute, Farmington Hills, Mich., pp. 87–117.

Grace, N. F., Soliman, A. K., Abdel-Sayed, G. and Saleh, K. R. (1998). "Behavior and Ductility of Simple and Continuous FRP Reinforced Beams." *ASCE Journal of composites for construction*, 2(4), 186-194.

Gravina, R. J., and Smith, S. T. (2008). "Flexural behaviour of indeterminate concrete beams reinforced with FRP bars." *Eng. Struct.*, 30(9), 2370–2380.

Habeeb, M. N., and Ashour, A. F. (2008). "Flexural behavior of continuous GFRP reinforced concrete beams." *J. Compos. Constr.*, 12(2), 115–124.

Hognestad, E., Hanson, N. W., and McHenry, D. (1955). "Concrete stress distribution in ultimate strength design." *ACI J.*, 52(12), 455–479.

Ilker Fatih Kara and Ashraf F. Ashour. (2012) "Flexural performance of FRP reinforced concrete beams". *Composite Structures*, 94(5), 1616-1625.

Ilker Fatih Kara. (2011). "Prediction of shear strength of FRP-reinforced concrete beams without stirrups based on genetic programming." *Advances in Engineering Software*, 42(6), 295-304.

ISIS Canada. (2001). "Reinforcing concrete structures with fibre reinforced polymers." *Design Manual No. 3*, ISIS Canada, Winnipeg, Manitoba, Canada.

Jaeger, L. G., Tadros, G., and Mufti, A. A. (1995). "Balanced section, ductility and deformability in concrete with FRP reinforcement."*Res. Rep., Joint U.S.-Can. Meeting at West Virginia Univ.,* Morgantown, W.Va.

Jaeger, L. G.; Mufti, A.; and Tadros, G. (1997). "The Concept of the Overall Performance Factor in Rectangular- Section Reinforced Concrete Beams," *Proceedings of the Third International Symposium on Non-Metallic (FRP) Reinforcement for Concrete Structures* (FRPRCS-3), V. 2, Japan Concrete Institute, Tokyo, Japan, pp. 551-558.

Japan Society of Civil Engineers (JSCE). (1997). "Recommendation for design and construction of concrete structures using continuous fiber reinforcing materials." *Concrete Engineering Series 23*. Machida, A. ed., Tokyo, Japan.

Kakizawa, T., Ohno, S., and Yonezawa, T. (1993). "Flexural behaviour and energy absorption of carbon FRP reinforced concrete beams."*Proc., Int. Symp. Fiber-Reinforced-Plastic Reinforcement for Concrete Structures,* A. Nanni and C. Dolan, eds., Vancouver, Canada, 585-598.

Kanakubo, T., Yonemaru, Y., Fukuyama, H., Fujisawa, M. and Sonobe, Y. (1993). "Bond Performance of Concrete Members Reinforced with FRP Bars." Fiber-Reinforced-Plastic Reinforcement for Concrete Structures, SP-138, Arnencan Concrete Institute, Detroit, 767-788.

Kassem, C., El-Salakawy, E., and Benmokrane, B. (2003). "Deflection Behavior of Concrete Beams Reinforced with Carbon FRP Composite Bars." Deflection Control for the Future, ACI SP-210, editor N.J. Gardner, ACI, Farmingtion Hills, MI, 173-190.

Kassem, C., Farghaly, A., and Benmokrane, B. (2011). "Evaluation of Flexural Behavior and Serviceability Performance of Concrete Beams Reinforced with FRP Bars." *J. Compos. Constr.*, 15(5), 682–695.

Larralde, J. and Silva-Rodriguez, R. (1993). "Bond and Slip of FRP Rebars in Concrete." *J. Mater. Civ. Eng.*, 5(1), 30–40.

Lee, W.K., Jansen, D.C., Berlin, K.B., and Cohen, I.E. (2010). "Flexural Cracks in Fiber- Reinforced Concrete Beams with Fiber-Reinforced Polymer Reinforcing Bars." *ACI Struct. J.*, 107(3), 321–329.

Makitani, E., Irisawa, I., and Nishiura, N. (1993). "Investigation of bond in concrete member with fibre reinforced plastic bars." *Fibre-Reinforced-Plastic Reinforcement for Concrete Structures-Int. Symp.*, ACI SP138-20, pp. 315-331.

Masmoudi, R., Béland, S., and Benmokrane, B. (1999). "Experimental evaluation of Kb factor for glass and carbon isorod FRP rebars". *Technical Report* No. 02-1999, submitted to Pultrall Inc., Thetford Mines, Qué.

Masmoudi, R., Benmokrane, B., and ChaaIlal, O. (1996a). "Cracking behaviour of concrete beams reinforced with FRP rebars." *Can. J. Civ. Engrg.*, 23(6), 1172–1179.

Masmoudi, R., Thériault, M., and Benmokrane, B. (1998). "Flexural behavior of concrete beams reinforced with deformed fiber reinforced plastic reinforcing rods." *ACI Struct. J.*, 95(6), 665 –676.

Masmoudi, R., Thériault, M., and Benmokrane, B. (I 996b). "Flexural behaviour of concrete beams reinforced with FRP C-BAR reinforcing rod," *Tech. Rep.* 2 *submitted to Marshal/Industries Composites. Inc.*, Dept. of Civ. Engrg., Univ. of Sherbrooke, Sherbrooke, Canada.

Member with Fibre Reinforced Polymer (FRP) Bars," *Construction and Building Materials,* 12(8), 453-462.

Metwally IM (2009). "Evaluation of existing model for predicting of flexural behavior of GFRP-reinforced concrete members", *HBRC J. Hous. Build. Res. Cent. Cairo, Egypt*, 5(1): 46-58.

Micelli F, Nanni A. (2001) "Mechanical properties and durability of FRP rods." In: CIES Report 00-22. Rolla, MO: University of Missouri-Rolla; 15–20.

Michaluk, C.R.; Rizkalla, S., H.; Tadros, G.; and Benmokrane, B. (1998), "Flexural Behavior of One-Way Concrete Slabs Reinforced by Fiber Reinforced Plastic Reinforcements", *ACI Structural Journal*, 95(3), 353–365.

Mohamed S. Issa, Ibrahim M. Metwally, and Sherif M. Elzeiny. (2011) "Influence of fibers on flexural behavior and ductility of concrete beams reinforced with GFRP rebars." *Engineering Structures* 33 (5), 1754-1763

Mostofinejad, D. (1997). "Ductility and Moment Redistribution in Continuous FRP Reinforced Concrete Beams," PhD thesis, Department of Civil and Environmental Engineering, Carleton University, Ottawa, Ontario, Canada.

Mota, C. M. (2005). "Flexural and shear behaviour of FRP-RC members." M.Sc. thesis, Dept. of Civil Engineering, Univ. of Manitoba, Winnipeg, Manitoba, Canada.

Mota, C., Alminar, S. and Svecova, D. (2006). "Critical Review of deflection formulas for FRP reinforced concrete." *ASCE Journal of Composites for construction*, 10(3), 183-194.

Mufti, A. A., Newhook, J. P. and Tadros, G. (1996). "Deformability versus ductility in concrete beams with FRP reinforcement." *Proc., 2nd Int. Conf. Adv. Composite Mat. In Bridges and Struct.*, El-Badry. Ed., Can. Soc. For Civ. Engrg., Montreal, Canada, 189-199.

Muhammad Masood Rafi and Ali Nadjai (2009) "Evaluation of ACI 440 Deflection Model for Fiber-Reinforced Polymer Reinforced Concrete Beams and Suggested Modification" *ACI Struct. J.*, 106(6), 762-771.

Nanni, A., (1993). "Flexural Behavior and Design of RC Members Using FRP Reinforcement," *ASCE J. of Struct. Engineering*, 119 (11), 3344 – 3359.

Nanni, A., Al-Zaharani, M. M., Al-Dulaijan, S. U., Bakis, C. E., and Boothby, T. E. (1995). ''Bond of FRP reinforcement to concrete experimental results.'' *Proc., 2nd Int. Symp. on Non-Metallic (FRP) Reinforcement for Concrete Struct.*, E & FN Spon, London, 135–145.

Nanni, A., and Dolan, C. W., eds. (1993). *Fiber-Reinforced- Plastic Reinforcement for Concrete Structures—International Symposium*, SP-138, American Concrete Institute, Farmington Hills, Mich., 977 pp.

Nawy, E. G., and Neuwerth, G. E. (1977). "Fiberglass reinforced concrete slabs and beams." *ASCE J. Struct. Div.*, 103(2), 421–440.

Newhook, J., Ghali, A. and Tadros, G. (2002). "Concrete flexural members reinforced with fiber reinforced polymer: design for cracking and deformability." *Canadian Journal of Civil Engineering*, 29(1), 125–134.

Park, R. and Paulay, T. (1975). *Reinforced Concrete Structures*. John Wiley and Sons, New York, NY.

Pecce, M., Manfredi, G., and Cosenza, E. (2000). "Experimental response and code models of GFRP RC beams in bending." *ASCE J. Compos. Constr.*, 4(4), 182–190.

Pilakoutas, K., Neocleous, K., and Guadagnini, M. (2002). "Design philosophy issues of fiber reinforced polymer reinforced concrete structures." *ASCE J. Compos. Constr.*, 6(3), 154–161.

Pilakoutas, K, FRP Composites in Construction. *T2 Materials and Constitutive relationships*, University of Seffield, 2010

Rasheed, H. A., Nayal, R. and Melhem H. G. (2004). "Response Prediction of Concrete Beams Reinforced with FRP Bars," *Compos. Struct.*, 65(2), 193-204.

Rashid, M. A., Mansur, M. A., and Paramasivam, P. (2005). "Behavior of Aramid Fiber- Reinforced Polymer Reinforced High Strength Concrete Beams under Bending." *ASCE J. of Composites for Construction*, 9(2), 117–127.

Razaqpur, A. G. and Mostofinejad, D. (1999). "Experimental Study for Shear Behavior of Continuous Beams Reinforced with Carbon Fiber Reinforced Polymer for Reinforced Concrete Structures." *Proceedings of the Fourth International Symposium*, 169-178.

Razaqpur, A. G., Svecova, D., and Cheung, M. S. (2000). "Rational method for calculating deflection of fiber-reinforced polymer reinforced beams." *ACI Struct. J.*, 97(1), 175–185.

Rizkalla, S., and Mufti, A. (2001). *Reinforcing concrete structures with fibre reinforced polymers—Design manual No. 3*, ISIS Canada, Winnipeg, Man., Canada.

Rizkalla, S., Hwang, L. S. and El Shahawai, M. (1983). "Transverse reinforcement effect on cracking behavior of RC members." *Canadian Journal of Civil Engineering*, 10(4), 566-581.

Saadatrnanesh, H., and Ehsani, M. R. (1991). "Fiber composite bar for reinforced concrete construction." *J. Compos. Mat.* 25(2), 188-203.

Shehata, E. F. G. (1999). "Fibre-Reinforced Polymer (FRP) for Shear Reinforcement in Concrete Prisms." Ph.D. Thesis, Department of Civil and Geological Engineering, University of Manitoba, Winnipeg, Manitoba.

Sim, J., Park, C., & Moon, D. Y. (2005), "Characteristics of basalt fiber as a strengthening material for concrete structures." Composites Part B: Engineering, 36(6-7), 504-512.

Tezuka, M., Ochiai, M., Tottori, S., and Sato, R. (1995). "Experimental study on moment redistribution of continuous beams reinforced or pretensioned with FRP." 2nd Int. Symp., Nonmetallic Reinforcement (FRP) for Concrete Struct., 387 -394.

Thériault, M. and Benmokrane, B. (1998). "Effects of FRP reinforcement ratio and concrete strength on flexural behaviour of concrete beams." *ASCE J. Compos. Constr.*, 2(1), 7 – 16.

Tighiouart, B., Benmokrane, B. and Gao, D. (1998). "Investigation of Bond in Concrete

Toutanji, H., and Deng, Y. (2003). "Deflection and crack-width prediction of concrete beams reinforced with glass FRP rods." *Construction and Building Materials J.*, 17, 69–74.

Toutanji, H.A. and Saafi, M. (2000). "Flexural behavior of concrete beams reinforced with glass fiber-reinforced polymer (GFRP) bars." *ACI Struct. J.*, 97(5), 712–719.

Tureyen, A. K., and Frosch, R. J., (2002), "Shear Tests of FRP Reinforced Concrete Beams without Stirrups," *ACI Structural Journal* 99(4), 427-434.

Tureyen, A. K., and Frosch, R. J., (2003), "Concrete Shear Strength: Another Perspective," *ACI Structural Journal* 100(5) 609-615.

Vijay, P. V. and GangaRao, H. V. (2001). "Bending Behaviour and Deformability of Glass Fiber-Reinforced Polymer Reinforced Concrete Members." *ACI structural journal,* 98(6), 834-842.

Vijay, P. V., Kumar, S. V. and GangaRao, H. V. S. (1996). "Shear and ductility behaviour of concrete beams reinforced with GFRP rebars." *Proc., 2nd Int. Conf. Adv. Composite Mat. In Bridges and Struct.*, El-Badry. Ed., Can. Soc. For Civ. Engrg., Montreal, Canada, 217-226.

Wegian, F. & Abdalla, H. (2005). Shear Capacity of Concrete Beams Reinforced with Fiber Reinforced Polymers. *Journal of Composite Structures* 71 (1), 130–138.

Wu, W. P., (1990), "Thermo mechanical Properties of Fiber Reinforced Plastic (FRP) Bars," PhD dissertation, West Virginia University, Morgantown, W.Va., 292 pp.

Yost, J. R., and Gross, S. P. (2002). "Flexure design methodology for concrete beams reinforced with fiber-reinforced polymers." *ACI Struct. J.*, 99(3), 308–316.

Yost, J. R., Gross, S. P., and Dinehart, D. W. (2003). "Effective moment of inertia for glass fiber reinforced polymer-reinforced concrete beams." *ACI Struct. J.*, 100(6), 732 – 739.

Yost, J. R.; Goodspeed, C. H.; and Schmeckpeper, E.R. (2001), "Flexural Performance of Concrete Beams Reinforced with FRP Grids", Journal of Composites for Construction, 5(1), pp.18–25.

Zhao, W., Maruyama, K., and Suzuki, H. (1995). "Shear behavior of concrete beams reinforced by FRP rods as longitudinal and shear reinforcement." *Non-Metallic (FRP) Reinforcement for Concrete Structures, Rilem Proc. 29*, E&FN Spon, London, 352–359.